Partitioning carbon fluxes in a permafrost landscape

Dissertation zur Erlangung des Doktorgrades an der Fakultät für Mathematik, Informatik und Naturwissenschaften

Fachbereich Geowissenschaften der Universität Hamburg

vorgelegt von

Tim Eckhardt

aus

Hamburg

Hamburg

2017

Tag der Disputation: 12.07.2017

Als Dissertation angenommen vom Fachbereich Geowissenschaften der Universität Hamburg auf Grund der Gutachten

von Prof. Dr. Eva-Maria Pfeiffer

und Dr. Christian Knoblauch

Parts of this dissertation have been published:

Eckhardt, Tim (2015): Verfahren zur Auftrennung der Bodenrespiration und deren Anwendungsmöglichkeiten in der polygonalen Tundra. In: Knoblauch, C., Fiencke, C., Berger, K. (Eds.): Böden im Wandel. Festschrift für Eva-Maria Pfeiffer. Hamburger Bodenkundliche Arbeiten, **77**, 49-60.

Eckhardt, Tim; Kutzbach, Lars (2016): MATLAB code to calculate gas fluxes from chamber based methods. *Institut für Bodenkunde, Universität Hamburg,* https://doi.pangaea.de/10.1594/PANGAEA.857799

Table of Contents

List of Figures

List of Tables

List of Abbreviations and Symbols

α	initial canopy quantum efficiency
AIC_c	Akaike Information Criterion
ALD	active layer depth
a.s.l.	above sea level
C	carbon
CH_4	methane
CH_3COOH	acetic acid
CO_2	carbon dioxide
CO_2-eq	carbon dioxide equivalent
C/N	carbon to nitrogen ratio
EC	Eddy covariance
GPP	gross primary productivity
GWP	global warming potential
H_2	hydrogen
H_2O	water
Hz	hertz
LAI	leaf area index
mg	milligram (= 10^{-3} g)
n	number of replicates
N	nitrogen
NDVI	normalized difference vegetation index
NEE	net ecosystem exchange
NPP	net primary productivity
p	probability value
PAR	photosynthetic active radiation
Pg	petagram (= 10^{15} g)
pH	negative decadal logarithm of hydrogen ion activity
P_{max}	maximum canopy photosynthetic potential
ppm	parts per million
Q_{10}	ecosystem sensitivity to changing temperatures

R^2	coefficient of determination
R^2_{adj}	adjusted coefficient of determination
R_A	autotrophic respiration
R_{base}	basal respiration
R_{eco}	ecosystem respiration
R_H	heterotrophic respiration
RMSE	root mean square error
RVI	ratio vegetation index
SOC	soil organic carbon
SOM	soil organic matter
SMR	soil microbial respiration
T_{air}	air temperature
Tg	teragram (= 10^{12} g)
TIC	total inorganic carbon
T_{soil}	soil temperature
T_{surf}	surface temperature
TOC	total organic carbon
VWC	volumetric water content
WT	water table
µg	microgram (= 10^{-6} g)

Summary

Arctic tundra ecosystems have acted as a historical sink for atmospheric carbon (C). Therefore, these ecosystems contain significant amounts of carbon in their frozen soils and sediments. The function as strong C sink is a product of short summers, low temperatures, well-adapted vegetation and water-saturated conditions, which causes low degradation and mineralization rates of soil organic matter (SOM). The Arctic is currently facing amplified climate warming and the rate of this warming is expected to accelerate. A number of changes are predicted in response to warming. On the one hand, warming is expected to cause the deeper thaw of permafrost-affected soils leading to both the enhanced production of carbon dioxide (CO_2) due to the increasing degradation of SOM, and increased methane (CH_4) formation, which could create a positive climate feedback to global warming. On the other hand, due to higher temperatures the assimilation of CO_2 by vegetation will increase. Therefore, it remains uncertain how the C sink function of arctic tundra landscapes will react to future changes in climate.

This study aimed to determine the CO_2 and CH_4 fluxes at the soil-plant-atmosphere interface in an arctic tundra ecosystem and to identify the main environmental drivers of these fluxes. Furthermore, as the processes governing CO_2 net ecosystem exchange (NEE) react differently on a changing climate, the CO_2 fluxes were partitioned into gross primary productivity (GPP) and ecosystem respiration (R_{eco}). R_{eco} was further partitioned into its autotrophic (R_A) and heterotrophic respiration (R_H) components. The study was conducted using chamber measurements on the microscale (1 m – 10 m) in a polygonal tundra environment in the Lena River Delta in 2014 and 2015. In order to estimate the CO_2 fluxes over the complete growing season in 2015, they were reproduced using flux models.

This work finds the polygonal tundra in the Lena River Delta to be a robust sink for atmospheric CO_2 and a source for CH_4. The CO_2 sink strength was highly heterogeneous on the microscale. The net CO_2 uptake at a wet-depressed polygonal center over the 2015 growing season was more than twice as high as measured at a drier polygonal rim. In addition to higher GPP fluxes, the differences in NEE between the two microsites were primarily caused by lower R_{eco} fluxes at the center compared to the rim. Here, the contrasting hydrological conditions cause the CO_2 flux differences between the microsites,

where high water levels lead to lower decomposition rates due to anoxic conditions. For the first time, the different response of *in situ* measured R_A and R_H fluxes to hydrological conditions was determined. It was shown that a high water table can lower R_A fluxes, most likely due to the submersion of plants; while a low water table lead to enhanced R_H fluxes and can desiccate mosses, therefore lowering R_A fluxes. The R_H fluxes presented in this study are the first *in situ* measured R_H fluxes, which cover an almost complete growing season from the vast Russian arctic tundra.

The environmental parameter with the highest explanatory power for the CH_4 fluxes was the active layer depth (ALD), although in general CH_4 fluxes were poorly correlated with environmental parameters, which highlights the complicated identification of factors influencing CH_4 fluxes. In contrast to previous studies, the dry tundra (polygonal rim) was not found to act as sink for atmospheric CH_4, most probably due to the low soil temperatures and high substrate availability at the study site.

The calculation of CO_2 and CH_4 budgets for the polygonal tundra revealed that the polygonal rims were a stronger net CO_2 sink than the centers in 2015 due to the high coverage of dry tundra at the study site. Considering the global warming potential (GWP) of CH_4 compared to CO_2, the radiative forcing of CH_4 emissions were five-fold lower in magnitude than the strength of the CO_2 sink in 2015. However, in 2014 both the CO_2 and the CH_4 budgets were marginally positive, denoting that the area functioned as a net source for atmospheric C. This finding highlights the pronounced inter-annual variability of C fluxes between the soils and atmosphere at the study site.

The partitioning of CO_2 fluxes provides unique insights into the individual contributions of each of the processes governing the CO_2 NEE. Improved knowledge of these contributions is of crucial importance to gain a better understanding of the reaction of arctic ecosystems to changing climatic conditions as these processes react differently to environmental parameters. Estimates of the CH_4 source strength of different microsites in the arctic tundra improves estimates of the C budgets from these contrasting environments. Furthermore, the presented results provide an improved understanding of the response of CO_2 and CH_4 fluxes to environmental controls from different arctic tundra sites, which is needed to optimize model simulations of future C fluxes.

Zusammenfassung

Über lange Zeiträume wirkten Ökosysteme der arktischen Tundra als Senke für atmosphärischen Kohlenstoff. Daher befinden sich in den gefrorenen Böden und Sedimenten dieser Ökosysteme enorme Mengen organischer Substanz. Die starke Senken-Funktion ist ein Produkt kurzer Sommerperioden, niedriger Temperaturen, einer an die Bedingungen angepassten Vegetation und wassergesättigter Böden, welches zu einer geringen Zersetzungsrate organischer Substanz im Boden führt. Die momentane Erwärmung der Arktis führt unter anderem zu einem tieferen Auftauen von permafrost-beeinflussten Böden, welches eine erhöhte Freisetzung von CO_2 und höhere CH_4-Produktion, aufgrund steigender Zersetzung organischer Substanz, bedingt. Dies könnte zu einer weiteren Verstärkung der globalen Erwärmung führen. Die Änderungen der Umweltbedingungen bedingen jedoch auch vermehrte CO_2-Aufnahme durch Pflanzen. Somit bleibt unklar, ob arktische Tundra-Ökosysteme in Zukunft eine Quelle oder Senke für atmosphärischen Kohlenstoff darstellen werden.

Ziel dieser Arbeit war es, die CO_2- und CH_4-Austauschflüsse zwischen Boden und Atmosphäre in einem arktischen Tundra-Ökosystem zeitlich hochaufgelöst zu bestimmen und den Einfluss verschiedener Umweltfaktoren auf diese Flüsse zu ermitteln. Der CO_2-Austauschfluss kann in einzelne Prozesse unterteilt werden: Die Primärproduktion sowie die Ökosystemrespiration, welche sich in autotrophe und heterotrophe Respiration aufteilt. Da diese Prozesse unterschiedlich auf sich ändernde Umweltfaktoren reagieren, wurde ihr Beitrag zum CO_2-Austauschfluss einzeln ermittelt. Die Untersuchungen wurden in den Jahren 2014 und 2015 an zwei unterschiedlichen Standorten in der polygonalen Tundra auf der Insel Samoylov im Lena Delta durchgeführt. Um die Beiträge der CO_2-Austauschflüsse während einer gesamten Messperiode zu bestimmen, wurden diese mit Hilfe von Modellen reproduziert.

Die polygonale Tundra stellt eine robuste CO_2-Senke und eine CH_4-Quelle dar. Beide Austauschflüsse zeigen eine hohe Heterogenität auf kleinräumlicher Skala (1 – 10 m): In einem wassergesättigten Polygonzentrum wurde eine mehr als doppelt so hohe CO_2-Aufnahme ermittelt als auf einem verhältnismäßig trockenen Polygonwall. Neben der höheren Primärproduktion führen hauptsächlich Unterschiede in der

Ökosystemrespiration zu unterschiedlichen CO_2-Austauschflüssen. Diese können anhand gegensätzlicher hydrologischer Bedingungen erklärt werden, da ein hoher Wasserstand eine geringere Zersetzung organischen Materials bedingt. Zusätzlich wurden unterschiedliche Reaktionen der heterotrophen und autotrophen Respiration auf hydrologische Bedingungen festgestellt: Ein hoher Wasserstand kann zur Überschwemmung der Pflanzen führen, welches eine Minderung der autotrophen Respiration bedingt. Ein niedriger Wasserstand kann wiederum zu erhöhter Zersetzung organischen Materials führen, welches die heterotrophe Respiration erhöht. Weiterhin kann ein niedriger Wasserstand Moose austrocknen und damit zu verringerter Primärproduktion führen. Die gemessenen heterotrophen Respirationsflüsse stellen die ersten *in situ* ermittelten Flüsse aus einem der weit verbreiteten Tundra-Gebiete der russischen Arktis dar.

Die gemessenen CH_4-Austauschflüsse korrelieren am besten mit der Auftautiefe. Allerdings lassen sich die Flüsse nur schwach mit verschiedenen Umweltvariablen erklären, welches die komplizierte Ermittlung der, die CH_4-Produktion, -Oxidation und den -Transport beeinflussenden Umweltvariablen hervorhebt. Unter Berücksichtigung des CH_4-Treibhauspotenzials übertrifft die CO_2-Senken-Funktion die CH_4-Emissionen um etwa das Fünffache während der Messperiode in 2015. Allerdings zeigten Kalkulationen, dass das Ökosystem in 2014 eine geringe Quelle für atmosphärischen Kohlenstoff darstellte, welches die hohe inter-annuelle Variabilität der Austauschflüsse verdeutlicht.

Die Auftrennung des CO_2-Austauschflusses in Einzelprozesse erlaubt einen einzigartigen Einblick in die Beiträge der Einzelflüsse zum gesamten CO_2-Austauschfluss. Die Bestimmung der Beiträge dieser Einzelflüsse ist von hoher Bedeutung, da diese unterschiedlich auf sich ändernde Umweltbedingungen reagieren. Kenntnisse der CH_4-Emissionen verschiedener Standorte der polygonalen Tundra helfen bei der Aufstellung von Kohlenstoff-Bilanzierungen für arktische Ökosysteme. Zusätzlich liefern die Resultate einen Erkenntnisgewinn zur Steuerung der Austauschflüsse durch Umweltvariablen, welcher notwendig ist, um Modell-Simulationen zukünftiger Kohlenstoff-Austauschflüsse zwischen Boden und Atmosphäre in arktischen Tundra-Ökosystemen zu verbessern.

1. Introduction and objectives

The amount of carbon (C) stored in northern high-latitude permafrost soils is with more than 1300 Petagram (Pg) distinctly higher as the current amount of C in the atmosphere (832 Pg) (Ciais *et al.*, 2013, Hugelius *et al.*, 2014). Of this 1300 Pg, about 500 Pg are stored in the seasonally thawed active layer, while ~800 Pg are stored in perennially frozen ground (Hugelius *et al.*, 2014). Given this large amount of C stored in permafrost soils, the response of the Arctic C cycle to a changing climate is of global importance (McGuire *et al.*, 2009). Over thousands of years the C was stored in permafrost soils due to a long freezing period and poor drainage, resulting in water-saturation (Ping *et al.*, 2015). Since a few decades, arctic ecosystems are facing amplified warming (Chapin *et al.*, 2005), which will cause a longer and deeper thawing of permafrost-affected soils.

As a consequence of longer and deeper thawing periods there will be an enhanced production of carbon dioxide (CO_2) through the increasing degradation of soil organic matter (SOM) (Knoblauch *et al.*, 2013, Schuur *et al.*, 2009, Zimov *et al.*, 2006). On the other hand, due to higher temperatures the assimilation of CO_2 by vegetation increases because of higher plant productivity (Jia *et al.*, 2009, Schuur *et al.*, 2007). Belshe *et al.* (2013) showed that the net CO_2 uptake increased since the 1990's in northern high-latitude tundra ecosystems, but also observed an increase in CO_2 winter emissions and therefore suggested that on an annual scale these ecosystems represent a source of atmospheric CO_2 in recent years. However, data of CO_2 fluxes from the vast Siberian permafrost landscapes are very scarce. This is critical as arctic ecosystems are highly heterogeneous and are therefore expected to show huge differences in flux strength on the microscale to macroscale (French, 1996).

Methane (CH_4) has a 34-fold higher global warming potential (GWP) as CO_2 on a 100-year timescale (Myhre *et al.*, 2013) and is therefore an important greenhouse gas in the climate system. The arctic tundra displays a substantial source of atmospheric CH_4, but this estimate is accompanied by a large uncertainty (McGuire *et al.*, 2012). This uncertainty can be attributed to the variability of CH_4 fluxes on spatial and temporal scales. For reliable estimates of the CH_4 source strength from arctic tundra landscapes, it is essential to perform continuous measurements across all land cover types as CH_4 emissions are

unevenly distributed in these landscapes and most likely occur during short periods of time (Marushchak *et al.*, 2016) and may show distinct emission peaks (Mastepanov *et al.*, 2008).

This study focussed on an arctic tundra region which holds tremendous amounts of soil organic carbon (SOC) (Zubrzycki *et al.*, 2013). The region is a substantial sink of atmospheric CO_2 (Kutzbach *et al.*, 2007b, Runkle *et al.*, 2013) and a source of CH_4 (e.g. Knoblauch *et al.*, 2015, Sachs *et al.*, 2010, Wille *et al.*, 2008). However, it still remains unclear which effects future climate warming will have on the C budget of permafrost-affected soils as a better understanding of the response of underlying processes of the C fluxes to warming is needed. For instance, Walz *et al.* (2017) have shown that the CO_2 release by heterotrophic respiration (R_H) due to decomposition of SOM will increase significantly if formerly frozen parts of the soils will thaw. Therefore, it is essential to gain a quantitative understanding of the underlying processes of CO_2 net ecosystem exchange (NEE) on different time scales and land cover classes. Partitioning NEE into photosynthesis, autotrophic and heterotrophic respiration is necessary to identify the response of these ecophysiological processes to a changing climate. To improve estimates of the C budgets from different tundra sites, it is necessary to investigate the CH_4 source strength intensely. Furthermore, a better understanding of the environmental controls on these processes is needed to improve model simulations of future C fluxes.

This study presents results of *in situ* chamber measurements of CO_2 and CH_4 fluxes conducted during two expeditions in a polygonal tundra in the Lena River Delta during summer 2014 and 2015.

The main objectives of this study were

1) to partition the net ecosystem exchange of CO_2 into the underlying processes by
   - determination of CO_2 fluxes and partitioning into gross primary productivity (GPP) and ecosystem respiration (R_{eco}) with chamber measurements
   - *in situ* measurements of R_H fluxes over a summer period from an arctic Russian tundra site using a root-trenching approach
2) to quantify the spatio-temporal variability of the individual processes of the CO_2 and CH_4 fluxes by

- calibrating flux models of GPP, R_{eco} and R_H as well as CH_4 fluxes with the measured chamber fluxes over a period of three months during the arctic growing season
- identifying dominant processes and the environmental controls governing these fluxes

The following main hypotheses were tested:

H1) The different microsites in the polygonal tundra act as sinks for atmospheric C over the measurement period

H2) The CO_2 fluxes differ between the microsites mainly due to contrasting hydrological conditions

H3) The contribution of R_H to R_{eco} during the growing season is less than 50%

H4) The contribution of R_H to R_{eco} show a distinct seasonality and increases by the end of the growing season

H5) The soil temperature is the environmental parameter with the highest explanatory power of the CH_4 fluxes

H6) Due to dry soil conditions, the polygonal rim represents a sink for CH_4

H7) On the ecosystem scale, the polygonal rims display a stronger net sink for atmospheric CO_2 than the polygonal centers

2. State of the Art

2.1. Permafrost

Permafrost is defined as soil, sediment or rock which remain below 0 °C for at least two consecutive years (van Everdingen, 2005). Almost one quarter of the total land surface of the northern hemisphere is underlain by permafrost, which are about 23 million km^2 (Zhang *et al.*, 2008) (Figure 1). Based on the spatial distribution, the permafrost can be separated into continuous, discontinuous, sporadic and isolated permafrost. The permafrost depths in the continuous zone are typically ranging between 350 and 650 meters, but can reach depths of more than 1000 meters, while permafrost depths in the discontinuous zone have a much lower thickness (Schuur *et al.*, 2008). The uppermost layer of permafrost-affected soils, the so-called active layer, thaws during the short summer period when temperatures at the surface are above 0 °C. The active layer is the layer of biological activity and hence crucial for C-cycling. The active layer depth (ALD) is important for hydrological processes, vegetation composition, quantity of SOM and all microbial degradation processes. Active layer thickness ranges from several meters in the discontinuous permafrost zone, to meters or just a few tens of centimeters in the continuous permafrost zone (Schuur *et al.*, 2008).

Figure 1: Permafrost distribution in the Arctic. Based on the spatial distribution, the permafrost can be partitioned into isolated, sporadic, discontinuous and continuous (marked by purple colors). The study area is located in the Lena River Delta (black circle). Map by Philippe Rekacewicz and UNEP/GRID-Arendal (1998), data from International Permafrost Association, 1998.

2.2. Permafrost-carbon feedback

Temperatures in northern high-latitude regions have risen twice as fast as the global average with 0.6 °C per decade over the last 30 years (IPCC, 2013). This increase can lead to a positive feedback between the release of C, stored in permafrost-affected soils and the temperature changes, and this feedback is expected to accelerate (Koven *et al.*, 2011, Schneider von Deimling *et al.*, 2012) (Figure 2).

The arctic permafrost regions are of major interest within the context of global climate change because permafrost-affected soils store huge amounts of C (Hugelius *et al.*, 2014, McGuire *et al.*, 2009, Tarnocai *et al.*, 2009). The SOC content of permafrost-affected soils is often distinctly higher than the SOC content of soils of temperate climatic zones as the decomposition of soil organic matter is inhibited due to a short growing season, low temperatures and often saturated soil water regimes as well as permanent freezing of SOC in permafrost (Hugelius *et al.*, 2014, Ping *et al.*, 1998, Zubrzycki *et al.*, 2013). As a result, permafrost-affected soils acted over thousands of years as substantial sinks for atmospheric C. With rising temperatures and thawing permafrost, the formerly frozen carbon will be mobilized, resulting in an enhanced degradation of SOM (Grosse *et al.*, 2011, Kuhry *et al.*, 2010), which will cause an enhanced production of CO_2 (Knoblauch *et al.*, 2013, Schuur *et al.*, 2009). Further consequences of thawing permafrost are, among others, increased coastal erosion and subsided thermokarst pits (Jones *et al.*, 2013, Jorgenson & Grosse, 2016).

About one quarter of the permafrost land surface is covered by tundra ecosystems (CAVM-Team, 2003). These highly heterogeneous, treeless ecosystems, whose vegetation consists primarily of grasses, sedges, herbs, shrubs, lichens and mosses, which are adapted to the extreme environmental conditions, but react sensitive to a changing climate (Kutzbach, 2006). For instance, higher temperatures will lengthen the growing season (Johnson *et al.*, 2000), growth forms of different plant species become taller and larger (Hudson *et al.*, 2011) and the expansion of trees and shrubs changes the plant-species composition of permafrost landscapes (Pearson *et al.*, 2013, Tape *et al.*, 2006). This will lead to positive feedback mechanisms on regional warming and permafrost thaw due to changes of the albedo dynamics of arctic tundra landscapes (Loranty *et al.*, 2011) and increasing evapotranspiration (Swann *et al.*, 2010), but can also cause lower ALD due to shrub expansion and therefore negative feedback mechanisms and higher CO_2 uptake (Blok *et al.*, 2010). Furthermore, higher temperatures and permafrost thaw will also have impacts on microbial mineralization rates and nutrient availability in permafrost-affected soils (Beermann *et al.*, 2015, Salmon *et al.*, 2016, Schaeffer *et al.*, 2013), which could increase the primary productivity and cause another negative feedback on regional warming (Natali *et al.*, 2012, Walker *et al.*, 2006).

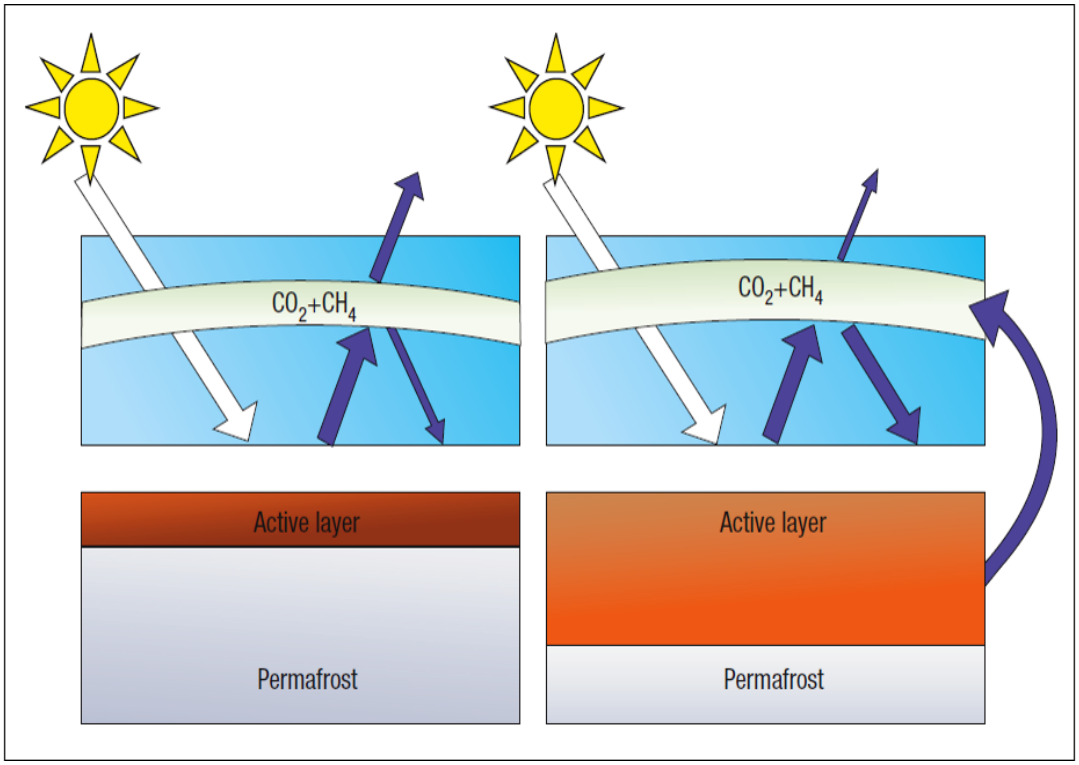

Figure 2: Simplified interactions between the climate system and the carbon cycle in the Arctic. The upper layer of permafrost will thaw due to global warming which will increase the active layer thickness. This will result in the release of previously frozen carbon as CO_2 or CH_4. This additional release of these greenhouse gases could create a positive feedback to global warming, as it will enhance the radiative forcing of the climate system (figure from Beer (2008)).

Although warming of arctic soils will enhance both the CO_2 uptake via GPP as well as CO_2 release by R_{eco} (Mauritz *et al.*, 2017) a further warming is suggested to decrease net CO_2 uptake (Parmentier *et al.*, 2011), which is in good agreement with other studies (Schuur *et al.*, 2013, Schuur *et al.*, 2009). On the other hand, most recently it was suggested that on a short-term scale (decades) arctic wetlands will give a positive feedback to climate warming due to increasing CO_2 emissions, while this feedback could turn negative on a long-term scale (centuries) due to enhanced net C deposition (Wilson *et al.*, 2017). However, due to additional thawed permafrost, the decomposition of formerly frozen soil organic matter could contribute substantially to future CO_2 release fluxes from permafrost-affected soils (Walz *et al.*, 2017).

To estimate the effects of changing climate conditions on permafrost regions it is essential to investigate the recent carbon dynamics on the soil-atmosphere interface. Therefore, measurements of CO_2 and CH_4 fluxes are needed to improve estimates of the future sink and source function of these greenhouse gases from arctic tundra regions.

2.3. CO_2 - fluxes and processes in arctic permafrost landscapes

2.3.1. Uptake and release processes

To obtain a better understanding of the effect of further rising temperatures due to changing climate conditions on CO_2 fluxes from arctic permafrost regions, it is essential to gain a quantitative understanding of the processes underlying the CO_2 NEE, namely photosynthesis, autotrophic and heterotrophic respiration on spatial and temporal scales (Table 1). The NEE of CO_2 between the land surface and the atmosphere is composed of (1) the CO_2 uptake by plants due to photosynthesis, where atmospheric CO_2 (inorganic carbon) is converted into organic carbon (carbohydrates) and incorporated into plant biomass, described by GPP and (2) the release of CO_2 from soils and plants, described by R_{eco} (Chapin *et al.*, 2006). Contributors to R_{eco} are autotrophic respiration by plants and roots (R_A), which includes the usage of carbohydrates for plant growth and maintenance, and R_H, where litter and SOM are decomposed by soil microorganisms and used as energy supply (Luo & Zhou, 2006). In terrestrial ecosystems, sinks and sources of inorganic C are generally neglected because of their minor contribution to NEE (Elsgaard *et al.*, 2012, Kuzyakov, 2006). Therefore, to partition NEE into the underlying fluxes, the quantification of GPP, R_{eco}, R_A and R_H fluxes are required (Figure 3).

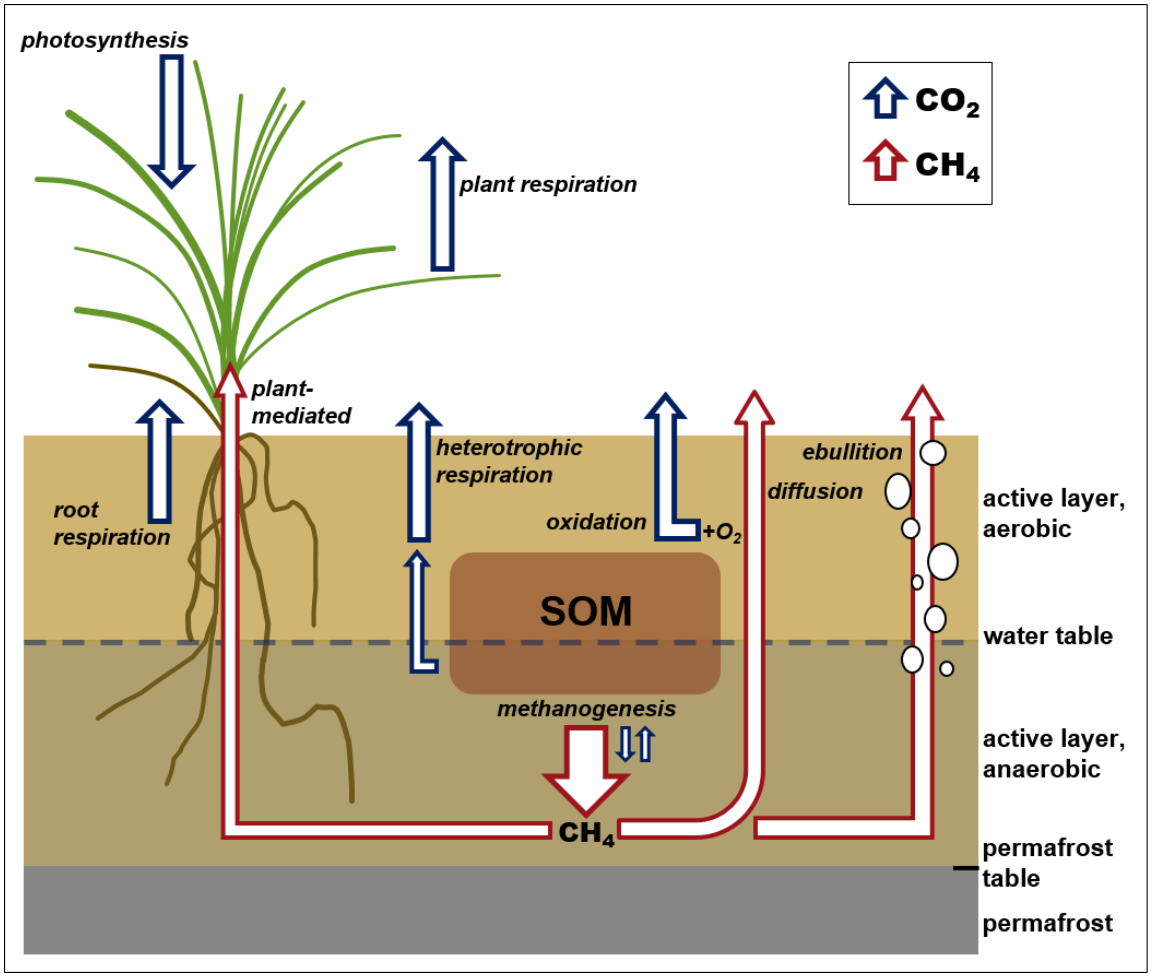

Figure 3: CO_2 and CH_4 processes in permafrost-affected soils. The most important CO_2 uptake process is photosynthesis. CO_2 release processes are plant and root respiration, together autotrophic respiration (R_A), and methane oxidation as well as the decomposition of soil organic matter, called heterotrophic respiration (R_H). CH_4 is produced in the anaerobic active layer and released by molecular diffusion, by ebullition in form of gas bubbles and through the aerenchyma of vascular plants, namely plant-mediated transport. In the aerobic active layer, CH_4 is oxidized to CO_2 by methanotrophs.

As sunlight represents the energy source of the CO_2 uptake by vegetation from the atmosphere, one of the dominant controls of GPP is the photosynthetically active radiation (PAR; Schlesinger, 2013). Beside PAR, the amount of C fixed by plants due to photosynthesis depends on temperature, plant species, water availability, air humidity, the green plant biomass and the atmospheric CO_2 concentration (Schlesinger, 2013). The temperature is also an important factor controlling ecosystem respiration fluxes because it affects almost all aspects of respiration processes (Luo & Zhou, 2006). The quality and quantity of the substrate exerts another strong influence on R_{eco} (Högberg *et al.*, 2001, Schlesinger, 2013) and soil moisture is suggested to have also a large impact on R_{eco} fluxes (Xu *et al.*, 2004). Additional factors controlling these fluxes are oxygen concentration,

nitrogen availability (carbon to nitrogen ratio (C/N)), soil texture and pH values as well as the composition of the heterotrophic community (Luo & Zhou, 2006, Schlesinger, 2013).

Table 1: Summary of ecosystem CO_2 fluxes. The CO_2 net ecosystem exchange (NEE) can be divided into gross primary productivity (GPP) and total ecosystem respiration (R_{eco}). R_{eco} can be divided into autotrophic (R_A) and heterotrophic respiration (R_H). The net primary productivity (NPP) is the sum of GPP and R_A.

Concept	Abbreviation	Definition
Gross Primary Productivity	GPP	CO_2 uptake by plants during photosynthesis
Autotrophic Respiration	R_A	Respiratory loss of CO_2 by plants and roots
Heterotrophic Respiration	R_H	Respiratory loss of CO_2 by soil microbial microorganisms
Ecosystem Respiration	R_{eco}	$R_A + R_H$
Net Ecosystem Exchange	NEE	GPP – R_{eco}
Net Primary Productivity	NPP	GPP – R_A

2.3.2. Partitioning ecosystem respiration

The release of CO_2 from soils by R_{eco} is the largest efflux of C from terrestrial ecosystems to the atmosphere (Biasi *et al.*, 2014). Therefore, changes in respiration rates can have large effects on atmospheric CO_2 concentration. R_A can be separated into aboveground plant respiration and belowground root respiration as well as in respiration of root-derived, recent components. Due to the decomposition of SOM by heterotrophic soil organisms, R_H is also called soil microbial respiration (SMR). It is challenging to separate belowground respiration fluxes into autotrophic and heterotrophic components because roots and microorganisms are closely linked within the soil (Hanson *et al.*, 2000). There is a wide spectrum of methods to partition ecosystem respiration (Kuzyakov, 2006, Subke *et al.*, 2006) and each of these approaches has its advantages and disadvantages. For different ecosystems not every approach is feasible. In ecosystems with a high root density and sparsely decomposed dead roots, like most arctic tundra ecosystems, partitioning methods based on the separation of roots are difficult to realize. Isotope labelling techniques based on ^{13}C are principally achievable in arctic tundra landscapes (Dorrepaal *et al.*, 2009). However, because isotopic label is spread after first usage into the whole soil, it is only useful for single estimates as considerable subsequent corrections are needed for investigations on the temporal scale (Hanson *et al.*, 2000). ^{14}C partitioning methods have been successfully applied in arctic ecosystems (Biasi *et al.*, 2014, Hicks Pries

et al., 2013, Schuur *et al.*, 2009), but its usage on a seasonal scale to partition R_{eco} with a high temporal resolution is very expensive and technically challenging.

A commonly applied method to partition belowground respiration fluxes *in situ* is root-trenching, where roots are physically isolated by digging a trench and the active plant biomass is removed (Bond-Lamberty *et al.*, 2011, Subke *et al.*, 2006). Despite some disturbance on the plant-soil interface, root-trenching can give accurate estimates of the rates of R_A and R_H (Diaz-Pines *et al.*, 2010). Nevertheless, there are some drawbacks related to the root-trenching technique as it is associated with disturbances of the soil-root continuum (Figure 4). One of the main drawbacks is the additional decomposition of residual roots, which leads to an overestimation of R_H if measurements are conducted shortly after trenching (Bond-Lamberty *et al.*, 2011, Diaz-Pines *et al.*, 2010, Subke *et al.*, 2006). It is therefore preferable, that the removal of living plant biomass is conducted at least several months before the measurements are started as after this time it can be assumed that decomposition of residual roots contributes little to R_H (Shurpali *et al.*, 2008). However, the impact of other drawbacks can increase over time. The missing input of photosynthates and litter into the soil as well as turnover from roots can lead to a significant underestimation of R_H (Epron *et al.*, 2006). Furthermore, root-trenching can also have an impact on abiotic factors. For instance, Edwards and Ross-Todd (1983) have shown that root-trenching is associated with changes in soil temperatures as well as its diurnal variability. Also changes in soil moisture are ascertained to occur on trenched plots (Epron *et al.*, 2006) which could lead to an overestimation of R_H. Subke *et al.* (2006) mentioned that the underestimation because of the lack of litter turnover and the overestimation because of soil moisture differences could cancel each other out in particular cases. On the other hand, it is assumed that hydrological conditions are re-established within days as well as soil temperature conditions are returning within weeks after root-trenching to those before the treatment (Bond-Lamberty *et al.*, 2011, Kuzyakov, 2006). Despite the known drawbacks, it was shown that root-trenching produced similar results compared to a ^{14}C partitioning approach in an arctic tundra ecosystem (Biasi *et al.*, 2014).

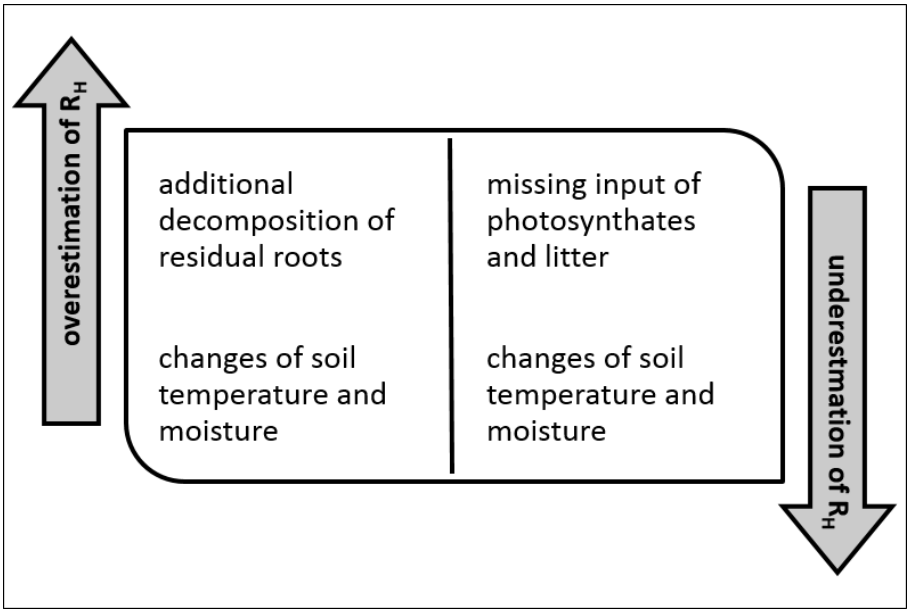

Figure 4: Summary of disturbances accompanied by root-trenching. The disturbances can lead either to an overestimation (left) or to an underestimation (right) of the natural R_H fluxes. The impact of these disturbances is both variable across different land cover classes and on temporal scale.

To date there are just a few estimates on the contribution of R_H to R_{eco} from tundra ecosystems during the growing season (Biasi *et al.*, 2014, Nobrega & Grogan, 2008), and data are lacking so far for polygonal tundra ecosystems. This is critical as warming of the Arctic will influence R_{eco} fluxes direct and indirect: Warming will increase decomposition of soil organic matter (R_H) and ensures a deeper thawing of permafrost, which will expose previously frozen SOM to decomposition (Dorrepaal *et al.*, 2009, Schuur *et al.*, 2011). This could cause a substantial reduction of the carbon sink function of arctic tundra ecosystems as gross ecosystem productivity is less temperature sensitive than ecosystem respiration in these ecosystems (Dorrepaal *et al.*, 2009, Grogan & Chapin, 2000). Furthermore, warming could decrease microbial biomass C and soil moisture (Frey *et al.*, 2008, Suseela *et al.*, 2012) as well as increase R_A due to increasing aboveground biomass, which can lead to a lower contribution of R_H to R_{eco} (Chen *et al.*, 2016, Hicks Pries *et al.*, 2015). The increase of R_A and R_H fluxes due to warming might be compensated by higher net primary production (Hicks Pries *et al.*, 2013), but whether this is valid for the complete growing season and across highly heterogeneous arctic ecosystems remains uncertain.

2.3.3. Fluxes in arctic permafrost regions

To date, a set of studies focused on C balances of the arctic tundra to consider if these ecosystems act as sink or source for atmospheric CO_2 (e.g. Kutzbach *et al.*, 2007b, Marushchak *et al.*, 2013, Oechel *et al.*, 2000). McGuire *et al.* (2012) suggested that arctic tundra regions act recently as a sink for atmospheric CO_2 on an annual basis with a total CO_2 uptake of 110 Teragram (Tg) C yr^{-1}. On the other hand, Belshe *et al.* (2013) found that these ecosystems act as source for atmospheric CO_2 (462 Tg C yr^{-1}). But due to limited data from Russian arctic tundra ecosystems this estimate is spatially biased. Even if this ambivalence can partly be explained by differences in the included vegetation types and a lack of data from Russian tundra within the calculation of Belshe *et al.* (2013), it clearly shows the need of intensified CO_2 and CH_4 flux observations in northern high-latitude ecosystems. Therefore, a better understanding of recent C dynamics in permafrost-affected soils is needed to improve estimates of future C balances of arctic tundra regions. Several studies determined NEE and R_{eco} fluxes on the microsite scale in permafrost landscapes in Alaska, Canada and Greenland (e.g. Natali *et al.*, 2011, Nobrega & Grogan, 2008, Oechel *et al.*, 2000, Olivas *et al.*, 2011, Ström *et al.*, 2012, Trucco *et al.*, 2012), but only a few studies are available from Russian tundra ecosystems (Heikkinen *et al.*, 2004, Kwon *et al.*, 2016, Zamolodchikov *et al.*, 2000). These ecosystems clearly need more attention considering their vast extent of 3 million km^2 (CAVM-Team, 2003), which is more than half of northern high-latitude tundra ecosystems, and their pronounced heterogeneity. Otherwise, estimates of the recent carbon balance of the arctic tundra and its future reaction on changing climate conditions are biased.

2.4. CH_4 - fluxes and processes in arctic permafrost landscapes

2.4.1. CH_4 production, oxidation and transport mechanisms

In water-saturated arctic tundra soils, CH_4 is produced as the end product of anaerobic mineralization of SOM by archaeal methanogens. Hereby, different microorganisms are converting SOM stepwise to acetate or hydrogen (H_2) and CO_2, the main reactants responsible for CH_4 production (Lai, 2009, Olefeldt *et al.*, 2013). Within this “food-web” hydrolytic and fermenting bacteria are decomposing complex organic polymers to

alcohols, fatty acids as well as CO_2 and H_2 (Whalen, 2005). CH_4 is then produced by methanogens via two main reactions (Whalen, 2005): Hydrogenotrophic methanogens are reducing CO_2 with H_2 as electron donor:

$$4H_2 + CO_2 \rightarrow CH_4 + 2H_2O \quad (1)$$

while acetotrophic methanogens produce CH_4 and CO_2 by usage of acetate as substrate:

$$CH_3COOH \rightarrow CH_4 + CO_2 \quad (2)$$

In northern organic soils (SOC content > 20%), Lee *et al.* (2012) found the hydrogenotrophic methanogenesis to be dominant, while the acetotrophic methanogenesis dominanted in mineral soils. However, Vaughn *et al.* (2016) reported an opposing finding in polygonal tundra soils.

After production, the CH_4 is released from the soil to the atmosphere via three main pathways, namely (1) molecular diffusion, (2) plant-mediated transport and (3) ebullition (Chanton, 2005) (Figure 3).

1.) Due to the production of CH_4 in the anaerobic soil layers, there is typically a CH_4 concentration gradient and molecules are moving from higher to lower concentration following Fick's first law (Lai, 2009). Compared to the other transport mechanisms, the molecular diffusion is rather slow, but it is important as it facilitates the contact of methanotrophic bacteria with CH_4, controlling the rate of microbial CH_4 consumption (Lai, 2009, Whalen, 2005).
2.) A major pathway for CH_4 transport is provided through the aerenchyma of some vascular plants, whereby the aerobic soil layer is bypassed (Kutzbach *et al.*, 2004). This internal gas-space ventilation system provides aeration under anaerobic soil conditions and transports oxygen into the rhizosphere, while in the opposite direction CH_4 is transported to the atmosphere (Joabsson *et al.*, 1999). At completely submerged arctic tundra sites, the plant-mediated transport can account for 70 to 90% of the total CH_4 emissions from the soil to the atmosphere (Knoblauch *et al.*, 2015).
3.) Another pathway in water-saturated soils is the sudden release of CH_4 from the soil by ebullition, which can contribute substantially to total CH_4 fluxes (Tokida *et*

al., 2007). These gas bubbles are formed when the partial pressure of all dissolved gases in solution exceeds the hydrostatic pressure in the soil (Lai, 2009).

In the aerobic soil layers, parts of the produced CH_4 is consumed as energy source for growth and maintenance by methanotrophs (Hanson & Hanson, 1996). Hereby, CH_4 is sequentially oxidized to methanol, formaldehyde, formate and eventually CO_2 (Whalen, 2005):

$$CH_4 \rightarrow CH_3OH \rightarrow HCHO \rightarrow HCOOH \rightarrow CO_2 \quad (3)$$

In peatlands, the highest methanotrophic activity is located at the aerobic-anaerobic interface close to the water table as these interface provides the optimal ratio of the substrates, oxygen and CH_4 (Dedysh, 2002, Knoblauch *et al.*, 2015, Lai, 2009, Preuss *et al.*, 2013).

2.4.2. Environmental controls on CH_4 fluxes

CH_4 emissions from arctic wetlands are a product of the balance between methanogenesis and oxidation, which is substantially influenced by the presence of oxygen, one of the most important factors controlling CH_4 emissions (Whalen, 2005). If anaerobic conditions exist, the substrate supply is the limiting factor of methanogenesis (Ström *et al.*, 2012, Yavitt & Lang, 1990). Similar to CO_2 respiration fluxes, the (soil) temperature is one of the main factors controlling both methanogenesis as well as methane oxidation (Knoblauch *et al.*, 2008, Lai, 2009). Vegetation composition can influence CH_4 oxidation rates as there is evidence for symbiotic-like relations of methanotrophs with moss species (Liebner *et al.*, 2011). Wagner *et al.* (1999) found soil texture to be an important parameter influencing CH_4 production. Also, the soil and porewater pH has an impact on CH_4 production and oxidation mechanisms, but the limiting and the optimal pH values are varying with different ecosystems (Whalen, 2005). Furthermore, CH_4 emissions are heavily affected by fluctuations of the water table depth, which can be explained with changes of the thicknesses of potential CH_4 production and oxidation zones (Lai, 2009).

The water table depth is one of the main predictors of CH_4 emissions as it affects significantly the production and oxidation rates (Marushchak *et al.*, 2016, McEwing *et al.*, 2015) and is mostly negatively correlated with the CH_4 fluxes (Lai, 2009). Another

important predictor is the vegetation composition (Davidson *et al.*, 2016); especially the presence of sedges can have large impacts on the rate of CH_4 emissions as they promote plant-mediated transport (King *et al.*, 1998, Knoblauch *et al.*, 2015, Kutzbach *et al.*, 2004, Olefeldt *et al.*, 2013). CH_4 emissions data from Eddy covariance (EC) measurements showed near-surface turbulence to be one of the main drivers of CH_4 emissions (Sachs *et al.*, 2008, Wille *et al.*, 2008). If the ALD and permafrost degradation can serve as parameter influencing CH_4 emissions is highly uncertain (Olefeldt *et al.*, 2013, Prater *et al.*, 2007, van Huissteden *et al.*, 2005). Various studies have identified the temperature as one of the main controls of CH_4 emissions (e.g. Mastepanov *et al.*, 2013, Sachs *et al.*, 2010, Schneider *et al.*, 2016, Wille *et al.*, 2008). This relationship is based on the temperature dependence of microbial activity (Conrad, 1996, Wagner *et al.*, 2007).

2.4.3. CH_4 flux estimates from arctic permafrost landscapes

Due to often water-saturated and anaerobic conditions, the arctic tundra displays a significant source of atmospheric CH_4 with about 19 Teragram (Tg) C yr^{-1}, ranging from 9 to 35 Tg C yr^{-1} (McGuire *et al.*, 2012). Considering worldwide CH_4 emissions from wetlands between 133 and 213 Tg C yr^{-1} (Ciais *et al.*, 2013) and total global emissions of 550 Tg C yr^{-1} (Dlugokencky *et al.*, 2011), arctic tundra regions are a substantial source of atmospheric CH_4. Therefore, changes in the CH_4 source strength of arctic tundra regions in the future can have large impacts on the global greenhouse gas budgets. For instance, rainfall is predicted to increase in high-latitudes (Christensen *et al.*, 2013), and as a result of that CH_4 emissions could increase as anaerobic soil conditions are expected to expand with higher precipitation rates (Sachs *et al.*, 2010). Furthermore, thaw-induced subsidence is predicted to increase CH_4 emissions (Johnston *et al.*, 2014, Olefeldt *et al.*, 2013). On the other hand, permafrost thaw causes morphological changes of arctic landscapes, resulting in increased drainage (Godin *et al.*, 2014) and arctic warming causes more evaporation which leads to less summer inundation (Koven *et al.*, 2011). Both processes can cause a reduction of the CH_4 source strength from arctic tundra regions. Furthermore, non-saturated soils in high-latitudes can also act as substantial sinks for atmospheric methane (Jørgensen *et al.*, 2015, Zhu *et al.*, 2014) and also water-saturated sites can act as sinks when exposed to high radiation (Liebner *et al.*, 2011). The CH_4 sink

strength of non-saturated soils is suggested to increase in future simultaneously to warmer soil conditions (Jørgensen *et al.*, 2015).

The annual CH_4 fluxes in high-latitudes are suggested to be dominated by fluxes during the short growing season (e.g. Whalen & Reeburgh, 1992, Wille *et al.*, 2008), but recently, the emissions from the cold season (September to May) are found to contribute significantly to annual CH_4 budgets (Zona *et al.*, 2016). Nevertheless, a detailed understanding on the environmental controls and sensitivities of growing season CH_4 emissions is needed to assess the impact of future changing climate conditions on CH_4 fluxes.

2.5. Chamber measurement technique

Closed chamber methods are widely used to quantify emissions of trace gases (Livingston *et al.*, 2005) as they allow a good spatial coverage. They are low in cost, simple to use and can be applied in remote, low-stature canopies like arctic tundra regions (Kutzbach *et al.*, 2007a). However, the use of closed chambers is related to a set of potential errors, including (1) the disturbance of soils during collar installation, (2) the disturbance of pressure gradients during chamber deployment, (3) changes of turbulence strength, (4) inaccuracies in the calculation of headspace volume and leakage closure as well as (5) the alteration of the natural gas concentration gradient inside the chamber headspace (Davidson *et al.*, 2002, Hutchinson & Livingston, 2001, Kutzbach *et al.*, 2007a, Lai *et al.*, 2012, Redeker *et al.*, 2015). All of these potential errors can lead to a serious bias of the measured fluxes and the latter leads to non-linear concentration-over-time curves of chamber headspace air (Kutzbach *et al.*, 2007a, Pedersen *et al.*, 2010). A non-linear flux evaluation can also have methodological reasons. For instance, if the chamber is not equipped with large openings on top, air is pressed into the soil during chamber deployment on the soil, which can lead to initial pressure shocks (Christiansen *et al.*, 2011, Schneider *et al.*, 2011). These initial pressure shocks can cause a sudden release of gases from the soil, which is perturbing the concentration-over-time curve of a chamber measurement and lead to substantial overestimation of the fluxes. However, Görres *et al.* (2014) found out that the flux calculation with a linear regression model is more appropriate to describe CO_2 fluxes even if the concentration-over-time curves are

non-linear. Furthermore, chambers have to be equipped with a fan to allow continuous headspace mixing, and should be in an adequate size as both can lead flux underestimation (Christiansen *et al.*, 2011, Hutchinson & Livingston, 2001, Pihlatie *et al.*, 2013). However, the use of fans to mix chamber headspace air is part of current discussion (Redeker *et al.*, 2015). Some studies showed that realistic flux estimates of trace gas emissions can be achieved only in chambers where the air was mixed by a fan (Christiansen *et al.*, 2011, Denmead, 2008), but some authors suggested that chambers that are equipped with fans give unreliable readings (Davidson *et al.*, 2002). Another important factor to keep potential errors to a minimum is the exclusion of the data from the very beginning of the chamber measurement to allow steady headspace mixing and prevent that disturbances caused by chamber deployment are included into the flux calculation (Christiansen *et al.*, 2011, Koskinen *et al.*, 2014). This exclusion is also important for measuring R_{eco} as CO_2 uptake can continue for a short time period after PAR is blocked in dark chambers (Laisk *et al.*, 1984).

If all these potential errors are kept to a minimum, the use of closed chambers is appropriate for the observation of the spatial and temporal variability of CO_2 and CH_4 fluxes. Arctic polygonal tundra landscapes are on the microscale (1 m to 10 m) highly heterogeneous landscapes (French, 1996). Therefore, measurements on this microscale are necessary as solely they can give insights into the processes controlling the CO_2 and CH_4 fluxes and the future reactions of these fluxes on changing climate conditions. Chamber measurements can provide reliable estimates of gas fluxes from this microscale. These estimates can further be used to reproduce the gas fluxes over complete seasons by developing flux models based on the measured fluxes. The models provide crucial information on the dependence of the gas fluxes from environmental parameters and they can give reliable estimates of cumulative fluxes. Therefore, they can be used for the quantitative contribution of single fluxes and microsites to the arctic C cycle.

3. Study area

3.1. Lena River Delta

The Siberian Lena River Delta (72.0 – 73.8°N, 122.0 – 129.5°E) is the third-largest river delta worldwide and the largest delta in the Arctic and covers a surface area of 29,000 km^2 (Schneider *et al.*, 2009) (Figure 6). This fan-shaped delta is characterized by a network of rivers and channels with more than 1,500 islands of different sizes. The Lena River Delta can be geomorphologically divided, into three main river terraces of different ages and the flood-plain levels (Grigoriev, 1993 in Schwamborn *et al.*, 2002). The first terrace includes active flood-plains, large thermokarst lakes and ice-wedge polygonal tundra. This youngest terrace, formed in the Middle Holocene, occupies about two-third of the total delta area, primary occurring in the central and eastern parts of the delta (Bolshiyanov *et al.*, 2015, Schwamborn *et al.*, 2002). The second terrace occurs in the northwestern part of the delta and is characterized by sandy sediments with a low ice content; it was formed between the Late Pleistocene and the Early Holocene and covers about 23% of the delta (Schneider *et al.*, 2009). The oldest terrace consists of fine-grained, organic- and ice-rich sediments and is an erosional remnant of a Late Pleistocene plain, characterized by polygonal ground and thermokarst processes (Boike *et al.*, 2013).

The delta is located in the continuous permafrost zone with permafrost depths of about 500 to 600 m (Grigoriev, 1960) and relatively low temperatures of -7.8 °C at 1.7 m soil depth (Boike *et al.*, 2013). A mean annual permafrost temperature of -8.6 °C at 10.7 m depth demonstrates that the Lena River Delta is one of the coldest permafrost regions on the earth (Romanovsky *et al.*, 2010).

The climate in the Lena River Delta is arctic-continental and characterized by both low temperatures and precipitation (Boike *et al.*, 2008). Despite comparatively low precipitation, the climate of the delta has to be considered as humid because of low evaporation rates due to low temperatures (Kutzbach, 2006). At the weather station in Tiksi (about 120 km southeast of the study site in the delta), the mean annual air temperature over a 30-year period (1981-2010) was -12.8 °C and the mean annual precipitation 321 mm (Figure 5). The mean temperatures of the warmest (August: 7.8 °C)

and the coldest month (January: -30.2 °C) highlight the extreme climatic contrast between the seasons, typical for continental polar regions. The summer growing season, defined in this study as the period with consecutive positive daily average air temperatures, usually lasts about three months, from mid-June until mid-September. The mean summer precipitation at the study site during the period 1998-2011 was 125 mm, ranging from 52 mm to 199 mm (Boike *et al.*, 2013), which is about 40% of the annual precipitation. The central delta region experiences rapidly changing weather conditions during summer by advection of cold and moist or warm and dry air from the Arctic Ocean or continental Siberia, respectively (Runkle *et al.*, 2013). Polar day lasts from 7 May until 8 August and polar night lasts from 15 November to 28 January. River ice break-up and snowmelt starts usually in the first half of June.

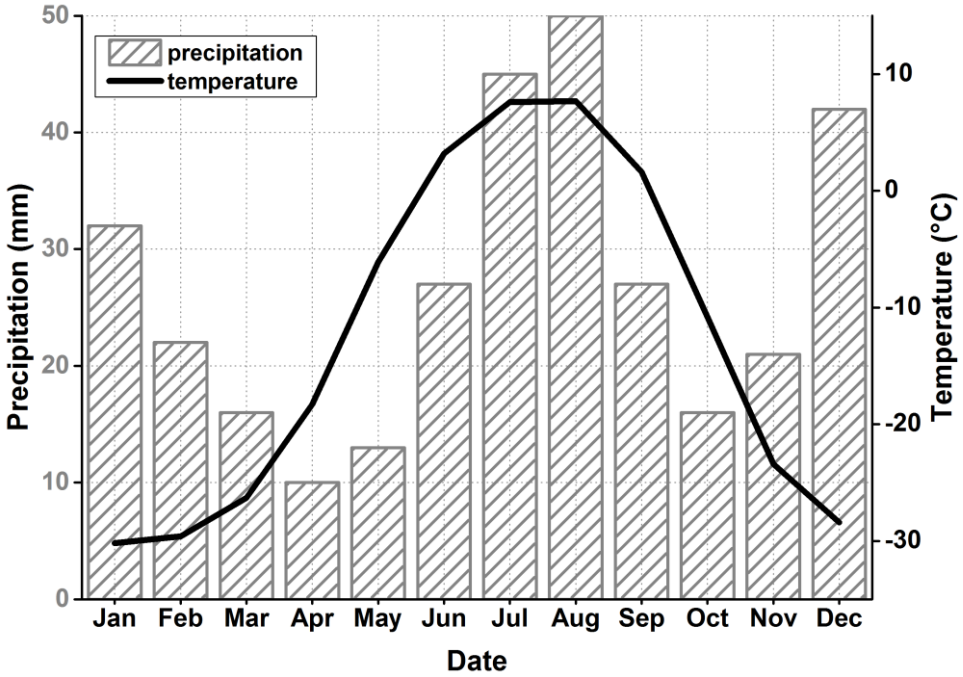

Figure 5: Climate chart of Tiksi over the period 1980-2011. The reference site is located ~120 km southeast of the study site. The precipitation and temperature data are shown as monthly mean values.

3.2. Samoylov Island

The study area is located on Samoylov Island in one of the main river channels, the Olenyokskaya Channel, in the southern central Lena River Delta (72°22'N, 126°28'E; Figure 6). During the past two decades, a number of studies with focus on geomorphology, microbiology, soil science as well as gas and energy exchange were

conducted on Samoylov Island (e.g. Boike *et al.*, 2008, Kutzbach *et al.*, 2007b, Muster *et al.*, 2012, Sachs *et al.*, 2010, Schwamborn *et al.*, 2002). Samoylov Island covers an area of around 5 km^2. The island can be geomorphologically divided in two parts: In the western part of the island is an active flood-plain (2 km^2) with elevations from 1 to 5 m above sea level (a.s.l) which is occasionally flooded during river break-up. The study site is located in the eastern part of the island in the wet ice-wedge polygonal tundra on a Late Holocene river terrace (3 km^2) with elevations from 10 to 16 m a.s.l. This River terrace is only partly flooded during extreme flooding events.

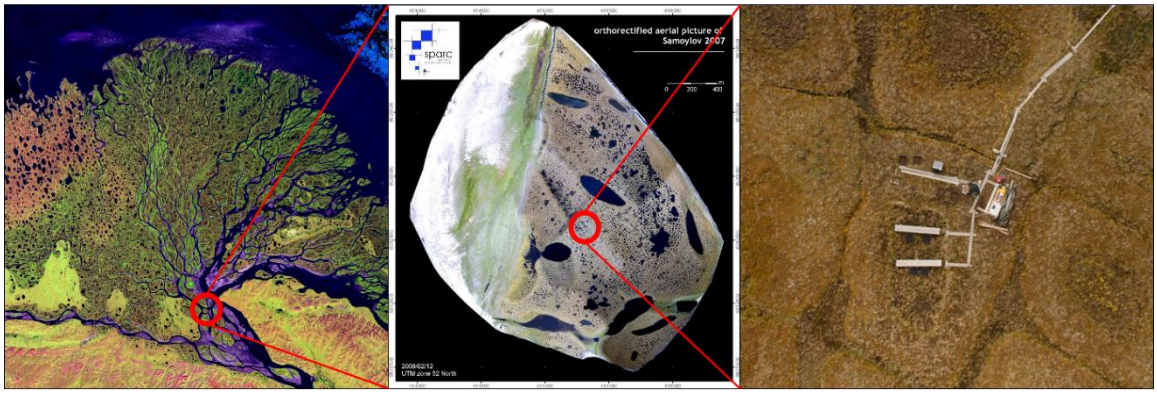

Figure 6: The study site on Samoylov Island, Lena River Delta in Northeastern Siberia (72°22'N, 126°28'E). (Images: Lena River delta - left: NASA Landsat program: Lena River Delta in Landsat 7; available at: http://earthobservatory.nasa.gov/IOTD/view.php?id=2704, 2002; Samoylov Island - middle: Boike *et al.* (2012); Study site - right: Boike *et al.* (2015))

Wet polygonal tundra landscapes are typical for the Late Holocene River Terrace in the Lena River Delta (Figure 7). Polygonal structures are developing due to thermal contraction in the winter season, which leads to cracks of the surface followed by ice-wedge growth when melting water freezes in these cracks. This process produces a honeycomb-like surface structure with high- and low-centered polygons as well as polygonal ponds. In low-center polygons (hereinafter 'polygonal center') drainage is impeded due to the underlying permafrost and as a result of that, anaerobic accumulation of organic material is feasible (Wagner *et al.*, 2003). In contrast to that, in the soils of the higher situated polygonal rims, which are surrounding the polygonal centers, less SOM is accumulated due to oxic conditions in the upper soil part. The elevation differences between wet polygonal centers and comparatively dry polygonal rims is about 0.5 m.

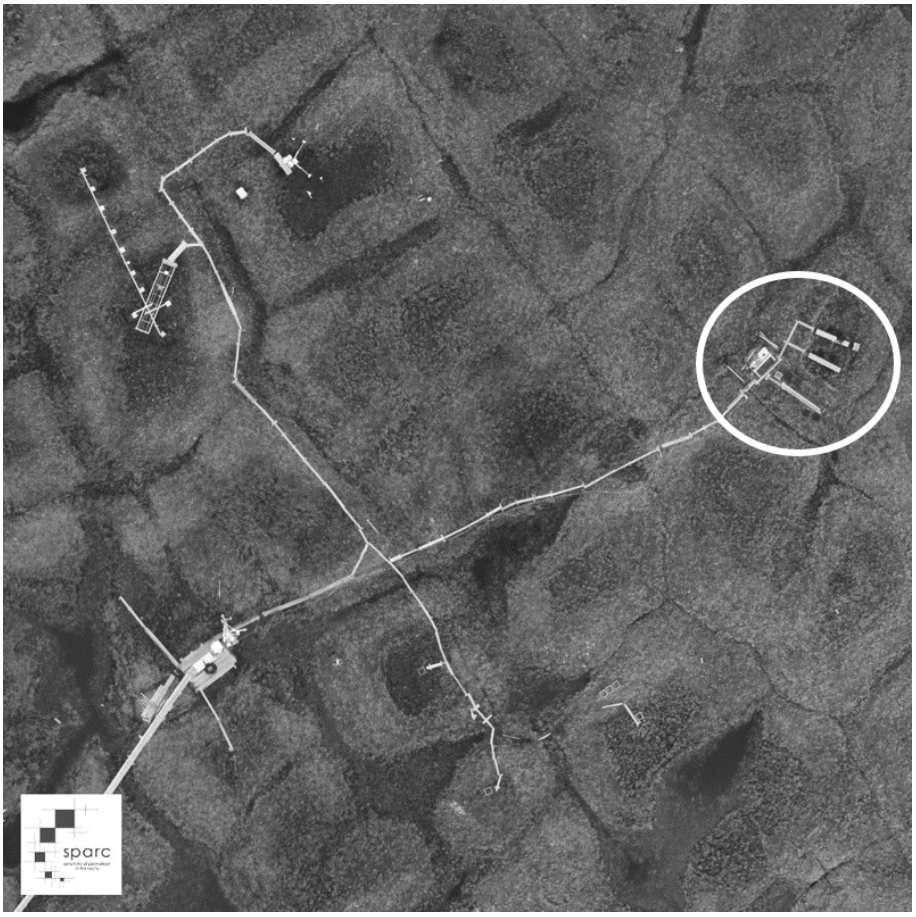

Figure 7: The polygonal tundra on Samoylov Island. Polygons are formed due to thermal contraction in winter that produces cracks where ice-wedges can grow when melting water freezes later inside these cracks. The study site (white circle), the soil measurement station (upper left) and the eddy covariance system (bottom left) are connected with boardwalks to avoid disturbance. Image from Boike *et al.* (2015)

On both parts of the island an eddy covariance (EC) system for measurements of energy, wind and gas fluxes was installed (Kutzbach *et al.*, 2007b, Runkle *et al.*, 2013, Wille *et al.*, 2008). The study site in the current work is located within the footprint area of the EC system on the river terrace. Surface classification of aerial images had shown that polygonal rims (dry tundra) represent about 50% while depressed polygonal centers (wet tundra) represent approximately 40% and open water bodies represent around 10% of the EC footprint area (Muster *et al.*, 2012). With more than 25 kg m^{-2} SOC in the uppermost meter these landscapes contain a significant pool of SOM (Zubrzycki *et al.*, 2013).

In this study, two different microsites were investigated (Figure 8): a wet-depressed polygonal center and its surrounding elevated polygonal rim (72°22,442 N; 126°29.828 E). At this polygon, the maximum ALD is deeper at the polygonal center with about 40 cm

compared to the polygonal rim with about 30 cm. Nutrient input into this rather nutrient-limited ecosystem comes from upward migration of fluvial sediments due to cryoturbation at the polygonal rims and maybe from aeolian deposits. According to WRB (2014) the soils at the polygonal center are typically classified as *Histic Cryosols* with water tables close to the soil surface. The polygonal rim soils are characterized by cryoturbation, a rearrangement of soil material due to freeze-thaw processes. Therefore, the soils at the polygonal rim are classified typically as *Turbic Glacic Cryosols* with a water table just a few centimeters above the permafrost table. High contents of SOM (> 10%) are usually occurring in the first 15 cm within the soils of the polygonal rim and are underlain by cryoturbated mineral horizons, while high SOM contents at the polygonal center are common in the entire active layer (40 cm). The vegetation of the polygonal rim is dominated by the moss species *Hylocomium splendens* as well as *Dryas punctata, Astragalus frigidus* and lichens (*Peltigera spp.*), whereas vegetation of the polygonal centers is dominated by the hydrophilic sedge *Carex aquatilis* and mosses (*Drepanocladus revolvens, Meesia triqueta, Scorpidium scorpioides*).

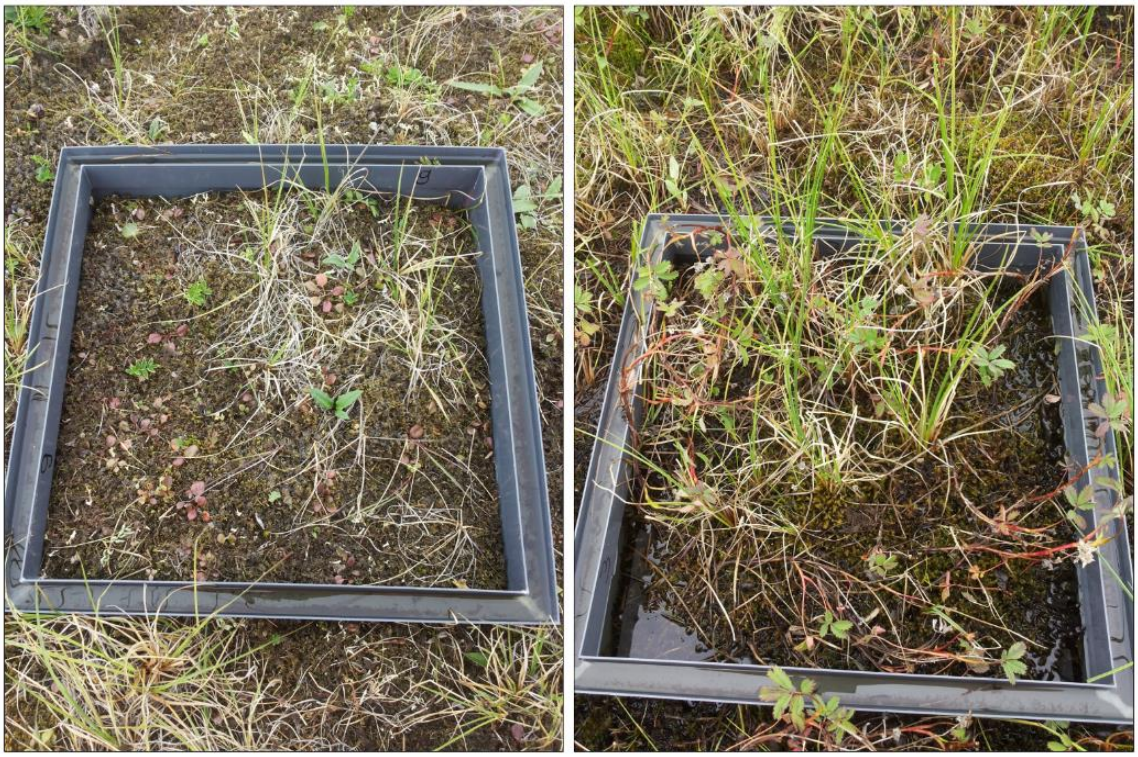

Figure 8: Polygonal rim and center at the study site. The typical vegetation of **polygonal rims** (left) is moss-dominated with small amounts of lichens and various vascular plants, while **polygonal centers** (right) can be considered as sedge-moss-dominated.

4. Methods

4.1. Meteorological data

Meteorological variables were recorded in 30 min intervals at the nearby EC system and an adjacent meteorological station, 40 m southwest from the study site. An ultrasonic anemometer (Solent R3, Gill Instruments Ltd, UK) measured wind velocity components in three dimensions. Further data on relative humidity and air temperature (MP103A, ROTRONIC AG, Switzerland), air pressure (RPT410F, Druck Messtechnik GmbH, Germany) and photosynthetic active radiation (PAR; wavelength: 400 – 700 nanometer; QS2, Delta-T Devices Ltd., UK) as well as the incoming and reflected components of shortwave and longwave radiation, respectively (CNR 1, Kipp and Zonen, Netherlands) were collected. The radiative surface temperature (T_{surf}) was calculated after Kutzbach *et al.* (2007b) using the formula

$$T_{surf} = \left(\frac{L\uparrow_B}{\varepsilon\, 5.67\times10^{-8}}\right)^{1/4} \quad (4)$$

where $L\uparrow_B$ is the upward infrared radiation and the emissivity ε was assumed to be 0.98.

4.2. Soil, vegetation and porewater analysis

Soil analysis was done in July 2014. At the polygonal rim a total of six soil samples were taken using steel rings between the soil surface and the frozen ground with a depth of 12-16 cm and 6 cm in inner diameter. These samples were separated into an organic-rich and a mineral soil layer based on soil texture. Between these soil layers a transition layer was determined, developed due to cryoturbation processes. At the polygonal center one soil sample was taken from the surface to the frozen ground with a spade and separated vertically into three replicates. These samples were separated into horizontal layers after SOM decomposition status. Living plant biomass from the top was removed from all soil samples. For further analysis, the samples were dried at 70 °C and milled. Soil organic carbon contents were measured with a liquiTOC II coupled with a solids module (Elementar Analysesysteme GmbH, Hanau, Germany) and total contents of carbon and nitrogen (N) were measured with an Element analyzer (VarioMAX cube, Elementar Analysesysteme GmbH, Hanau, Germany). These values were used to calculate the C/N

ratio. The weight difference between wet and dried (105 °C) soil samples were used to calculate soil water contents. Soil pH values were measured in a suspension of 5 g soil in 12.5 mL distilled water (CG820, Schott AG, Mainz, Germany).

Furthermore, to compare CO_2 and CH_4 fluxes with vegetation community structure each chamber collar (50 x 50 cm) was divided into 10 x 10 cm subplots. In four of these subplots the plant species were recorded and their abundance (% of the surface cover) was determined. This procedure was conducted at every single measurement plot in mid-July and at the end of August in 2015.

Depth profiles of pH values at the water-saturated polygonal center were analyzed with a field pH meter (340i, WTW, Xylem Inc., Weilheim, Germany). Therefore, porewater was extracted from the center using a steel rod with small openings at the bottom and an attached syringe at the top. At first, the rod and the syringe were flushed with water from the required depth. In a second step, 150-200 mL of porewater were extracted from the soil. Porewater samples were taken in 2015 from 5, 10, 15, 20, 25, 30 and 35 cm soil depth in weekly intervals. Samples from the latter were taken when the active layer was thawed to this depth (first on 26 August). Description of pH values were made following the protocol of Schoeneberger *et al.* (2012).

4.3. Chamber measurements

4.3.1. Light and dark chamber measurements

A total of eight PVC chamber collars (50 x 50 cm), four at each microsite, were permanently installed in July 2014 at the sampling site for CO_2 as well as CH_4 flux measurements (Figure 9). Both microsites were equipped with boardwalks to avoid disturbance. The chamber collars had boreholes with 5 cm in diameter on each of the four sides in 15 cm soil depth to allow lateral water movement and were inserted 20 cm deep into the active layer. The collars were equipped with an U-shaped frame filled with water to avoid gas exchange between the chamber headspace and ambient air. The chamber used for CO_2 and CH_4 flux measurements was made of clear plexiglas (Plexiglas SunActive GS, Evonik Industries AG, Germany) with dimensions of 50 x 50 x 50 cm and a thickness of 4 mm. For R_{eco} measurements the chamber was covered with an optically opaque box

(dark chamber measurements). The chamber was equipped with a fan for continuous mixing of headspace air (axial fan, 12V/DC, Conrad Electronic SE, Germany). Furthermore, a PAR sensor (SKP212, Skye Instruments Ltd., UK) and a temperature probe (107 Thermistor probe, Campbell Scientific Ltd., USA) were installed inside the chamber. Including the volume inside the chamber collars, the chamber enclosed a volume between 124-143 L. In 5 cm soil depth, soil temperature and volumetric water content (VWC – GS3, Decagon Devices, Inc., USA) were measured during every single chamber measurement right beside the chamber collar. A Diver (Schlumberger Ltd., USA) was installed at the polygonal center to measure water table (WT) fluctuations in 15 min intervals. To prevent pressure induced emission shocks during chamber closure, two openings (3 cm in diameter) were installed at the top of the chamber that were left open during the chamber placement and closed immediately after placing the chamber on the collars. On every measurement day soil temperature between the surface and the frozen ground in 5 cm intervals and ALD were measured at both microsites. CO_2, CH_4 and water vapor (H_2O) concentrations in the chamber headspace were measured with an Ultra-Portable Gas Analyzer (UGGA 30-p, Los Gatos Research, USA). The chamber headspace was pumped in a closed loop via transparent PUN tubes (inner diameter 4 mm, each 10 m length) through the analyzer with a flowrate of 200 mL min^{-1}. Gas concentrations of CO_2, CH_4 and water vapor were logged together with PAR as well as soil and air temperature with a frequency of 1 hertz (Hz) on a data logger (CR800series, Campbell Scientific Ltd., USA). Each chamber measurement was restricted to 120 seconds to minimize warming effects inside the chamber.

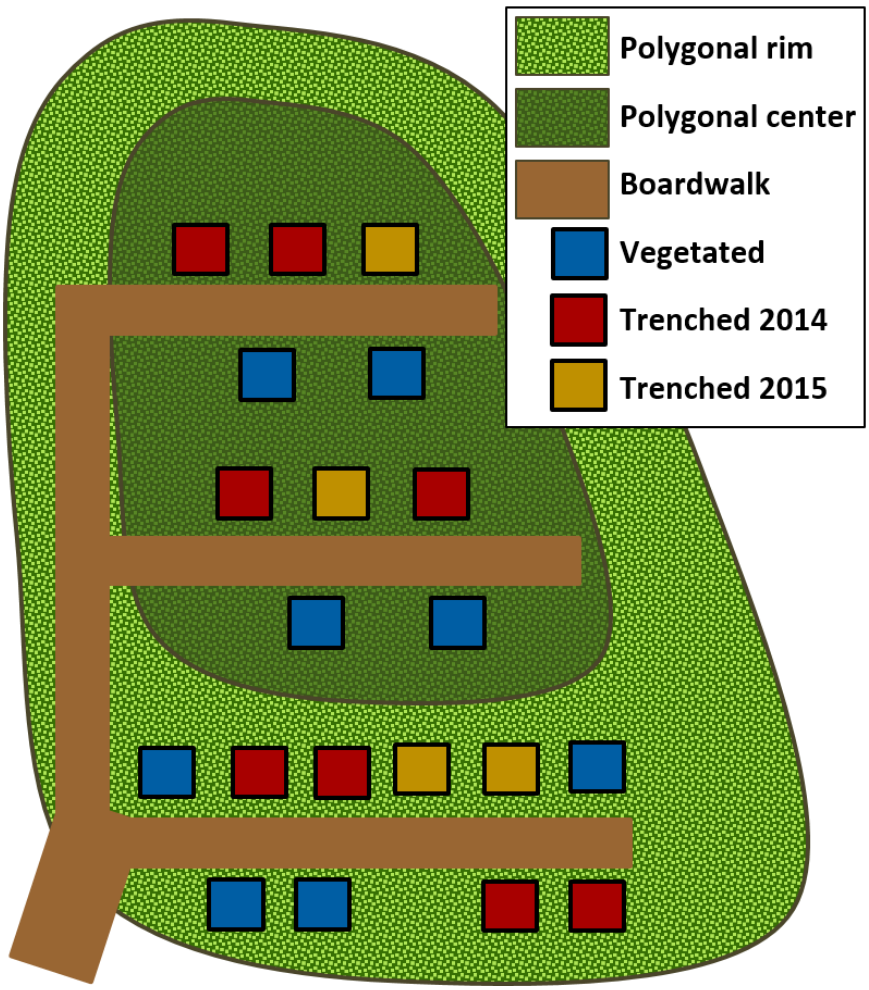

Figure 9: Diagram of the study site and the installed measurement plots. An elevated polygonal rim surrounds a wet-depressed center. Overall, 20 PVC collars, 10 on each microsite, were installed in 2014 (16) and 2015 (4) for CH_4 and CO_2 measurements and a boardwalk to avoid disturbances.

A total of 2,020 chamber measurements were conducted in summer 2015 from 11 July until 22 September. Except the weeks from 2 to 9 August (shift change) and 17 to 24 August (storm event) measurements were done at least every third day between 6 am and 9 pm (local time). Between measurements, atmospheric background concentration were achieved inside the chamber by holding the open-bottom of the chamber to the wind. Two consecutive measurements were performed at each collar: First, NEE and CH_4 (n = 679) were measured simultaneously with the transparent chamber followed by an R_{eco} measurement (n = 679) with the dark chamber. The four collars of one microsite were measured in a row before moving to the other microsite. The GPP fluxes were calculated from the sum of the measured R_{eco} and NEE fluxes.

Furthermore, 860 chamber measurements have been made from 23 July to 20 August in 2014 to observe CO_2 and CH_4 fluxes at the polygonal center and rim. The measurement procedure was identical to those of the chamber measurements in 2015.

4.3.2. Root-trenching approach

For R_H measurements the root-trenching method was applied at both microsites (Figure 10). By inserting PVC collars 20 cm deep into the soil, which is below the main rooting zone, lateral roots were cut off. All living plant biomass including mosses inside the collars was removed carefully in 2014. To prevent re-growth, the living plant biomass was removed periodically during the complete measurement period. This manipulation causes the die-off of roots (excludes R_A) and hence R_H fluxes can be determined. In total, the living plant biomass was removed from the inside of eight collars, four at each microsite. Repeatedly light and dark chamber measurements were made consecutive at the same plot to ensure the absence of photosynthesis. R_H fluxes (n = 662) were measured in 2015 during the same periods and with the same measurement interval as NEE, CH_4 and R_{eco} measurements on unaltered collars. In 2014, 226 chamber measurements on the altered plots were made.

To test if R_H fluxes are related to artefacts due to the root-trenching approach, four additional (two on each microsite) PVC collars were installed in 2015 and the living plant biomass was removed. The sampling protocol was the same to those plots where the root-trenching was applied in 2014. 302 R_H flux measurements were made on these newly installed plots. The differences of the mean R_H fluxes of every single plot that were trenched in 2014 and 2015 were analyzed using a student's t-test. R_A fluxes were calculated by subtracting the measured R_H fluxes from the measured R_{eco} fluxes that were measured simultaneously. The calculated R_A fluxes were used to calculate the net primary productivity fluxes (NPP), which is the sum of GPP and R_A fluxes.

Figure 10: The root-trenching approach at the polygonal center. The living plant biomass was removed from the measurement plots (left) to measure R_H fluxes, while the vegetation at other measurement plots was left intact (right) to measure CH_4, NEE and R_{eco} fluxes at the same microsite. The root-trenching was conducted in 2014. In 2015 the method was applied at four additional measurement plots to observe if the R_H fluxes are related to artefacts.

4.4. Flux calculation

CO_2 and CH_4 fluxes (in microgram (µg) CO_2/CH_4 m^{-2} s^{-1}) were calculated in MATLAB® R2015a (The MathWorks Inc., Natick, MA, 2000) with a routine which calculates flux rates with linear and different non-linear regression models and provides information criteria to find the regression that fits best (Eckhardt & Kutzbach, 2016). The regression models are described in detail in Kutzbach *et al.* (2007a). For flux rate calculations, a linear regression model and a Taylor power series expansion of the exponential model were used. The results of the power series expansion model are practically identical to those obtained from the exponential function, but the power series expansion model directly estimates the initial slope of the flux curve which results in lower error estimates for the initial slope. To determine if the fluxes are best represented by the linear or the power series expansion function the *Akaike* Information Criterion for finite sample sizes (AIC_c) was used (Burnham & Anderson, 2004) and the adjusted non-linear coefficient of determination (R^2_{adj}). It revealed that for the CO_2 fluxes, the linear model provided a better fit in most cases, with a lower AIC_c value in 71% and a higher R^2_{adj} in 53% of cases. For the CH_4 fluxes the linear regression model provided better fit with a lower AIC_c in 88% and a higher R^2_{adj} in 67% of cases.

The CO_2 and CH_4 fluxes were calculated using the following equation:

$$F_{CO_2,CH_4} = \frac{M_{CO_2,CH_4}}{R} \times \frac{V}{A} \times \frac{P_{atm}}{T_{ch}} \times \frac{dc_{CO_2,CH_4}}{dt} \quad (5)$$

where M_{CO_2,CH_4} is the molar mass of CO_2 and CH_4, respectively (g mol^{-1}), R is the ideal gas constant (J K^{-1} mol^{-1}), V is the chamber headspace volume (m^3), A is the chamber surface area (m^2), P_{atm} is the atmospheric pressure (Pa) and T_{ch} is the temperature inside the chamber during the measurement in Kelvin. The last term ($\frac{dc_{CO_2,CH_4}}{dt}$) describes the concentration evolution of the investigated gas in the chamber headspace over time.

Due to possible perturbation of the concentration-over-time curve during chamber setting, the first 30 seconds of each 2-minute measurement period were discarded and the remaining 90 data points were used for flux calculation. According to the manufacturer, the precision of the Gas Analyzer with 1 s signal filtering is < 0.3 parts per million (ppm) for CO_2 and < 0.005 ppm for CH_4. Typically, the root mean square error (RMSE) of chamber measurements and model fitting did not exceed these values and therefore higher RMSE values indicate failed model fitting or disturbed chamber measurements. Therefore, if RMSE exceed 0.3 ppm for CO_2 fluxes and 0.005 ppm for CH_4 fluxes, the flux curve was re-inspected. If irregularities could be removed by adjusting the measurement period, the flux curve was re-calculated and if not the dataset was discarded. Variation of PAR during chamber employment due to shifts in cloud cover leads to perturbation of the CO_2 concentration-over-time curves (Schneider *et al.*, 2011). These perturbed curves show distinct autocorrelation of the residuals of the fit function. Therefore, they were filtered out using a threshold for residual autocorrelation indicated by the Durbin-Watson test (Durbin & Watson, 1950). Overall, in 2015 about 3% (n = 47) of the CO_2 flux measurements (NEE, R_{eco} and R_H measurements) were discarded from the dataset, because they did not meet the mentioned quality criteria. For the same reasons, almost 4% (n = 26) of the CH_4 flux measurements were removed. From the 2014 dataset a total of 37 chamber measurements (~4%) were discarded as they exceeded the thresholds of RMSE and/or Durbin-Watson test.

As the chamber in 2014 was not equipped with large openings until 3 August, the CH_4 flux measurements cannot be used from measurements made between 22 July and 2 August. Missing openings at the top of the chamber can lead to a substantial overestimation of CH_4 emissions due to caused initial pressure shocks (Christiansen *et al.*, 2011). Therefore, 180 chamber measurements were excluded from the CH_4 dataset (~45%).

4.5. Modelling carbon fluxes

4.5.1. CO_2 model

There are two different sign conventions for NEE: the ecological sign convention defines a positive NEE as net uptake of CO_2 by the plant-soil ecosystem, whereas the atmospheric sign convention defines it as a net release of CO_2 from the soil to the atmosphere. In this study the atmospheric sign convention is used where a positive NEE defines a net release of CO_2 from the soil to the atmosphere.

GPP, R_{eco} and R_H fluxes from 2015 were modeled separately. The chamber measurements from 2014 were not used for modelling as the dataset is too small in quantity as well as on temporal scale. Examples of the modeled GPP and R_{eco} fluxes are given in Figure 11. To calibrate the models, the measured GPP, R_{eco} and R_H fluxes were fitted to the used functions for the flux models. The resulting fitting parameters were used to reproduce the fluxes over the complete measurement period. The modelling was done with a moving window of 15 days during the measurement period. If less than eight chamber measurements were performed in these 15 days, the moving window was extended to 19 days. Each of the four measurement plots per microsite were modeled separately and the summed fluxes were used to analyze differences between both microsites with a student's t-test. Subsequently, the modeled fluxes for each measurement plot were averaged for each microsite. The empirical Q_{10} model (van't Hoff, 1898) was fitted to the measured R_{eco} and R_H fluxes:

$$R_{eco,H} = R_{base} \times Q_{10}^{\frac{T_{a,surf,soil} - T_{ref}}{\gamma}} \qquad (6)$$

where the fit parameter R_{base} is the respiration at the reference temperature T_{ref}. T_{ref} (15 °C) and γ (10 °C) were held constant according to Mahecha *et al.* (2010). Q_{10} is a fit parameter indicating the ecosystem sensitivity to a 10 °C change in temperature. For this

study a fixed Q_{10} of 1.52 was used, which represents the seasonal mean value of the bulk partitioning model for the EC footprint area (Runkle *et al.*, 2013). Air temperature (T_a), surface temperature (T_{surf}) and soil temperature (T_{soil}) measured at a depth of 5 cm were tested as input variables. Since it has been shown that the water table and volumetric water content are important environmental factors in explaining R_{eco} and R_H fluxes (Biasi *et al.*, 2014, Schneider *et al.*, 2011), the respiration fluxes from the polygonal center were also related to WT and from the polygonal rim to VWC:

$$R_{eco,H} = R_{base} \times Q_{10}^{\frac{T_{a,surf,soil} - T_{ref}}{\gamma}} \times exp^{(WT,VWC \times c)} \quad (7)$$

The additional fitting parameter *c* was set to -0.11 when the model was calibrated to fluxes from the center and to -0.5 when the model was calibrated to fluxes from the rim. These values constitute the medians of this parameter obtained from test runs when *c* was held variable.

The modeling was done with MATLAB® R2015a (The MathWorks Inc., Natick, MA, 2000). The model parameters were estimated by nonlinear least-squares fitting (*nlinfit* function) and the uncertainty of the parameters were determined by calculating the 95% confidence intervals using the *nlparci* function. The selection of the best performing R_{eco} and R_H model was based on comparing the R^2_{adj}. The selected model was chosen as model for all measurement plots, even though for a single plot another model had a better qualifying parameter.

For an estimate of GPP, the R_{eco} fluxes, which were measured directly after the NEE fluxes were subtracted from the NEE fluxes. GPP fluxes are reproduced with the rectangular hyperbola function as a function of PAR (in µmol m^{-2} s^{-1}):

$$GPP = -\frac{P_{max} \times \alpha \times PAR}{P_{max} + \alpha \times PAR} \quad (8)$$

The fit parameters P_{max} and α are the maximum canopy photosynthetic potential (hypothetical maximum of P_{max} at infinite PAR) and the initial canopy quantum efficiency (initial slope of the P_{max} -PAR curve at PAR = 0), respectively. The values for α were obtained from modelling the CO_2 fluxes with EC data (Kutzbach *et al.,* unpublished). From the determined values when α was variable, a function was formulated with specific values for every day of the growing season using the following function:

$$\alpha = b \times exp^{\left(-\frac{abs\left((x-c)^d\right)}{2\times e^2}\right)} + f \qquad (9)$$

where b = 0.042, c = 209.5, d = 2, e = 25.51, f = 0.008 and x = day of year 2015. Afterwards, these "semi-fixed" values (variable on daily basis) were used to reproduce GPP fluxes from chamber measurements over the complete measurement period.

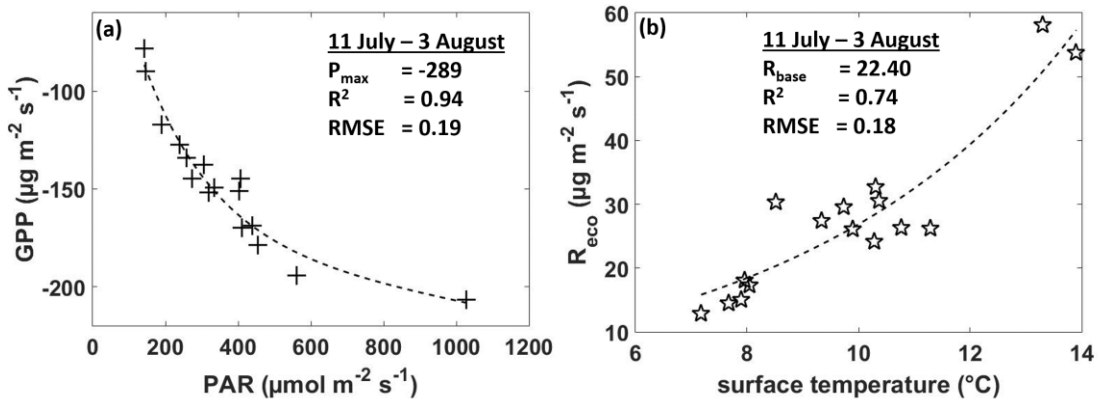

Figure 11: Examples of the models for the reproduction of GPP and R_{eco} fluxes. The relationship between PAR and GPP fluxes (left) is characterized by a light response curve (dotted line) and chamber measurements are shown as crosses. The temperature sensitivity of the R_{eco} fluxes (right) is exponential (dotted line). Stars display R_{eco} chamber measurements.

To consider the different phases of plant development throughout the growing season, three other GPP models were tested: (1) a rectangular hyperbola function including the normalized difference vegetation index (NDVI) as well as the ratio vegetation index (RVI) as input variable, (2) a sigmoidal model as well as a light response model including the leaf area index (LAI) and (3) a simple logistic function (Görres *et al.*, 2014, Marushchak *et al.*, 2013, Rodeghiero & Cescatti, 2005, Wohlfahrt *et al.*, 2010). The values of the NDVI and LAI were obtained from satellite images (ORNL DAAC, 2014). The values of the RVI were calculated using the following formula (Wilson & Meyers, 2007):

$$RVI = \frac{(NIR_{out}/NIR_{in})}{(PAR_{out}/PAR_{in})} \qquad (10)$$

where NIR_{out} and NIR_{in} (in W m^{-2}) are the outgoing and incoming near infrared radiation and PAR_{out} and PAR_{in} (in µmol m^{-2} s^{-1}) are the outgoing and incoming PAR, respectively. Unfortunately, all these models produced unrealistic fitting parameter and/or fluxes and where therefore not used in this study (Table 2).

Table 2: Failed GPP, R_{eco} and R_H models. All listed functions produced unrealistic fitting parameter and/or fluxes.

ID	Model formula	Remarks
A	$GPP = \frac{\beta \times RVI \times \alpha \times PAR}{\beta \times RVI + \alpha \times PAR}$	Modification of rectangular hyperbola model (after Görres *et al.* (2014)); Input variables are RVI and PAR, α and β are parameter.
B	$GPP = \frac{(\gamma + NDVI) \times P_{max} \times \alpha \times PAR}{P_{max} + \alpha \times PAR}$	Modification of model A with P_{max} and NDVI as input variables, γ is a parameter. In another test, NDVI was replaced by WT or VWC as input variable.
C	$GPP = \frac{P_{max} \times \alpha \times PAR}{\sqrt{(P_{max})^2 \times (\alpha \times PAR)^2}}$	Sigmoidal model after Wohlfahrt *et al.* (2010).
D	$GPP = \frac{P_{max} \times PAR}{(\varepsilon + PAR)} \times T_2 \times (\sigma + LAI)$	Light response model (Marushchak *et al.*, 2013); T_2 is the soil temperature at 2 cm soil depth and LAI is the leaf area index; ε and σ are parameter.
E	$R_{eco,H} = \frac{R_{max}}{1 + (\delta \times exp^{-\kappa \times T})}$	Simple logistic function (Görres *et al.*, 2014, Rodeghiero & Cescatti, 2005); R_{max} is the maximum respiration rate, δ determines the elongation along the x-axis and κ affects the steepness of the curve at its inflection.

The GPP model was calibrated with PAR values measured inside the chamber. Although the transmissivity of the Plexiglas is high (> 92%) it causes a reduction of the radiation. During the complete measurement period, the PAR values inside the chamber (mean of the first ten seconds of the measurement) were on average 20% lower than the PAR values measured every minute outside the chamber. A lower PAR is causing a lower photosynthetic uptake inside the chamber. Therefore, modelling of GPP was conducted in two steps. At first, the GPP model was calibrated using PAR values measured inside the chamber, and secondly, the reproduction of GPP fluxes over the growing season was carried out using PAR values measured outside the chamber. Without this two-step calibration the CO_2 uptake rates would have been seriously underestimated. The NEE and R_A fluxes were calculated as the sum of the modeled GPP and R_{eco} fluxes and of the modeled R_{eco} and R_H fluxes, respectively. Furthermore, NPP was calculated from the sum of R_A and GPP fluxes.

It was shown that CO_2 fluxes calculated with linear regression models can be seriously biased (Kutzbach *et al.*, 2007a), while non-linear regression models significantly improve flux calculations (Pihlatie *et al.*, 2013). On the other hand, Koskinen *et al.* (2014) have shown that, at least for respiration measurements, a linear regression model produced similar results and is more robust compared to other regression models, especially if chamber closure times are kept short. However, because the change in CO_2 and CH_4 concentration in the chamber was approximated best with a linear regression model (determined by AIC_c and R^2_{adj}) it was decided to run the models tentatively with two datasets. At first, only fluxes calculated with the linear regression were used for fitting. In a second step the fluxes which were calculated with the regression type which provided the best fit, determined by AIC_c, were used for fitting. This procedure revealed that model performance was best when fluxes were used, which were calculated with the linear regression model. On the basis of these findings, it was decided to use only the linear regression model for the calculation of chamber fluxes. This is in good agreement with Görres *et al.* (2014) who have shown that in some cases a linear regression model can produce a better CO_2 flux estimate for a non-linear concentration-over-time curve than a non-linear regression model.

4.5.2. CH_4 model

Similar to the CO_2 flux modelling, the measured CH_4 fluxes in 2015 were used to calibrate different CH_4 model approaches and the resulting fitting parameters were used to reproduce the CH_4 fluxes over the complete measurement period (Table 3). The functional relationship between environmental parameters and CH_4 emissions are known to be non-linear (Olefeldt *et al.*, 2013). Therefore, several exponential multiple regression models were used to correlate the CH_4 fluxes with WT, VWC, ALD, P_{max} (obtained from the GPP model) as well as different soil temperatures (at 2, 5, 10 and 15 cm soil depth) and the T_{surf}.

None of these model approaches explained the CH_4 flux variation acceptably as they produced unrealistic fitting parameter and/or CH_4 fluxes. Therefore, to gap-fill the CH_4 fluxes over the complete measurement period the fluxes were integrated over time using linear interpolation for the days between the measurements.

Table 3: Failed CH_4 models for the reproduction of CH_4 fluxes. All listed functions produced unrealistic fitting parameter and/or fluxes.

ID	Model formula	Remarks
A	$CH_4 = \alpha \times \beta^{[(T-T_{ref})/10]}$	Modified after Wille *et al.* (2008); input variables are soil or surface temperature. T_{ref} is the mean value of this variable during the measurement period; α and β are parameter.
B	$CH_4 = \alpha \times \beta^{[(T-T_{ref})/10]} \times exp^{(\gamma \times WT,VWC)} \times exp^{(\kappa \times ALD)}$	Modification of model A; Input variables are WT or VWC and ALD, γ and κ are parameter.
C	$CH_4 = \alpha \times \beta^{[(T-T_{ref})/10]} \times exp^{(\gamma \times WT_{full})}$	Modification of model A; WT_{full} is the thickness of the water-saturated soil horizon (WT_{full} = ALD - WT).
D	$CH_4 = \alpha \times \beta^{(T-10)/10} \times exp^{(\gamma \times WT)}$	Exponential model after Marushchak *et al.* (2016).
E	$CH_4 = \alpha \times exp^{(\beta \times T_{10})} \times exp^{(\gamma \times WT,P_{max})}$	Exponential multiple regression model (Saarnio *et al.*, 1997); T_{10} is the soil temperature at 10 cm depth, P_{max} is the maximum canopy photosynthetic potential obtained from the CO_2 model.

To investigate the environmental parameters controlling CH_4 emissions, a curve estimation with a linear and an exponential model was performed between CH_4 fluxes from 2015 and 2014 and a set of environmental variables (ALD, WT, surface temperature, as well as soil temperature at 2 and 15 cm) using SPSS software (IBM Corp, Released 2014. IBM SPSS Statistics for Windows, Version 23.0, NY: IBM Corp.).

4.6. CO_2 and CH_4 budgets

To estimate the CO_2 and CH_4 budgets of the complete measurement period in 2015, the polygonal tundra on Samoylov Island was classified by Muster *et al.* (2012) into dry tundra (65%), wet tundra (19%) and water bodies (16%) (thermokarst lakes (> 0.1 hectare) are not included in this classification). These amounts were used to calculate the contribution of the single microsites to the overall budget for the polygonal tundra on Samoylov Island. For an estimate of the CO_2 fluxes, cumulative fluxes obtained from the model results were used. The cumulative CH_4 fluxes were calculated from linear interpolated daily mean values.

5. Results

5.1. Environmental conditions

5.1.1. Meteorological conditions

During the measurement period from mid-July until the end of August in 2014, the total precipitation was 30 mm, with most of the rainfall in August (28 mm) (Figure 12). The ALD at the polygonal center increased from 37 to a maximum of 43 cm on 18 August, while at the rim the ALD increased from 20 to 32 cm. The soil temperature at the polygonal rim had a higher diurnal amplitude than at the center and maximum soil temperatures were 28 °C and 17 °C at rim and center, respectively. The averaged air temperature during August was almost 11 °C, which is 2 °C higher as the long-term mean temperature for August (Boike *et al.*, 2013). At the end of July, the air temperatures were highest with up to 30 °C. The WT ranged between -1 and -10 cm below the soil surface. Both WT and VWC fluctuations were tightly coupled with precipitation events (Figure 13). PAR reached continuously values of more than 1000 µmol m^{-2} s^{-1} during the measurement period (Figure 14). During the first week of the measurement period and at the beginning of August, the values were rather low for a few days.

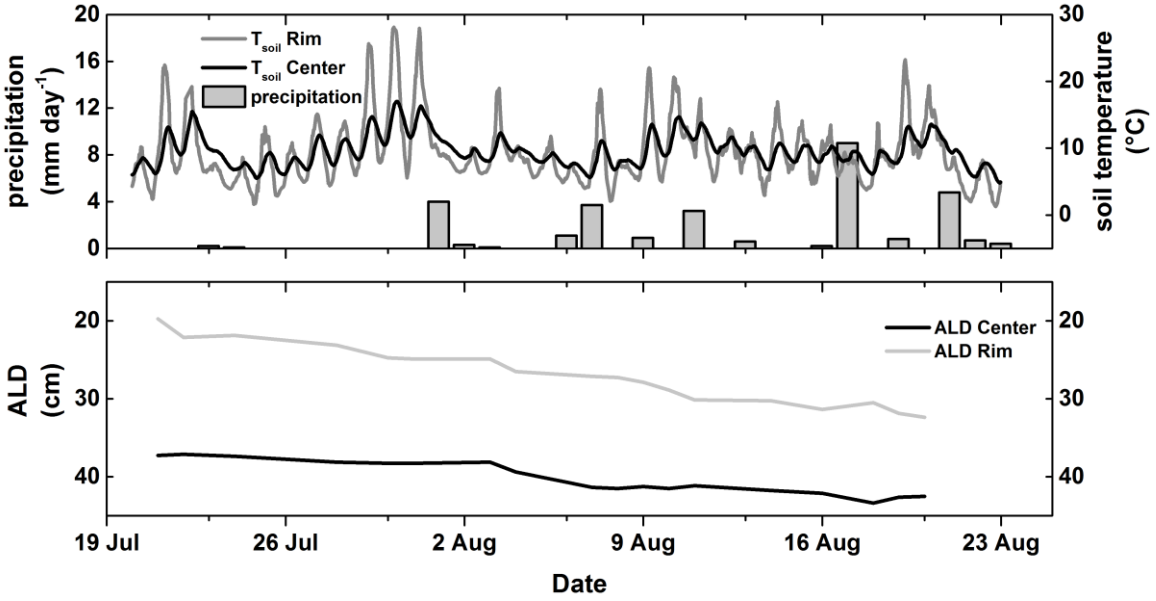

Figure 12: Soil temperatures, precipitation and active layer depths (ALD) at the study site in 2014. The upper graph shows the soil temperature at the polygonal center and rim as well as the daily precipitation rates during the measurement period. The bottom graph shows the evolution of ALD at both microsites.

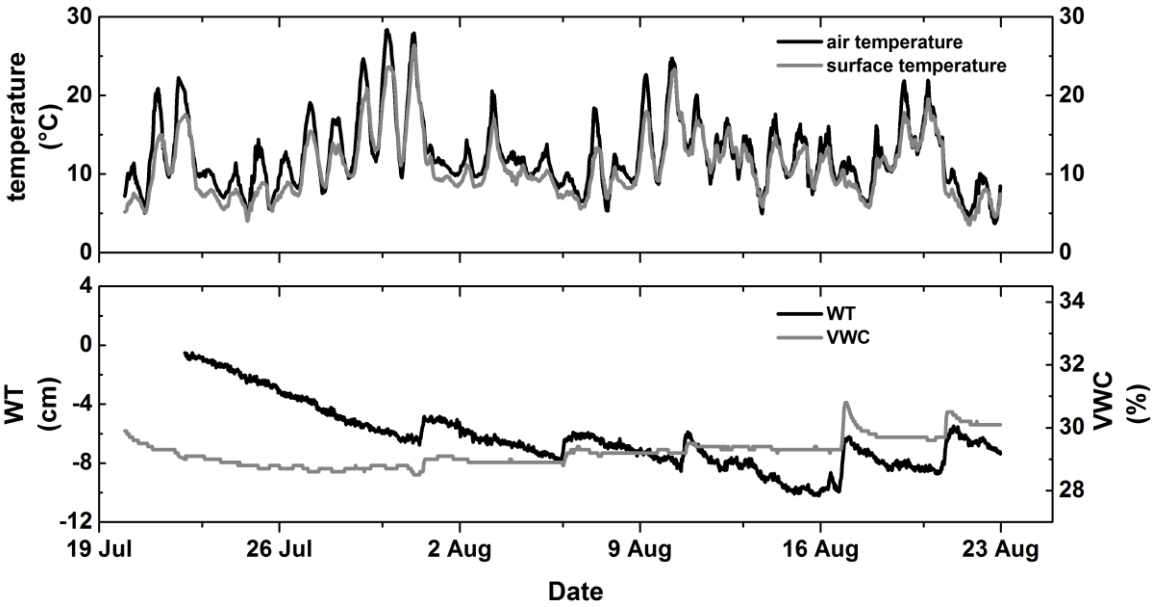

Figure 13: Air and surface temperature as well as water table (WT) and volumetric water content (VWC) at the study site in 2014. The upper graph shows the air temperature measured at the EC system at 2 m height and the surface temperature calculated with equation (4). The bottom graph shows the VWC at the polygonal rim measured at 5 cm soil depth and the WT in relation to the soil surface at the polygonal center during the measurement period.

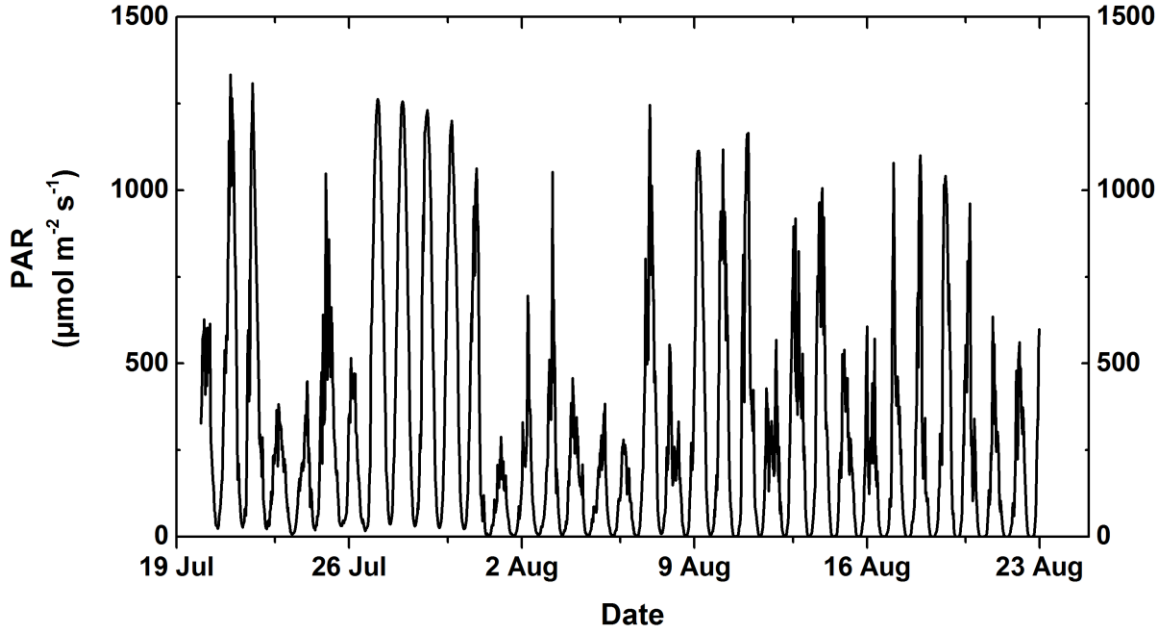

Figure 14: Photosynthetic active radiation (PAR) at the study site during the measurement period in 2014. PAR covers the wavelength range between 400 and 700 nanometer and was measured in 30-min intervals at the eddy covariance (EC) system.

During the measurement period from mid-July to end of September in 2015, the soil temperatures at 2 cm depth at the polygonal rim showed a higher diurnal variability than at the center (Figure 15). Highest soil temperatures of almost 25 °C occurred in mid-July and at the beginning of August. During the same periods, the soil temperature at the center reached its maximum of just 15 °C. At the end of the measurement period, the temperatures at both microsites were slightly negative. The air temperature ranged between 23 °C and -2 °C (Figure 16). There were two warm periods with temperatures above 20 °C, one in mid-July and one at the beginning of August recorded. After both periods, the temperatures remained around 10 °C for more than one week. A third warm period was recorded from 5 to 7 September with temperatures of up to 20 °C. After this period temperature started to decrease continuously and reached a daily minimum of -2 °C on 23 September. The average temperature in August 2015 (9 °C) was similar to the long-term mean temperature between 1998-2011 (Boike *et al.*, 2013), but about 2 °C colder than in 2014. Compared to the long-term mean, it was about 1°C colder during July (9 °C) but about 2 °C warmer during September (3 °C). A storm event with wind speeds of up to 11 m s^{-1} and precipitation of 18 mm day^{-1} reached the island around the 23 August (Figure 15). The total precipitation of the complete measurement period was 78 mm and at the end of September the precipitation was recorded as snow. While in 2014 28 mm of

rainfall was recorded between 3 and 20 August, the precipitation in 2015 during this period was almost 3-fold lower (10 mm). During July, nearly 50% (36 mm) of the total precipitation of the complete measurement period were recorded, while the total precipitation in September was just 9 mm. Longer periods without or with just light precipitation (≤ 0.1 mm day^{-1}) were recorded from 9 to 22 August and from 2 to 13 September.

ALD increased from the beginning of the campaign in mid-July until mid-September and then decreased slightly until the end of September (Figure 15). The ALD increased from 17 and 29 cm to a maximum of 36 and 37 cm at rim and center microsite, respectively. Maximum ALD was reached on 16 September at both microsites. At the polygonal center, the ALD nearly reached its maximum of 37 cm in July with depths of more than 35 cm and was almost constant at this depth until the values were decreasing at the end of September. In contrast to this, at the polygonal rim, the ALD was increasing almost constantly towards its maximum in September. During colder phases at the end of July and mid-August, the active layer depths were decreasing at both microsites. After the maximum was reached, the ALD decreased subsequently until the end of September by 3 cm and 4 cm at the polygonal center and the rim, respectively. WT fluctuations were coupled to precipitation. Throughout July, the WT was moving within few centimeters above the soil surface with a maximum of 5 cm on 21 July (Figure 16). During August, the water table dropped below the soil surface, but sharply increased after heavy rainfall on 23 August. Afterwards, accompanied by low precipitation, the WT decreased onto a minimum of 8 cm below the soil surface at the end of September. The volumetric water content at 5 cm soil depth was on average 30% at the polygonal rim. These values were peaking simultaneously to precipitation events.

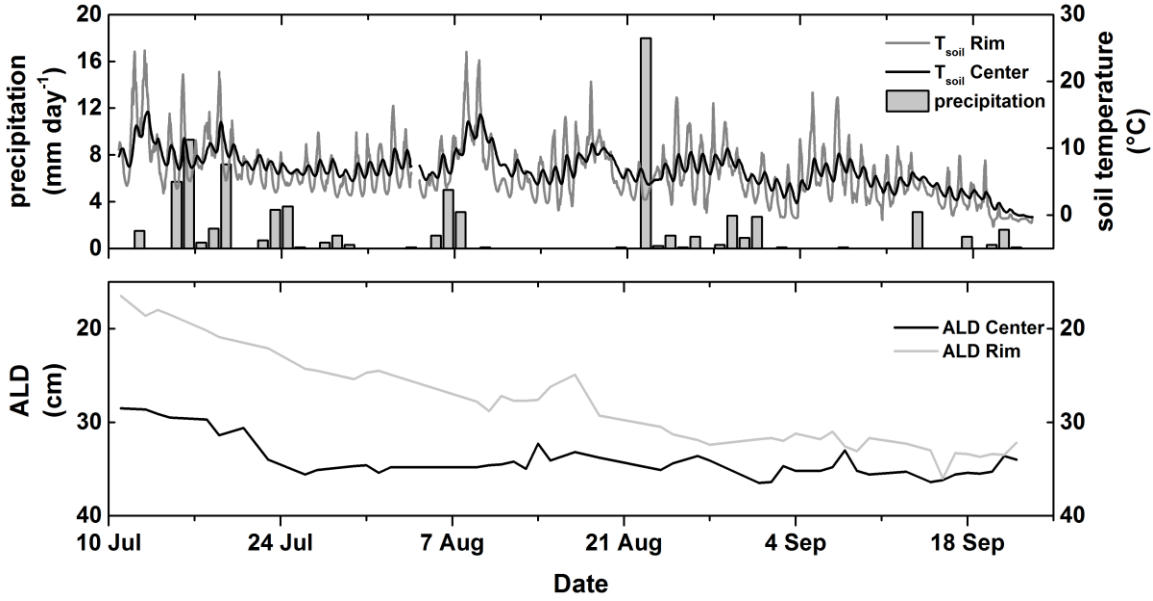

Figure 15: Soil temperatures, precipitation and active layer depths (ALD) at the study site in 2015. The upper graph shows the soil temperature at the polygonal center and rim as well as the daily precipitation rates during the measurement period. The bottom graph shows the evolution of ALD at both microsites.

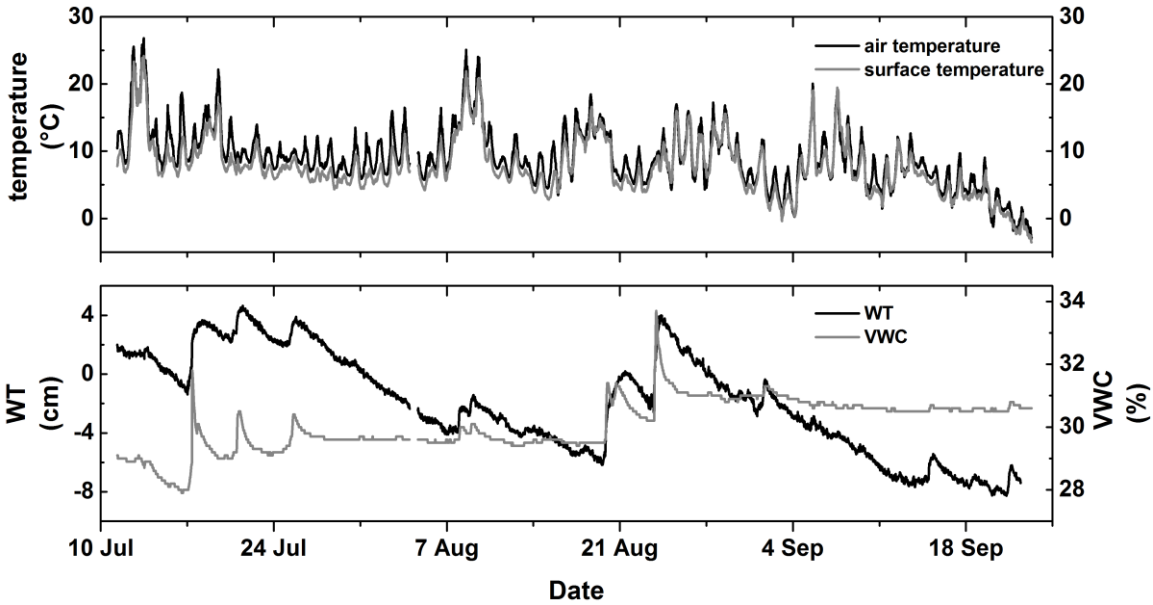

Figure 16: Air and surface temperature as well as water table (WT) and volumetric water content (VWC) at the study site in 2015. The upper graph shows the air temperature measured at the EC system at 2 m height and the surface temperature calculated with equation (4). The bottom graph shows the VWC at the polygonal rim measured at 5 cm soil depth and the WT in relation to the soil surface at the polygonal center during the measurement period.

The photosynthetic active radiation showed a strong diurnal variation with lowest PAR values during night times (Figure 17). From the beginning of the campaign until 12 August, the mean values during nighttime (9 pm – 3 am) did not dropped under 5 µmol m^{-2} s^{-1}.

Afterwards, with upcoming polar night conditions, the periods with low PAR values extended. High PAR values (PAR > 1000 µmol m^{-2} s^{-1}) were measured in mid-July, at the beginning of August and once at the end of August. Throughout September, the daily maximum PAR values were decreasing. Similar to the temperatures at the end of July and mid-August, the PAR values were comparatively low during these periods.

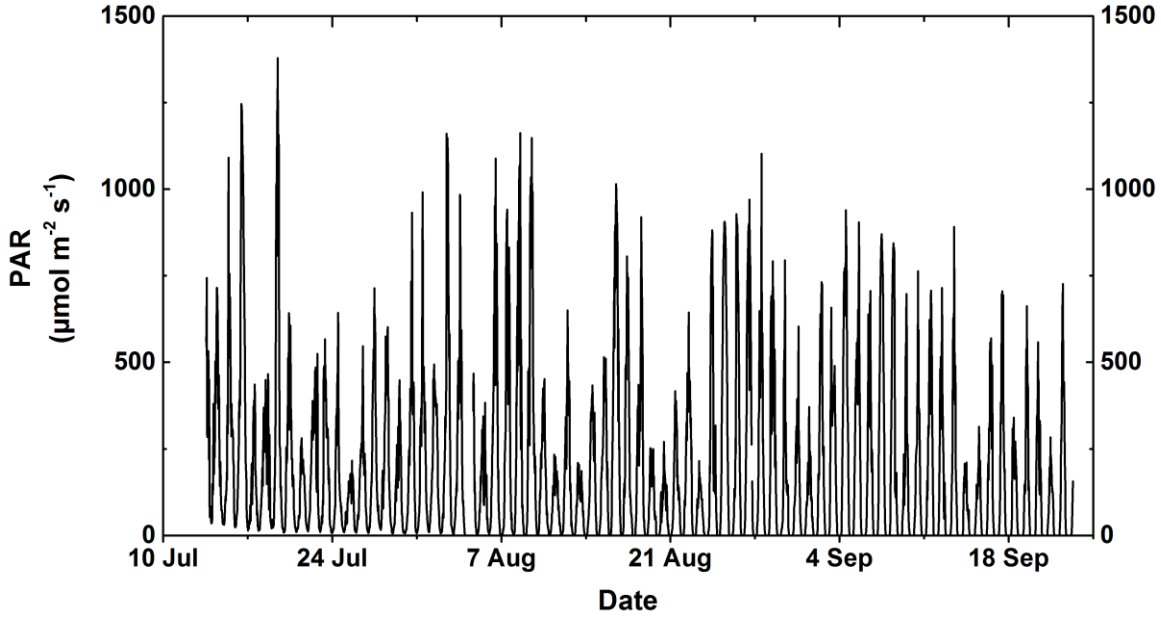

Figure 17: Photosynthetic active radiation (PAR) at the study site during the measurement period in 2015. PAR covers the wavelength range between 400 and 700 nanometer and was measured in 30-min intervals at the eddy covariance (EC) system.

5.1.2. Soil characteristics

At the polygonal rim, the soil bulk density increased sharply down the soil profile from 0.32 ± 0.03 g cm^{-3} in the organic-rich soil layer (0 to 6 cm) to 1.32 ± 0.08 g cm^{-3} in the mineral soil layer, while at polygonal center (0.36 ± 0.03 to 0.64 ± 0.01 g cm^{-3}) this increase was not as sharp (Figure 18 and Figure 19). The gravimetric water contents were distinctly higher at the center than on the rim with 75 to 85% and 38 to 53%, respectively. The total C contents were lower at the polygonal rim (2-12%) compared to the center (10-20%) and decreased down the soil profile. Total SOC contents were decreasing distinctly with increasing depths at both microsites. The nitrogen content at the center was almost constant down the soil profile with around 0.6%. This constant nitrogen content leads together with the SOC content to a decreasing carbon nitrogen ratio from 33.1 to 16.9. In contrast to that, at the polygonal rim the nitrogen content was considerably higher in the organic-rich layer compared to the mineral soil layer (0.5% vs. 0.1%) and the difference of the C/N ratios between different soil depths is smaller, compared to the center. Strongly acidic pH values were measured at every measurement depth at the polygonal center (around 5.3), while in the organic-rich layer and in the mineral soil layer at the rim pH values were moderately acidic with values of 5.7 and 6.0, respectivel

Polygonal center

Location: Samoylov Island, Lena River Delta
Geographic coordinates: 72°22.442 N, 126°29.828 E
Field location: center of low-center polygon

Date of profile acquisition: 10.07.2014
Thaw depth during sampling: 31 cm
Water level during sampling: -2 cm
Vegetation: sedge-moss tundra

Remarks: organic-layer very weakly decomposed, no evidence of cryoturbation

Classification:
World Reference Base for Soil Resources IUSS (WRB, 2014):
Reductaquic Cryosol (Hyperhumic) – abbreviation: CR-ra-jh
Russian classification (Elovskaya, 1987): Permafrost tundra humic-peatish

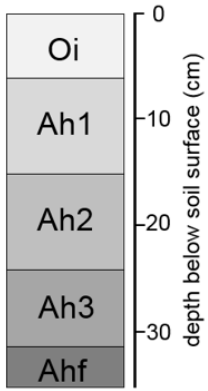

Horizon donation	Depth	TC	TIC	TOC	TOC	N	C/N	pH	Water content	Dry bulk density	Further characteristics
	cm	%	%	%	kg m^{-2}	%			wt%	g cm^{-3}	
Oi	0 to 6	19.8	0.2	19.6	4.2	0.60	33.1	5.18	85.4	0.36	Slightly decomposed plant material, *Carex* rhizomes
Ah1	6 to 15	13.2	0.2	13.0	6.2	0.51	25.7	5.34	75.4	0.53	Slightly humified plant material, *Carex* rhizomes, alpha-alpha-Dipyridyl positive
Ah2	15 to 23	11.7	0.2	11.5	5.8	0.57	20.6	5.22	77.1	0.62	Slightly humified organic matter, alpha-alpha-Dipyridyl positive
Ah3	23 to 31	10.1	0.2	9.9	5.1	0.60	16.9	5.56	81.2	0.64	Intermediate humified organic matter, alpha-alpha-Dipyridyl positive
Ahf	31+										frozen

Figure 18: Soil characteristics and soil classifications of the soil from the polygonal center.

Polygonal rim

Location: Samoylov Island, Lena River Delta
Geographic coordinates: 72°22.442 N, 126°29.828 E
Field location: elevated rim of low-center polygon

Date of profile acquisition: 10.07.2014
Thaw depth during sampling: 19 cm
Water level during sampling: -17 cm
Vegetation: moss-dominated tundra

Remarks: organic-rich layer weakly decomposed, evidence of cryoturbation (shown as @ in the horizon donation)

Classification:
World Reference Base for Soil Resources (WRB, 2014):
Turbic Glacic Cryosol – abbreviation: CR-gl.tu
Russian classification (Elovskaya, 1987): Permafrost tundra silty-peatish

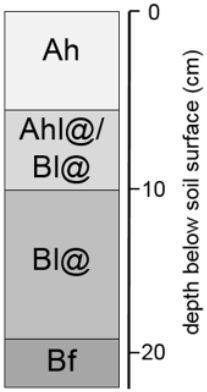

Horizon donation	Depth	TC	TIC	TOC	TOC	N	C/N	pH	Water content	Dry bulk density	Further characteristics
	cm	%	%	%	kg m^{-2}	%			wt%	g cm^{-3}	
Ah	0 to 6	12.3	0.2	12.1	2.3	0.49	24.6	5.69	52.9	0.32	Slightly decomposed plant material, some roots
Ahl@/Bl@	6 to 10	6.7	0.2	6.5	2.4	0.27	23.9	5.97	48.2	0.92	Transitional horizon, humified organic matter, capillary fringe mottling, mineral fraction increases
Bl@	10 to 19	2.1	0.2	1.9	2.3	0.10	19.2	6.02	38.2	1.32	Capillary fringe mottling, less organic matter, alpha-alpha-Dipyridyl negative
Bf	19+										frozen

Figure 19: Soil characteristics and soil classifications of the soil from the polygonal rim.

5.1.3. Vegetation units

The wet polygonal center was dominated by the moss species *Drepanocladus revolvens* and *Meesia triqueta* as well as the sedge *Carex aquatilis* and marsh cinquefoil (*Comarum palustre*). In a few spots at the center, the sedge species *Carex chodorrhiza* and in the transition zone between polygonal center and rim partially the willow species *Salix glauca* occured. The vegetation of the rim was made up mostly by the moss species *Hylocomium splendens* with a few parts consisting of *Polytrichum sp.* and *Rhytidium rugosum*. Vascular plants at this microsite were *Dryas punctata*, *Pyrola rotundifolia, Astragalus frigidus* and *Saussurea sp.* as well as some willow shrubs (*Salix glauca*, *Salix reticulata*). Furthermore, lichen species such as *Peltigera aphtosa*, *Stereocaulon sp.* and *Cladonia rangiferina* were present at the drier spots (Table 4).

Table 4: Mapping of vegetation species and abundance at polygonal rim and center. The abbreviation R- and C- are representing rim and center plots, respectively. The analysis was done in four subplots (10 x 10 cm) of the measurement plots (50 x 50 cm). Abundances are given in % of the surface cover.

Date		24.07.2015				22.08.2015			
Species/plot nr.		R-1	R-2	R-3	R-4	R-1	R-2	R-3	R-4
Polygonal rim									
Vascular plants									
	Astragalus frigidus	3	1	7	12	2	-	2	4
	Pyrola rotundifolia	14	12	2	11	5	3	-	5
	Salix reticulata	4	6	-	-	1	1	-	1
	Saxifraga cernua	-	2	1	1	1	1	-	-
	Dryas punctata	-	1	6	-	-	-	2	-
	Carex aquatilis	2	8	2	27	1	2	-	6
	Saussurea sp.	4	4	3	2	1	-	1	1
	Salix glauca	-	-	1	-	-	1	-	-
Lichens									
	Cladonia rangiferina	3	4	2	-	3	2	3	-
	Peltigera aphtosa	-	2	3	-	-	1	2	-
	Stereocaulon sp.	-	-	26	-	-	-	22	-
	Dactylina arctica	-	-	2	-	-	-	2	-
	Thamnolia vermicularis	-	3	-	-	-	4	-	-
Moss	*(Hylocomium splendens, Polytrichum sp., Rhytidium rugosum)*	>95	>95	>80	>95	>95	>95	>80	>95
		C-1	C-2	C-3	C-4	C-1	C-2	C-3	C-4
Polygonal center									
Vascular plants									
	Carex aquatilis	18	10	11	30	13	9	4	9
	Potentilla palustris	2	1	9	5	1	3	4	3
	Salix glauca	-	-	-	2	-	-	-	1
	Carex chodorrhiza	-	-	-	1	-	-	-	-
Moss	*(Drepanocladus revolvens, Meesia triqueta)*	>95	>95	>95	>80	>95	>95	>95	>80

5.1.4. Porewater conditions

The pH of the soil porewater at the water-saturated polygonal center showed a high variability with neutral pH values of 6.8 and strongly acidic pH values of 5.5 (Figure 20). At the beginning of the measurement period, neutral pH values were measured close to the soil surface at 5 cm soil depth, while towards the end of the growing season, most neutral pH values were measured at the bottom of the active layer in 35 cm soil depth.

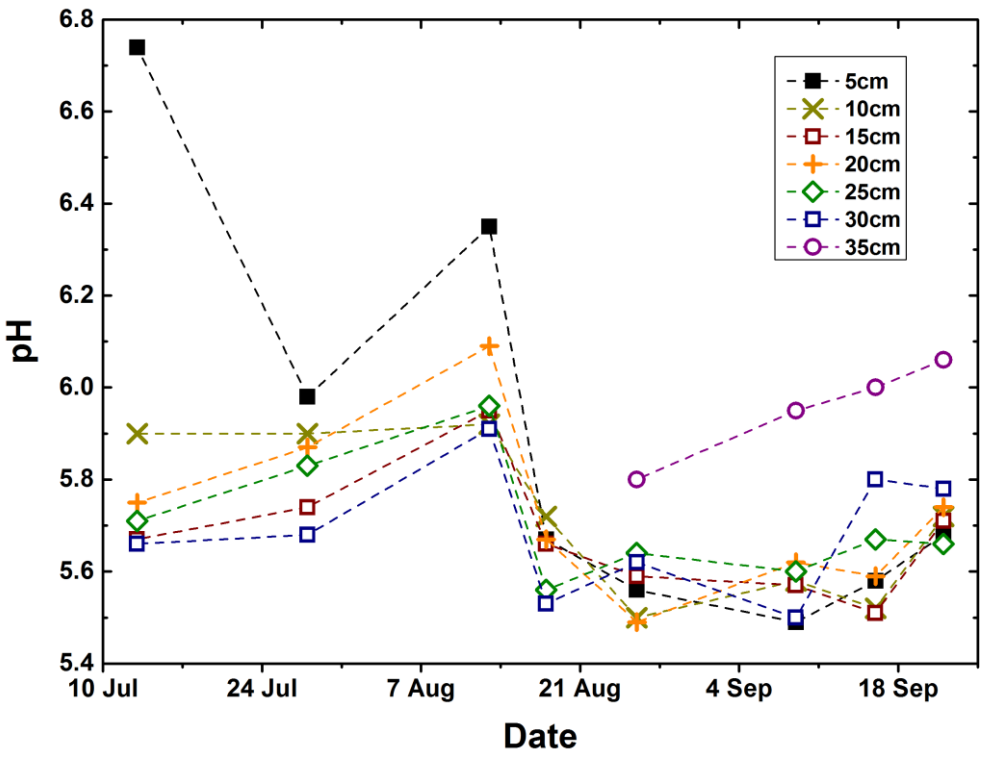

Figure 20: pH values of the soil porewater at the polygonal center in 2015. The pH was measured at different depths with an almost weekly interval. pH values from 35 cm soil depth were only measureable four times, as the soil was frozen at this depth until the end of August.

5.2. CO_2 fluxes

5.2.1. Chamber fluxes 2014

The CO_2 fluxes measured in 2014 at the polygonal rim and center are shown in Figure 21. During the measurement period in 2014, the center acted as a robust net CO_2 sink with an averaged NEE of -54 ± 16 µg m^{-2} s^{-1}. Highest net uptake of -83 ± 25 µg m^{-2} s^{-1} were measured at 3 August, while on 19 August a NEE of -25 ± 12 µg m^{-2} s^{-1} displayed the lowest uptake. In contrast, the polygonal rim was just a slight net CO_2 sink with an average of -2 ± 8 µg m^{-2} s^{-1}. On 3, 13 and 19 August the rim was a net source for atmospheric CO_2 with a NEE of more than 20 µg m^{-2} s^{-1}, while the highest net CO_2 uptake of -16 ± 5 µg m^{-2} s^{-1} was measured on 20 August. The daily averaged R_{eco} fluxes were higher at the polygonal center (69 ± 22 µg m^{-2} s^{-1}) compared to the rim (45 ± 4 µg m^{-2} s^{-1}). They ranged between 31 ± 4 and 116 ± 31 µg m^{-2} s^{-1} and 25 ± 6 and 73 ± 7 µg m^{-2} s^{-1} at the center and rim, respectively. At the end of July, smoke of a forest fire was blown towards Samoylov Island for about one week. This likely affected GPP during this time as NEE was low even though PAR and temperatures (Figure 13 + Figure 14) were favorable for high CO_2 uptake rates. The calculated mean GPP fluxes were -48 ± 20 µg m^{-2} s^{-1} and -123 ± 24 µg m^{-2} s^{-1} at the rim and center, respectively. Highest GPP fluxes of -162 ± 27 µg m^{-2} s^{-1} were measured at the center on 3 August and on 9 August at the rim (-74 ± 14 µg m^{-2} s^{-1}). The lowest GPP fluxes were measured at the rim on 13 August with just -4 ± 33 µg m^{-2} s^{-1}. At the polygonal center, the lowest GPP fluxes of -80 ± 9 µg m^{-2} s^{-1} were measured at the beginning of the measurement period.

The mean R_H fluxes were 30 ± 12 µg m^{-2} s^{-1} and 37 ± 14 µg m^{-2} s^{-1} at the polygonal center and rim, respectively. The lowest R_H fluxes were measured at the beginning of the measurement period at both microsites, while the highest R_H fluxes were measured simultaneously to highest air temperatures at the end of July. The averaged contribution of R_H to R_{eco} was 42% at the center. A distinctly higher contribution was observed at the rim with 85% and at more than half of the measurement days the measured R_H fluxes exceeded the R_{eco} fluxes. Based on these findings, R_A and NPP fluxes were not calculated from the sum of R_{eco} and R_H fluxes as well as GPP and R_A fluxes.

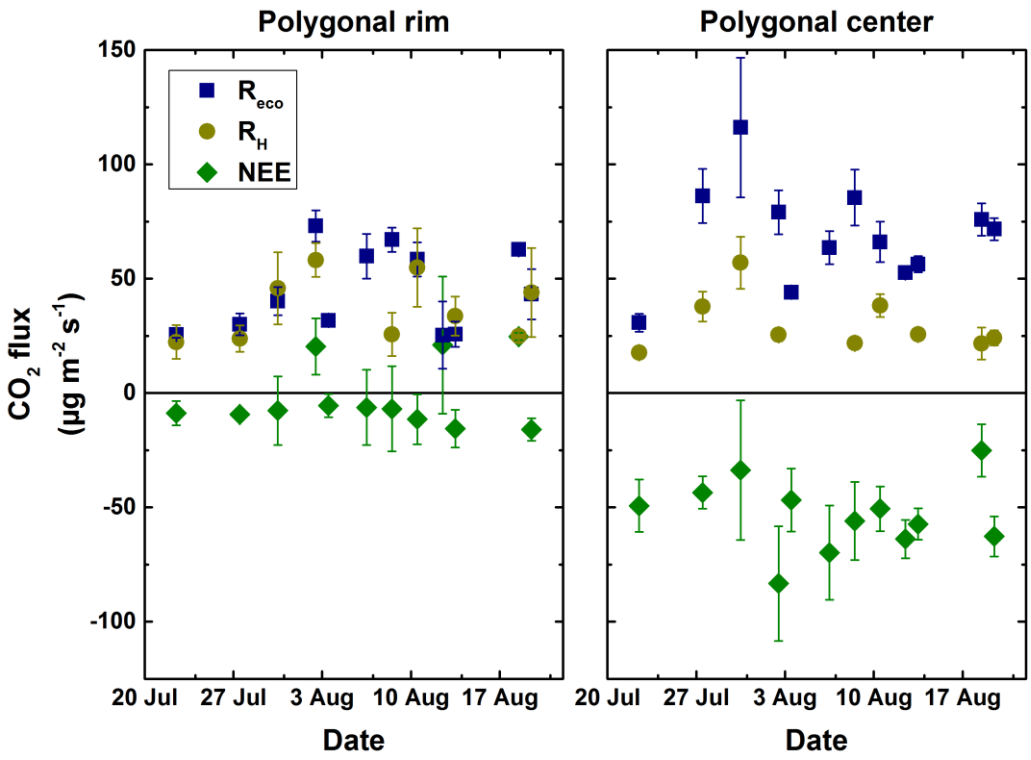

Figure 21: Chamber measurements of NEE, R_{eco} and R_H in 2014. The colored error bars denote the standard deviation between the four replicate measurements. The standard error of the replicate measurements is on average 3.6 µg m^{-2} s^{-1} at the center and 2.1 µg m^{-2} s^{-1} at the rim. Both NEE (n = 12) and R_{eco} fluxes (n = 12) were higher (in case of NEE more negative) at the center (right), while R_H fluxes (n = 9) were similar at both microsites.

5.2.2. Chamber fluxes 2015

The measured CO_2 fluxes in 2015 at the center and the rim are shown in Figure 22 and Figure 23, respectively. The standard error of the flux calculation was about 3.5 and 2.3 µg m^{-2} s^{-1} for polygonal center and rim, respectively and decreased slightly towards the end of the season. The net CO_2 uptake at the center was generally higher than at the rim (Figure 22). Highest NEE fluxes were measured at the end of July with -97.1 ± 27.0 µg m^{-2} s^{-1} and -208.6 ± 17.0 µg m^{-2} s^{-1} at the rim and center, respectively. In September, both microsites turned into small net sources for atmospheric CO_2. The highest net CO_2 release at the polygonal rim was measured on 17 August with 15.7 ± 4.7 µg m^{-2} s^{-1} and at the polygonal center on 19 September with 22.3 ± 3.2 µg m^{-2} s^{-1}.

In contrast to the NEE fluxes, the measured R_{eco} fluxes were on average higher at the rim compared to the center. Lowest ecosystem respiration fluxes at the polygonal center were observed on 23 July with 10.0 ± 2.5 µg m^{-2} s^{-1} and at the polygonal rim on 21 September

with 17.3 ± 1.3 µg m^{-2} s^{-1}. Highest ecosystem respiration fluxes of 79.7 ± 10.8 and 88.1 ± 10.4 µg m^{-2} s^{-1} for rim and center, respectively, were measured at 9 August, when temperatures reached more than 20 °C.

NEE and R_{eco} fluxes showed a clear seasonal trend. From mid-July the net CO_2 uptake increased until it peaked during the vegetation maximum at the end of July and beginning of August. Subsequently, NEE decreased until the end of September. This seasonality was more pronounced at the polygonal center than at the polygonal rim. Interestingly, the net CO_2 uptake at the polygonal rim was increasing from mid-September until the end of the measurement period. R_{eco} showed almost the same, but less distinct seasonal pattern and the peak of the highest R_{eco} fluxes was later in mid-August. In contrast, R_H followed no seasonal trend.

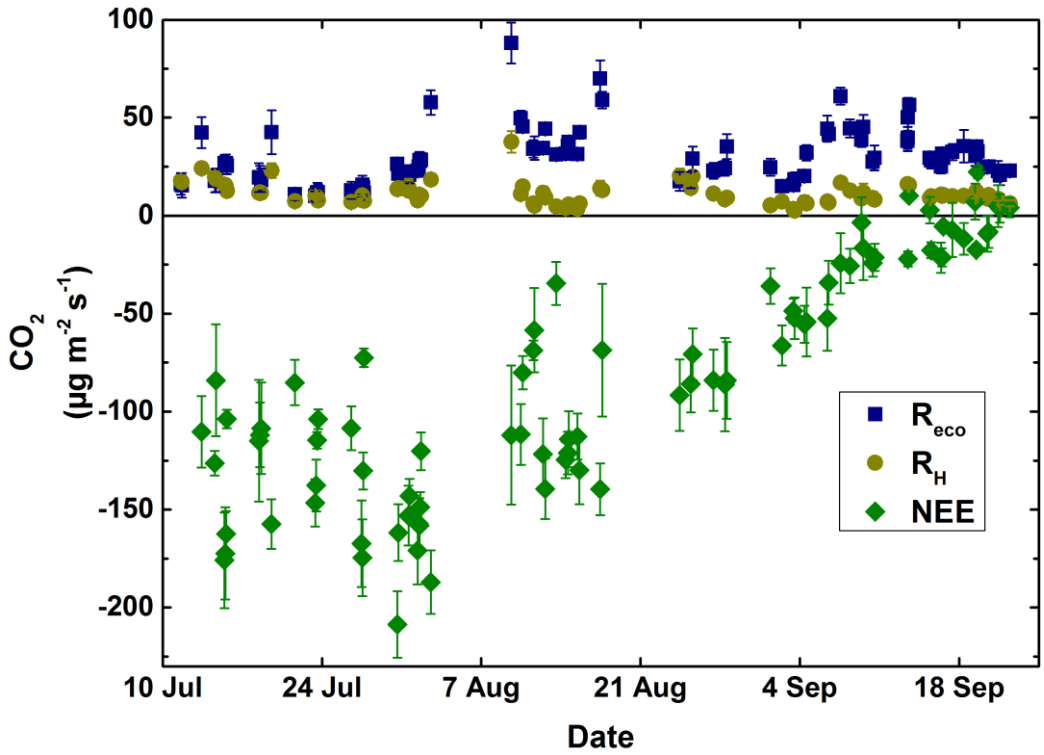

Figure 22: Chamber measurements of NEE, R_{eco} and R_H fluxes at the **polygonal center**. The error bars denote the standard deviation of the four replicate measurements. The averaged standard deviation of the flux calculation during the measurement period was 3.5 µg m^{-2} s^{-1}. Throughout the measurement period a pronounced seasonality of the NEE (n = 83) and R_{eco} fluxes (n = 85) was observed, while R_H fluxes (n = 85) showed no seasonal trend.

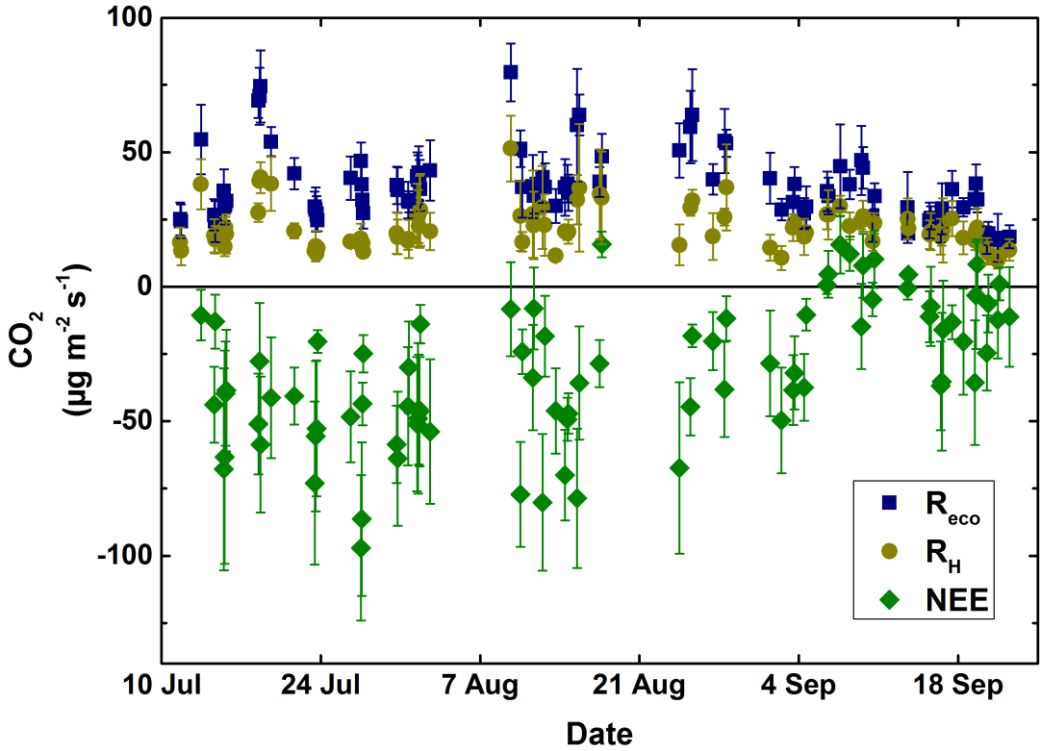

Figure 23: Chamber measurements of NEE, R_{eco} and R_H fluxes at the **polygonal rim**. The error bars denote the standard deviation of the four replicate measurements. The averaged standard deviation of the flux calculation during the measurement period was 2.3 µg m^{-2} s^{-1}. Similar to the polygonal center, the NEE (n = 83) and R_{eco} fluxes (n = 85) at the rim showed a seasonality, while no seasonal trend was observed for the R_H fluxes (n = 85).

The calculated GPP fluxes are naturally linked to determined fluxes of NEE and R_{eco} as they are derived from those values (Figure 24 + Figure 25). Lowest GPP fluxes of -10.4 ± 2.5 µg m^{-2} s^{-1} and -16.2 ± 5.7 µg m^{-2} s^{-1} for center and rim microsite, respectively, were observed at the end of the campaign were senescence of plants is well advanced. Maximum GPP fluxes are associated with the mature state of plants at the end of July. The highest GPP flux at the polygonal rim was measured on 27 July with -142.5 ± 33.4 µg m^{-2} s^{-1}, while at the polygonal center a maximum GPP flux of -244.8 ± 18.6 µg m^{-2} s^{-1} was measured on 2 August.

The calculated R_A fluxes at the polygonal center were on average 18.2 ± 13.9 µg m^{-2} s^{-1} with the highest fluxes of 56.0 ± 10.0 µg m^{-2} s^{-1} measured on 17 August. Occasionally, the R_A calculation revealed negative fluxes when R_H fluxes were exceeding R_{eco} fluxes, which occurred mostly during times of a high water table. At the polygonal rim, the averaged calculated R_A flux was 15.6 ± 8.2 µg m^{-2} s^{-1}. At this microsite, the highest R_A fluxes of

41.6 ± 7.3 µg m^{-2} s^{-1} were observed on 18 July and the lowest R_A fluxes were observed at mid-September with 3.1 ± 8.6 µg m^{-2} s^{-1}.

The calculated NPP fluxes showed, similar to the GPP fluxes, a distinct seasonality (Figure 24 and Figure 25). The mean NPP fluxes were -94 ± 61 and -55 ± 26 µg m^{-2} s^{-1} at the polygonal center and rim, respectively. The highest incorporation of CO_2 into the soil-plant continuum at the center was on 30 July with -222 ± 18 µg m^{-2} s^{-1}, which is three days earlier than the maximum GPP flux was determined. Similar to the highest GPP fluxes, the highest incorporation of CO_2 at the rim was determined on 27 July with -115 ± 29 µg m^{-2} s^{-1}. The lowest NPP fluxes were determined in September with -10 ± 11 µg m^{-2} s^{-1} at the rim and -2 ± 6 µg m^{-2} s^{-1} at the center.

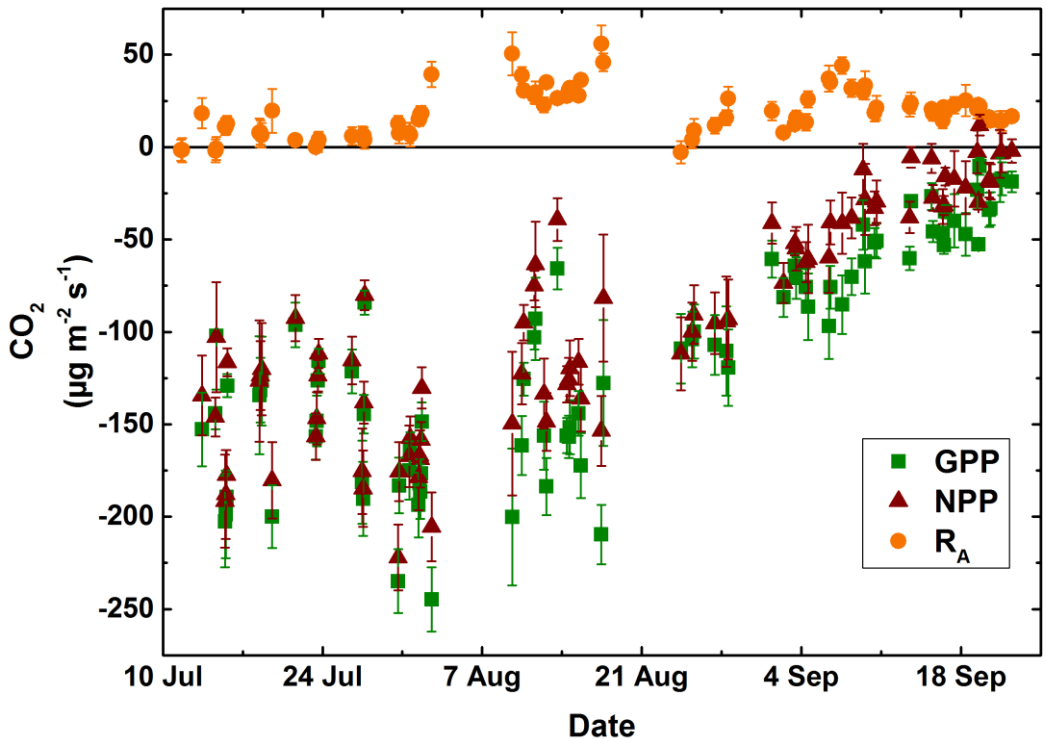

Figure 24: GPP, NPP and R_A fluxes at the **polygonal center** in 2015. GPP fluxes (n = 83) were calculated from NEE-R_{eco}, R_A fluxes (n = 85) were calculated from R_{eco}-R_H and NPP fluxes (n = 83) were calculated from GPP-R_A.

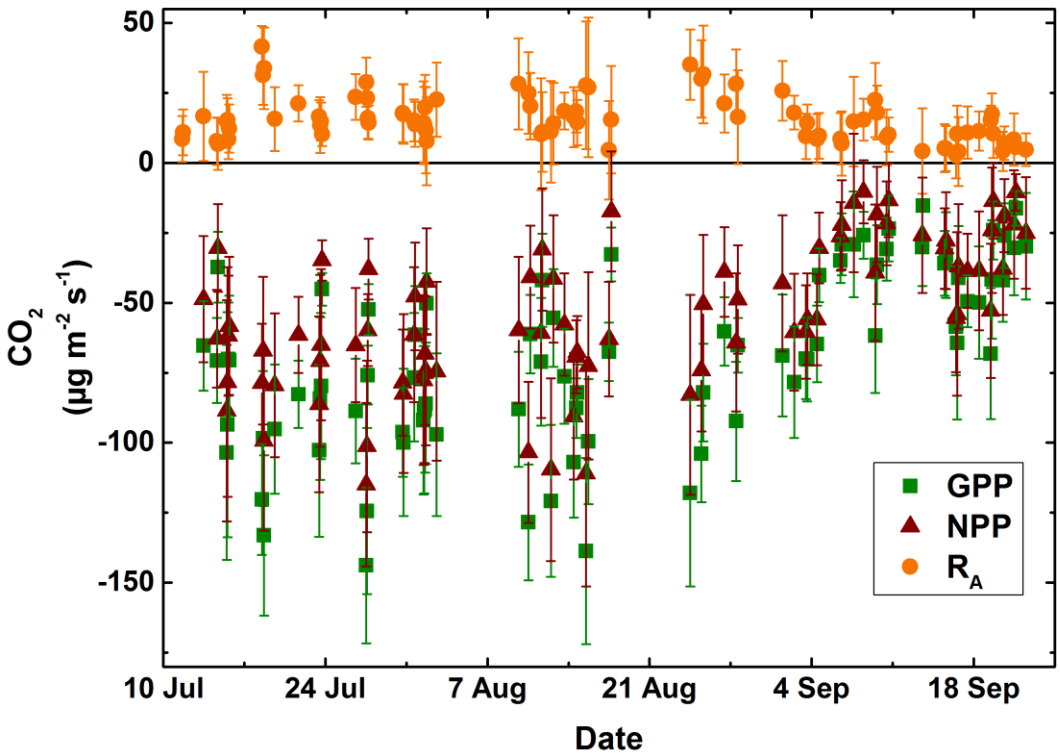

Figure 25: GPP, NPP and R_A fluxes at the **polygonal rim** in 2015. GPP fluxes (n = 83) were calculated from NEE-R_{eco}, R_A fluxes (n = 85) were calculated from R_{eco}-R_H and NPP fluxes (n = 83) were calculated from GPP-R_A.

Highest releases of CO_2 by R_H were measured on 9 August at the polygonal center and rim with 37.6 ± 5.5 and 51.4 ± 12.2 µg m^{-2} s^{-1}, respectively. The lowest R_H fluxes were measured at both microsites in September. On 3 September remarkably low R_H fluxes of 2.6 ± 1.1 µg m^{-2} s^{-1} were measured at the center, while at the rim lowest R_H fluxes of 9.8 ± 3.0 µg m^{-2} s^{-1} were observed at the end of September. Increased R_H fluxes after periodical re-clipping of the vegetation were not observed. The comparison of R_H fluxes from measurement plots that were trenched in 2014 with those that were trenched in 2015 revealed no significant differences (t-test, $p > 0.05$) between the years of root-trenching (Figure 26).

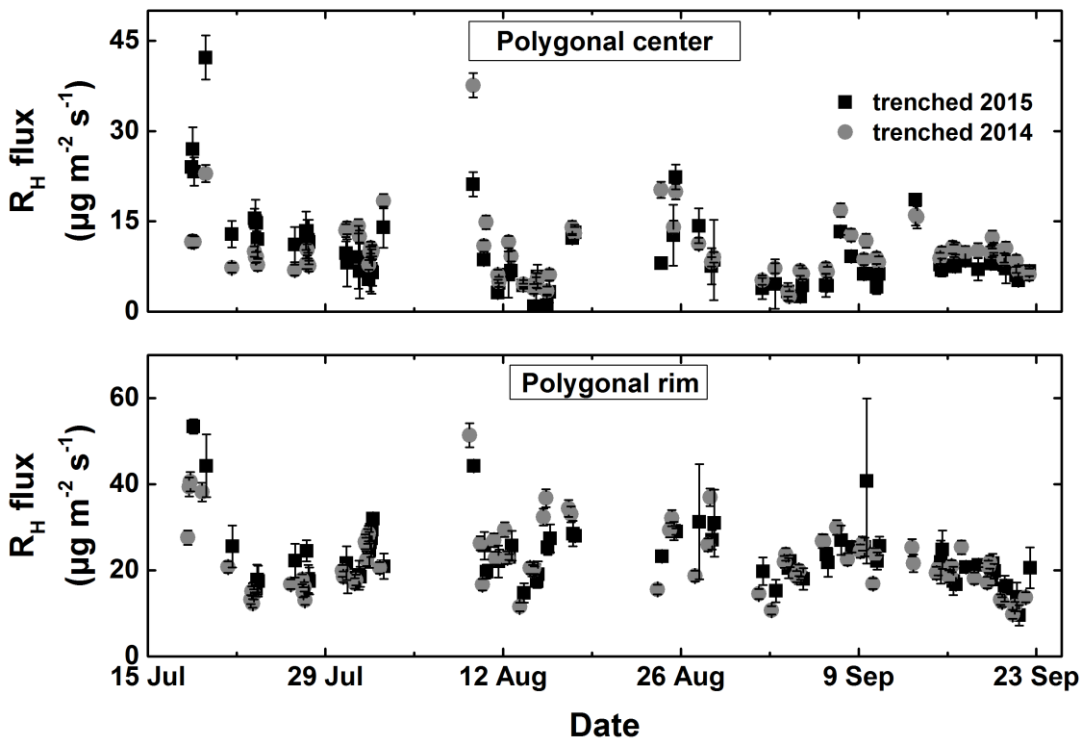

Figure 26: Comparison of R_H fluxes from plots trenched in 2014 and 2015. The measured fluxes are given with the standard deviation of the replicate measurements. The averaged standard error of the flux calculation is 1.0 and 1.5 µg m^{-2} s^{-1} at the center (n = 73) and rim (n = 70) that were trenched in 2015, respectively and 1.8 and 6.4 µg m^{-2} s^{-1} at the center (n = 76) and rim (n = 76) that were trenched in 2014, respectively. A student's t-test revealed no significant difference ($p > 0.05$) between plots that were trenched in 2014 and 2015.

The mean contribution of R_H to R_{eco} over the complete measurement period calculated from the flux measurements was 44% at the polygonal center and 61% at the rim. Both values showed no seasonal trend. High contributions of R_H to total ecosystem respiration were correlated with high WT at the polygonal center (Figure 27). During periods of lowest WT, the R_H/R_{eco} ratio increased again. Furthermore, R_A fluxes were low simultaneously to a high WT, but increased with a lowering of the WT, and decreased again, when the WT was at its minimum. In contrast to this, neither a trend to higher R_H fluxes during high water levels nor to lower R_H fluxes during low water levels was observed.

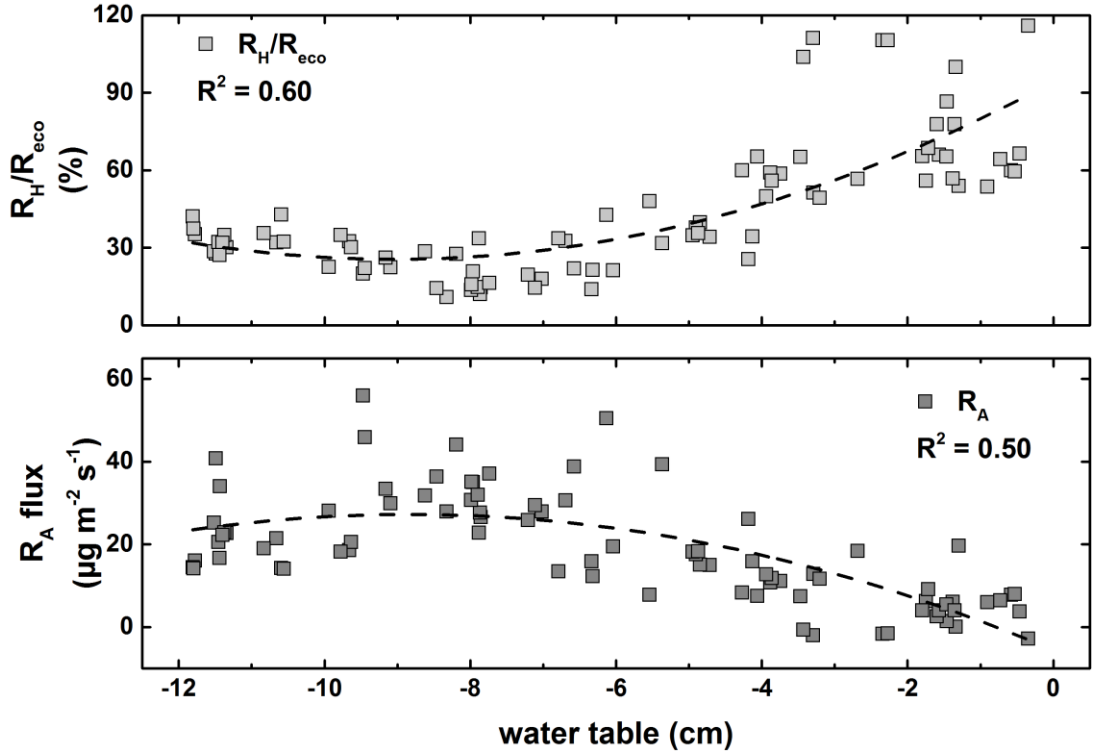

Figure 27: Relationship between water table fluctuations with the R_H/R_{eco} ratio and the R_A fluxes at the polygonal center. Negative values on the x-axis indicate a water table below the soil surface. The relationships are best described by a polynomial model with higher R_H/R_{eco} ratios (n = 85) and lower R_A fluxes (n = 85) towards higher water levels as well as lower water levels.

5.2.3. Model parametrization

Based on the modeled CO_2 fluxes and meteorological conditions, the measurement period in 2015 can be divided into (1) a peak season (11 July – 20 August), defined by mature state of vascular plants, highest CO_2 fluxes and temperatures and (2) a post season (21 August – 23 September) defined by upcoming senescence of vascular plants as well as lower temperatures and CO_2 fluxes.

The fitting parameters α and P_{max} as well as R_{base} showed a strong spatial and temporal variability (Figure 28) during the measurement period. In general, R_{base} were higher if the R_{eco} and R_H model was used to reproduce fluxes at the rim. The averaged R_{base} values of the R_H model did not differ significantly between peak and post season for center (15.4 ± 2.0 µg m^{-2} s^{-1} vs. 13.7 ± 1.8 µg m^{-2} s^{-1}) and rim (28.7 ± 3.7 µg m^{-2} s^{-1} vs. 29.3 ± 1.6 µg m^{-2} s^{-1}), but differed significantly between the microsites. Similarly, the averaged R_{base} values of the R_{eco} model differed between polygonal rim and center, but not significantly between the seasons (peak season: 18.7 ± 2.0 µg m^{-2} s^{-1} vs.

57.2 ± 7.2 µg m^{-2} s^{-1}; post season: 15.5 ± 2.6 µg m^{-2} s^{-1} vs. 56.1 ± 7.5 µg m^{-2} s^{-1}, for center and rim, respectively). For the GPP model, α values (mean: 1.47 ± 0.62) showed a high temporal variability with an average of 1.99 ± 0.18 during the peak season and 0.88 ± 0.34 throughout the post season, when plant senescence occurred. The P_{max} values showed a strong temporal variability when the GPP fluxes at the center were reproduced. Here, the mean P_{max} for the peak season was 334.4 ± 58.3 µg m^{-2} s^{-1}, while during the post season the averaged P_{max} was 156.0 ± 35.1 µg m^{-2} s^{-1}. Considerable differences in P_{max} were also observed between rim and center. The averaged values at the rim for the peak season was with 150.9 ± 25.3 µg m^{-2} s^{-1} much lower compared to the center. During the post season this difference was not as high as during the peak season; the averaged P_{max} at the rim was 119.0 ± 41.7 µg m^{-2} s^{-1}. Similar to the measured NEE fluxes, P_{max} was increasing at the rim towards the end of the measurement period and the highest P_{max} of 203.9 ± 151.3 µg m^{-2} s^{-1} was observed at the last day of the measurement period.

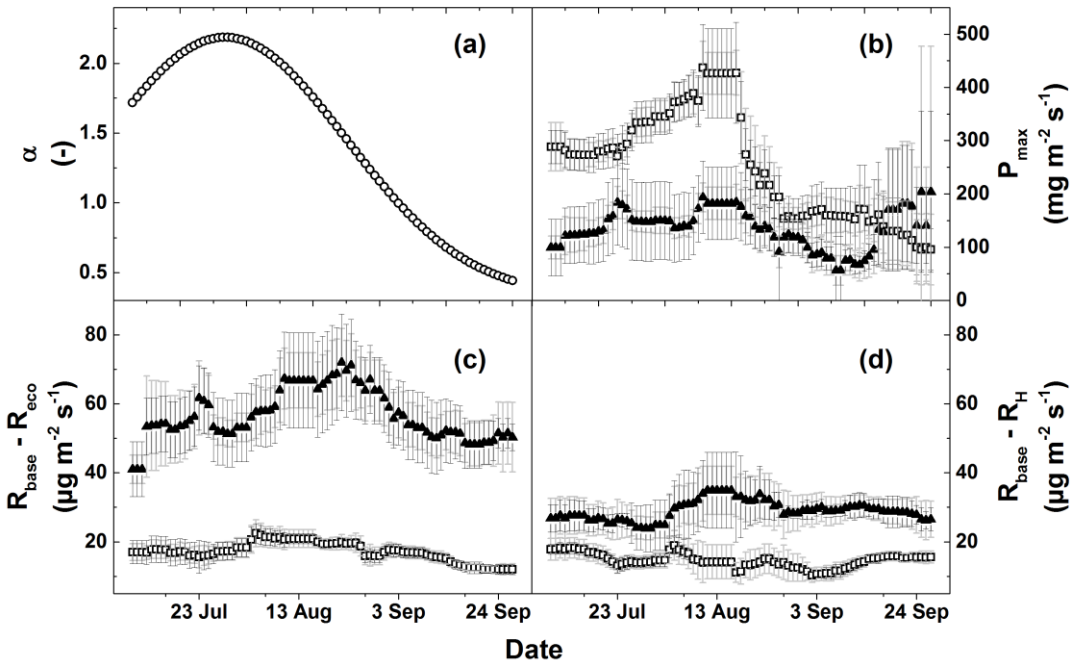

Figure 28: Fitting parameters of the CO_2 models. The values are given with the standard deviation of the model results of the single measurement plots (light grey error bars) and the confidence intervals (95%) of the fitting parameters (dark grey error bars). Panel (a) shows the initial canopy quantum efficiency α. The P_{max} values (panel b) show large differences between the polygonal center (white squares) and the rim (black triangles). Panel (c) shows R_{base} from the R_{eco} model and panel (d) R_{base} from the R_H model. Both models show higher R_{base} values for the rim.

For both microsites the R_{eco} model with an additional parameter (WT or VWC) suited best with a qualifying parameter R^2_{adj} of 0.46 and 0.78 for rim and center microsite,

respectively. Furthermore, the fluxes from the polygonal center (Figure 29) were best described by surface temperature, while for the polygonal rim (Figure 30) the soil temperature showed the best fitting compared to T_{soil} and T_{surf}. In contrast to the R_{eco} model the R_H model without an additional parameter produced the highest R^2_{adj} of 0.45 and 0.55 for polygonal rim and center, respectively, but the differences between the models in R^2_{adj} were small. The fluxes from the center were best described by air temperature, while at the rim the soil temperature was the parameter with the highest explanatory power. The R^2_{adj} of the GPP model was 0.82 for the polygonal center and 0.45 for the polygonal rim.

5.2.4. Modeled CO_2 fluxes

The modeled R_{eco} ranged between 12 ± 3 µg m^{-2} s^{-1} and 69 ± 7 µg m^{-2} s^{-1} with an average of 30 ± 4 µg m^{-2} s^{-1} at the polygonal center during the peak season (Figure 29). During the post season, the averaged R_{eco} values dropped slightly to 29 ± 3 µg m^{-2} s^{-1} with a range between 15 ± 1 µg m^{-2} s^{-1} and 52 ± 5 µg m^{-2} s^{-1}. At the polygonal rim, the modeled R_{eco} values were higher compared to the center throughout the first half of the growing season; they ranged between 23 ± 4 µg m^{-2} s^{-1} and 77 ± 14 µg m^{-2} s^{-1} with an average of 38 ± 7 µg m^{-2} s^{-1} (Figure 30). Afterwards, R_{eco} decreased to an average of 32 ± 6 µg m^{-2} s^{-1} (21 ± 3 µg m^{-2} s^{-1} to 63 ± 11 µg m^{-2} s^{-1}). The differences between the microsites were for both seasons not statistically significant (t-test, $p > 0.05$). Highest R_{eco} values of the measurement period where encountered at both microsites at the beginning of August during a hot period with surface temperatures of more than 20 °C. High fluxes where also observed during the other hot periods (see section 5.1.1.). At the polygonal rim, the lowest R_{eco} fluxes where obtained at the end of September accompanied by low soil temperatures. The lowest R_{eco} values at the polygonal center where encountered on 21 July, associated with the highest water table during the campaign. A steep decrease in the modeled R_{eco} fluxes at the center microsite was observed after the storm event on 23 August. In general, the values showed a larger diurnal amplitude at the rim compared to the center, which is in agreement with higher diurnal soil temperature variations at the rim (Figure 15).

At the polygonal rim, the modeled R_H fluxes ranged between 14 ± 4 µg m^{-2} s^{-1} and 46 ± 13 µg m^{-2} s^{-1} during the peak season and 14 ± 2 µg m^{-2} s^{-1} and 34 ± 5 µg m^{-2} s^{-1} during the post season with averaged values of 22 ± 5 and 19 ± 2 µg m^{-2} s^{-1}, respectively (Figure 30). At the polygonal center, the R_H fluxes were comparatively low; during the peak season they ranged between 8 ± 1 µg m^{-2} s^{-1} and 27 ± 2 µg m^{-2} s^{-1} with an average of 12 ± 1 µg m^{-2} s^{-1} (Figure 29). Also throughout the post season, the modeled R_H values were lower with 6 ± 1 µg m^{-2} s^{-1} to 15 ± 1 µg m^{-2} s^{-1} and an average of 9 ± 1 µg m^{-2} s^{-1}. The differences between the microsites were highly significant (t-test, $p < 0.001$) during the post season and significant ($p < 0.01$) during the peak season. The lowest R_H fluxes of the measurement period at the center were encountered on 3 September accompanied by low air temperature. The highest value was observed during the first hot period in July. The highest and lowest R_H fluxes at the polygonal rim were encountered at the same time as modeled R_{eco} fluxes (8 August and 20 September). Similar to the R_{eco} fluxes the R_H fluxes at the rim had a larger diurnal amplitude compared to the center. By comparing the R_H and the R_{eco} model over the complete measurement period, the contribution of R_H to R_{eco} is on average 42% at the polygonal center and 60% at the rim. This contribution was distinctly higher during the peak season (47%) than throughout the post season (35%) at the center. At the polygonal rim, an opposed trend was observed, although the differences were with 57% during the peak season and 62% during the post season was substantial lower.

The modeled GPP fluxes showed a distinct seasonal trend. From the mid of July until 12 August gross primary productivity took place for 24 hours per day because of polar day conditions, even though the CO_2 uptake was low during night times. Afterwards, periods where gross primary productivity was zero extended due to arising polar night conditions. The averaged GPP fluxes for the peak season were -138 ± 11 µg m^{-2} s^{-1} and -81 ± 25 µg m^{-2} s^{-1} at the center and rim, respectively. At both microsites, the diurnal amplitude of GPP increased from the beginning of the campaign until it reached a maximum of -163 ± 57 µg m^{-2} s^{-1} and -342 ± 53 µg m^{-2} s^{-1} at the polygonal rim and center, respectively in mid-August. After this peak, the GPP values decreased continuously onto the lowest daily maximum of -62 ± 18 µg m^{-2} s^{-1} at 21 September at the center. The highest GPP fluxes during the post season were -184 ± 30 µg m^{-2} s^{-1}

and -123 ± 29 µg m^{-2} s^{-1} at the polygonal center and rim, respectively. Interestingly, the lowest daily maximum of GPP (-53 ± 5 µg m^{-2} s^{-1}) at the rim microsite was observed about a week earlier than at the center microsite. Later, the GPP at the polygonal rim increased again. The averaged GPP fluxes during the post season were distinctly lower than during the peak season with -53 ± 9 µg m^{-2} s^{-1} and -39 ± 7 µg m^{-2} s^{-1} at the center and rim, respectively. The differences between the microsites were statistically significant ($p < 0.01$) during the peak season, but not during the post season ($p > 0.05$).

The modeled GPP and R_{eco} fluxes were used to calculate NEE fluxes (Figure 29 + Figure 30). Throughout the peak season, the highest net CO_2 uptake was -117 ± 60 µg m^{-2} s^{-1} at the rim (23 July) and -288 ± 53 µg m^{-2} s^{-1} at the center (16 August). Highest net CO_2 release was measured in mid-August with 49 ± 10 µg m^{-2} s^{-1} and 54 ± 2 µg m^{-2} s^{-1} at the polygonal rim and center, respectively. The averaged NEE flux at the center during the peak season was -107 ± 12 µg m^{-2} s^{-1}. At the polygonal rim, the averaged NEE flux was much lower with -44 ± 27 µg m^{-2} s^{-1}. From 11 July until the 28 July, the NEE at the polygonal center was continuously negative, while first net CO_2 release at the polygonal rim was encountered on 17 July. The diurnal amplitude of NEE oscillation was greatest between the end of July and mid-August. In the post season, the NEE at the center ranged between -166 ± 30 µg m^{-2} s^{-1} and 43 ± 4 µg m^{-2} s^{-1}. At the polygonal rim, the maximum net uptake was lower compared to the center with -92 ± 46 µg m^{-2} s^{-1}, while the highest net release was similar with 43 ± 8 µg m^{-2} s^{-1}. Compared to the peak season, the averaged net CO_2 uptake was much lower during the post season with values of -23 ± 10 µg m^{-2} s^{-1} and -7 ± 11 µg m^{-2} s^{-1} for polygonal center and rim, respectively. Highest net uptake during the post season were encountered at the end of August. From that period on the net CO_2 uptake at the center decreased and at some days the NEE became positive on a daily average but even at the end of the measurement period a net CO_2 uptake was observed during daytime. Similar to the GPP fluxes, the NEE fluxes at the rim were increasing again towards higher net CO_2 uptake from mid-September until the end of the measurement period.

In the peak season, the R_A fluxes were ranging between 1 ± 3 µg m^{-2} s^{-1} and 55 ± 4 µg m^{-2} s^{-1} at the polygonal center (Figure 29) and between 5 ± 5 µg m^{-2} s^{-1} and 32 ± 19 µg m^{-2} s^{-1} at the rim (Figure 30). On average, the R_A fluxes were slightly higher at

the center with 18 ± 4 µg m^{-2} s^{-1} compared to 16 ± 9 µg m^{-2} s^{-1} at the rim. The lowest R_A fluxes were accompanied by a low VWC (rim) and a high water table (center). During the post season, the lowest R_A flux at the center was observed directly after the storm event with 5 ± 1 µg m^{-2} s^{-1} and at the rim at the end of the campaign (6 ± 4 µg m^{-2} s^{-1}). The maximum R_A flux in the post season of 40 ± 4 µg m^{-2} s^{-1} was observed at the center during the warm period in September. At the rim, the R_A flux was highest shortly after the storm event with 30 ± 12 µg m^{-2} s^{-1}, accompanied by a high VWC. On average, the R_A fluxes were 19 ± 3 µg m^{-2} s^{-1} and 13 ± 6 µg m^{-2} s^{-1} during the post season at the polygonal center and rim, respectively.

The NPP fluxes were calculated from the sum of GPP and R_A fluxes. In general, the NPP fluxes are closely linked to variations of PAR values. The averaged NPP fluxes during the peak season were -122 ± 12 µg m^{-2} s^{-1} and -66 ± 28 µg m^{-2} s^{-1} at the center and rim, respectively. At the polygonal center, the highest NPP fluxes during the peak season were determined on 16 August with -300 ± 53 µg m^{-2} s^{-1} and throughout the post season on 24 August with -178 ± 30 µg m^{-2} s^{-1}. The lowest daily maximum at the center was observed on 19 August with -114 ± 17 µg m^{-2} s^{-1} and in mid-September with -39 ± 14 µg m^{-2} s^{-1} during the peak and post season, respectively. At the rim on 13 July (-89 ± 40 µg m^{-2} s^{-1}) and on 14 September (-43 ± 8 µg m^{-2} s^{-1}) the lowest daily maxima were determined for peak and post season, respectively. The highest NPP fluxes at the rim during the peak season were observed on 16 August with -142 ± 57 µg m^{-2} s^{-1}. During the post season, the maximum NPP fluxes were determined rather late in the season on 22 September with -107 ± 46 µg m^{-2} s^{-1}

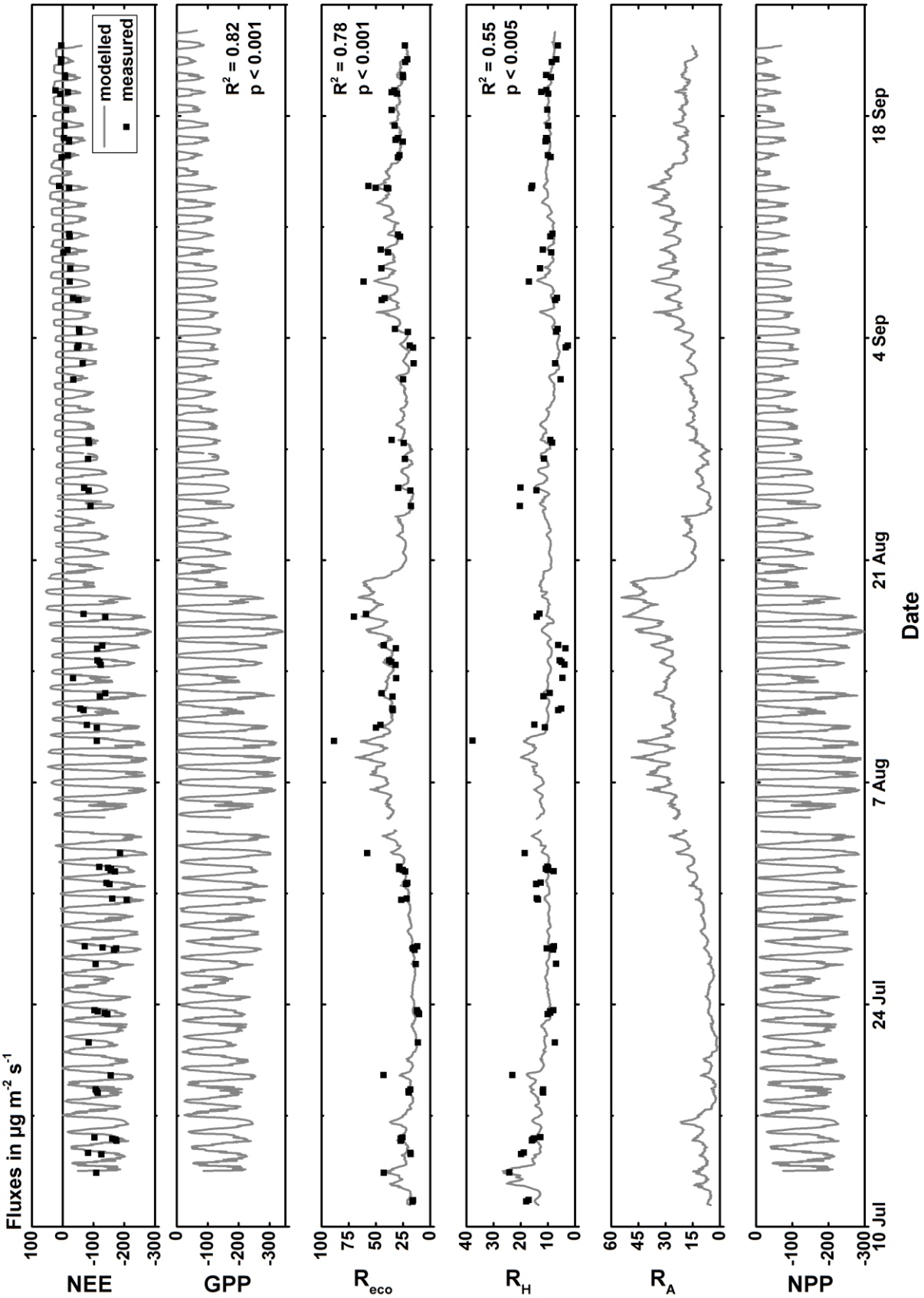

Figure 29: Modeled and measured CO_2 fluxes at the **polygonal center** in 2015. Measured fluxes are available for NEE, R_{eco} and R_H. NEE model fluxes are calculated from GPP-R_{eco}, R_A model fluxes from R_{eco}-R_H and NPP model fluxes from GPP-R_A. Note the different scales.

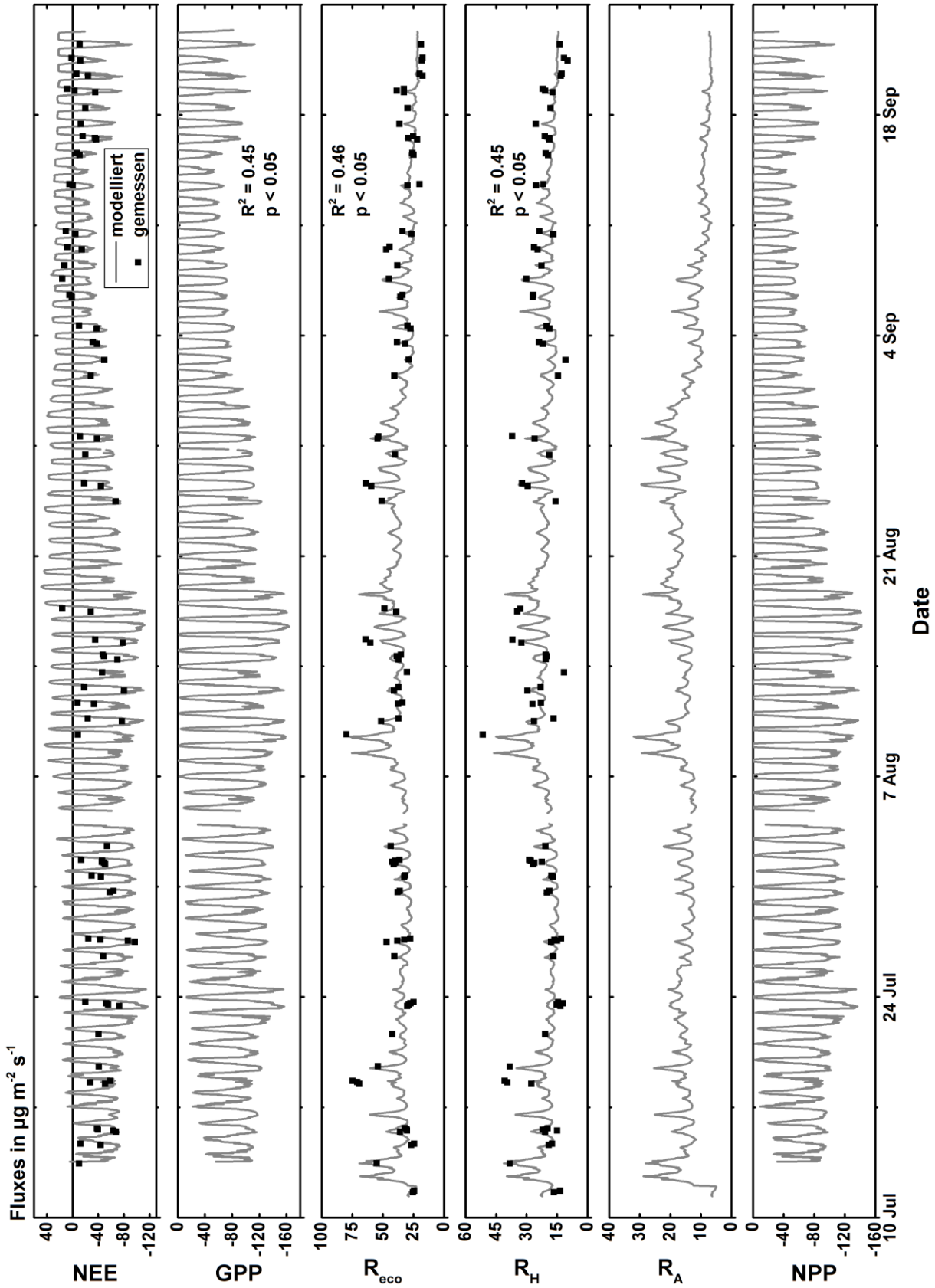

Figure 30: Modeled and measured CO_2 fluxes at the **polygonal rim** in 2015. Measured fluxes are available for NEE, R_{eco} and R_H. NEE model fluxes are calculated from GPP-R_{eco}, R_A model fluxes from R_{eco}-R_H and NPP model fluxes from GPP-R_A. Note the different scales.

5.2.5. Cumulative CO_2 fluxes

Based on the modeled CO_2 fluxes, the cumulative CO_2 fluxes were calculated (Table 5). The cumulative net CO_2 uptake during the peak season is more than twice as high at the center compared to the rim. During the post season, the differences in NEE fluxes between the microsites increased slightly. Partitioning of NEE fluxes into the underlying processes revealed that the cumulative GPP flux at the polygonal center is higher than at the polygonal rim during the peak season. Also throughout the post season, the cumulative GPP flux at the center is higher compared to the rim, but the gap between these fluxes decreased sharply (Table 5). Interestingly, the cumulative R_{eco} fluxes at the rim are higher than at the center. Similar to R_{eco}, the cumulative R_H fluxes were higher at the rim compared to the center during peak and post season. The cumulative GPP and R_A fluxes were used to calculate the net primary productivity (NPP). Over the complete measurement period, the NPP was almost twice as high at the center compared to the rim, but similar to the GPP fluxes the gap in NPP between the microsites was distinctly lower in the post season. At the center, the cumulative NPP was more than four-fold higher during the peak season compared to the post season. Similar to the center, more carbon was accumulated in the soil at the rim throughout the peak season compared to the post season.

Table 5: Cumulative CO_2 fluxes in 2015. The values were calculated from the model results. The cumulative fluxes show distinct differences between the peak and the post season. The values are given in g C m^{-2}. In total, both microsites are representing a net CO_2 sink over the measurement period with highest NEE throughout the peak season, whereas during the post season the respiration fluxes gained more importance.

		NEE	**GPP**	**R_{eco}**	**R_H**	**R_A**	**NPP**
Center	*total*	-411 ± 53	-595 ± 50	184 ± 17	68 ± 4	116 ± 17	-479 ± 53
	peak	-343 ± 34	-447 ± 32	104 ± 11	41 ± 3	62 ± 12	-385 ± 34
	post	-68 ± 25	-148 ± 24	80 ± 6	27 ± 1	53 ± 6	-95 ± 25
Rim	*total*	-154 ± 103	-376 ± 96	222 ± 38	131 ± 20	91 ± 42	-285 ± 105
	peak	-133 ± 83	-263 ± 80	130 ± 23	75 ± 15	55 ± 27	-208 ± 85
	post	-21 ± 25	-112 ± 19	92 ± 16	56 ± 6	36 ± 17	-77 ± 25

5.3. CH_4 fluxes

5.3.1. Chamber fluxes 2014

The measured CH_4 emissions in 2014 showed distinct differences between the microsites (Figure 31). The CH_4 fluxes at the center were with a mean of 0.45 ± 0.03 µg m^{-2} s^{-1} more than one order of magnitude higher than the CH_4 emissions from the rim (0.019 ± 0.008 µg m^{-2} s^{-1}). Highest CH_4 emissions at the rim were measured on 19 August with 0.045 ± 0.005 µg m^{-2} s^{-1}, while the lowest CH_4 fluxes at this microsite of 0.01 ± 0.004 µg m^{-2} s^{-1} were measured just one day after the maximum on 20 August. The CH_4 emissions at the center showed a much lower range over the measurement period compared to the rim. The lowest emissions of 0.36 µg m^{-2} s^{-1} were measured on 9 August and highest emissions at the same day a few hours later (0.51 ± 0.05 µg m^{-2} s^{-1}).

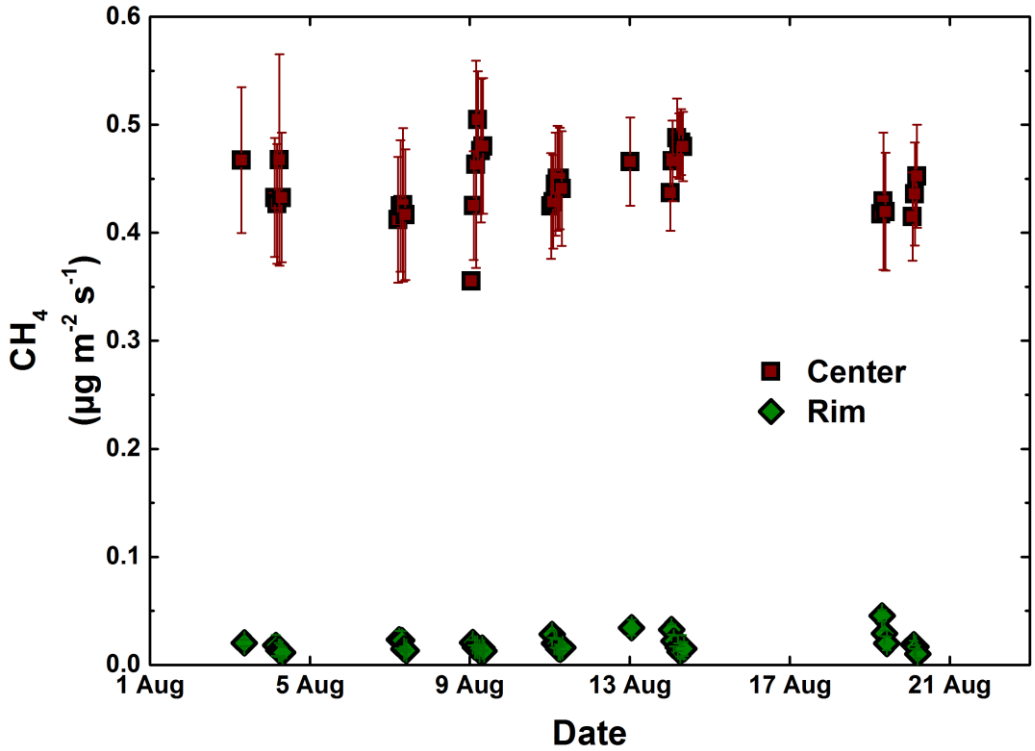

Figure 31: Measured CH_4 fluxes at polygonal rim and center in 2014. The error bar denote the standard deviation between the four replicate measurements. The averaged standard error of the flux calculation was 0.026 and 0.002 µg m^{-2} s^{-1} at the center and rim, respectively. The measured CH_4 emissions were about one order of magnitude higher at the center (n = 34) compared to the rim (n = 34).

5.3.2. Chamber fluxes 2015

The results of the CH_4 flux chamber measurements in 2015 for the polygonal center and rim are shown in Figure 32. The standard error of the flux calculation was about 0.016 µg m^{-2} s^{-1} at the center and 0.002 µg m^{-2} s^{-1} at the rim. These values were slightly increasing towards the end of the measurement period. Both investigated microsites were a source for atmospheric CH_4, but the source strengths differ considerably.

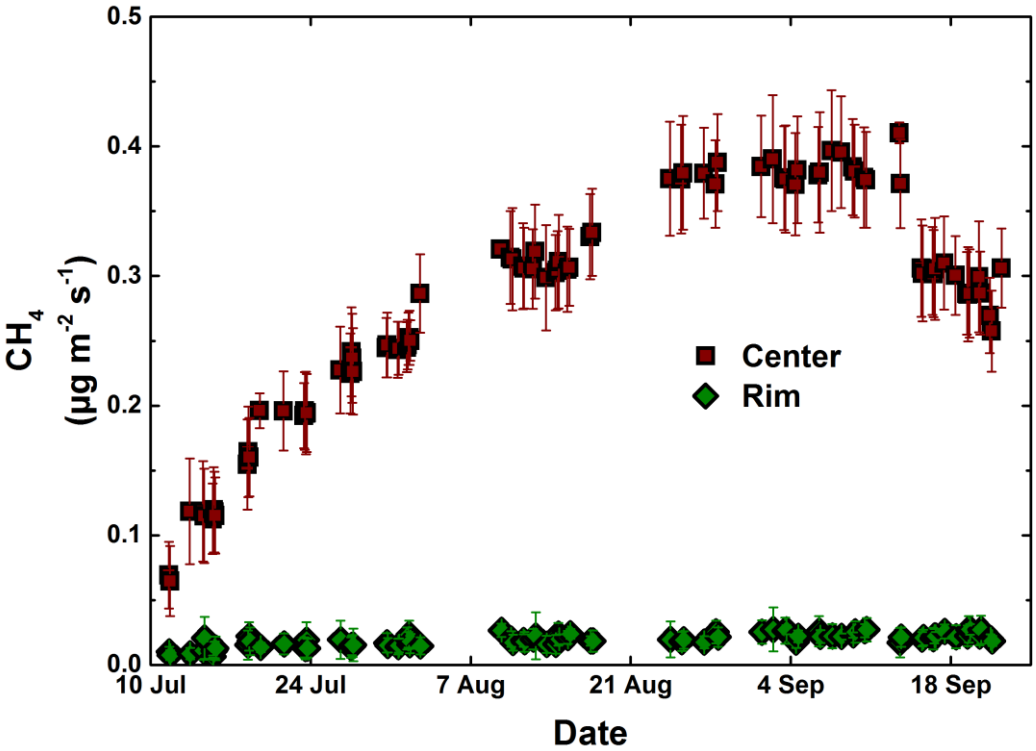

Figure 32: Measured CH_4 fluxes at the polygonal rim and center in 2015. The error bar denote the standard deviation between the four replicate measurements. The averaged standard error of the flux calculation was 0.016 and 0.002 µg m^{-2} s^{-1} at rim (n = 84) and center (n = 85), respectively. The fluxes show a pronounced seasonality at the center with highest fluxes at the beginning of September.

With a mean of 0.30 ± 0.08 µg m^{-2} s^{-1} compared to 0.017 ± 0.004 µg m^{-2} s^{-1} the CH_4 emissions were more than one order of magnitude higher at the polygonal center than at the rim, respectively. The highest CH_4 emissions of 0.41 ± 0.024 µg m^{-2} s^{-1} were measured at the center on 13 September while the lowest emissions were measured on 11 July with just 0.065 ± 0.004 µg m^{-2} s^{-1}. The CH_4 fluxes at the center showed a distinct seasonality with increasing emissions from July on until they reached a peak in mid-September. Afterwards, the CH_4 emissions were decreasing but were still rather high compared to emissions from July. At the polygonal rim, the same seasonal curve was observed, but less

pronounced as at the center. Here, CH_4 emissions were also increasing from the beginning of the measurement period, but no decrease was observed towards the end of September. The highest CH_4 flux at the rim was measured in mid-September with 0.027 ± 0.003 µg m^{-2} s^{-1} while the lowest emission of 0.006 ± 0.002 µg m^{-2} s^{-1} was measured on 15 July. Similar to the CO_2 fluxes, the measurement period can be divided into a peak and a post season. At both microsites, higher CH_4 emissions were measured during the post season. At the polygonal rim, the averaged mean CH_4 fluxes were 0.017 ± 0.004 µg m^{-2} s^{-1} during the peak season and 0.022 ± 0.003 µg m^{-2} s^{-1} throughout the post season. At the polygonal center the CH_4 emissions were about one third lower during the peak season (0.24 ± 0.08 µg m^{-2} s^{-1}) compared to those of the post season (0.36 ± 0.04 µg m^{-2} s^{-1}).

The comparison between the measured CH_4 fluxes from 2014 and 2015 revealed similar emissions at the polygonal rim. At the center, the mean CH_4 emissions in 2014 were higher than the highest single CH_4 fluxes measured in 2015.

5.3.3. Correlation with environmental parameters

Overall, the CH_4 fluxes from 2015 at the polygonal rim and center were poorly explained with environmental variables (Table 6). For both microsites, the environmental variable with the highest explanatory power for the CH_4 emissions was the ALD. However, the ALD explained just 27% and 45% of the CH_4 flux variance at the rim and center, respectively. Furthermore, no clear difference between the tested linear and exponential model was observed. Smaller explanatory power were given by the WT fluctuations and T_{soil} at 2 cm for CH_4 emissions from the center. At the polygonal rim, no further substantial correlation (> 20%) with environmental variables was observed.

The CH_4 fluxes from 2014 at the polygonal rim and center did not correlate significantly with any of the environmental variables. Neither a linear regression nor an exponential regression model was statistically significant ($p < 0.05$).

Table 6: Linear and exponential relationship between CH_4 emissions and environmental parameters in 2015. All relationships at the center (n = 331) and rim (n = 322) were statistically significant (significance level < 0.001). The goodness of the relationships are described by the R^2_{adj}.

Center	R^2_{adj}	**Rim**	R^2_{adj}
ALD lin	0.38	ALD lin	0.27
ALD exp	0.45	ALD exp	0.25
WT lin	0.24	VWC lin	0.14
WT exp	0.23	VWC exp	0.14
T_{surf} lin	0.04	T_{surf} lin	0.03
T_{surf} exp	0.07	T_{surf} exp	0.04
T_{soil} 2 cm lin	0.20	T_{soil} 2 cm lin	0.03
T_{soil} 2 cm exp	0.23	T_{soil} 2 cm exp	0.03
T_{soil} 15 cm lin	0.03	T_{soil} 15 cm lin	0.01
T_{soil} 15 cm exp	0.04	T_{soil} 15 cm exp	0.01

6. Discussion

This discussion focusses on CO_2 and CH_4 fluxes measured in 2015. The flux data from 2014 are just sporadically discussed. The dataset, the variability of fluxes and environmental parameters as well as the measurement period were too small and too short in 2014, which renders a profound interpretation of the data impossible.

6.1. CO_2 fluxes

In this study, the first values of net ecosystem exchange, gross primary productivity, net primary productivity as well as ecosystem respiration, heterotrophic respiration and autotrophic respiration fluxes obtained from modelling approaches for different microsites of the polygonal tundra were presented (Figure 29 and Figure 30). These fluxes are of crucial importance as they show the different response of the underlying processes of NEE to environmental controls over the growing season on a spatial and temporal scale. Good correlations were observed of GPP fluxes with PAR. R_{eco} fluxes correlated with soil and surface temperature, but also with VWC and WT for rim and center, respectively. However, for R_H fluxes the correlations with environmental parameters were smaller than for GPP and R_{eco} fluxes, which demonstrates the complexity and the still limited understanding of the factors controlling these fluxes. Both microsites acted as net sinks for atmospheric CO_2 during the measurement period in 2015, which supports Hypothesis 1. The CO_2 sink strength differed substantially between the microsites (Table 5). This difference is most likely mainly in response to different hydrological conditions, but also to soil temperature and vegetation composition. This finding supports Hypothesis 2, that contrasting hydrological conditions mainly drive the differences in CO_2 fluxes. The cumulative R_{eco} fluxes at the rim are higher as at the center. This is remarkable as high R_{eco} fluxes are generally associated with high GPP fluxes (Bubier *et al.*, 2003), since CO_2 uptake via photosynthesis displays the source of R_A fluxes. This might be caused by comparatively low R_A fluxes at the polygonal center. Despite substantial higher GPP fluxes, the R_A fluxes at the center are within the same range with those from the rim. The comparatively low R_A fluxes at the center might be an effect of contrasting hydrological conditions between both microsites. In total, these differences lead to an almost two-times higher NPP at the polygonal center in relation to the rim.

6.1.1. CO_2 fluxes in comparison with other studies

The daily averaged CO_2 fluxes obtained from the CO_2 models were compared with CO_2 fluxes from other arctic tundra sites that are similar in vegetation and soil composition to the polygonal tundra in the Lena River Delta (Table 7). It has to be noted that measurement periods, plant growth forms and density as well as climatic conditions can differ among the studies. These differences can lead to differences in CO_2 fluxes. However, all values are representing at least a rough estimate of growing season CO_2 surface-atmosphere fluxes of an arctic tundra ecosystem.

The R_{eco} fluxes at both microsites are at the lower end in comparison with other arctic tundra sites (Table 7). Solely, a wet tundra site in the Komi Republic, Russia (Heikkinen *et al.*, 2004), a wet sedge site at Daring Lake, Canada (Nobrega & Grogan, 2008) and a polygonal center site (Oechel *et al.*, 1995) showed R_{eco} fluxes that were within the same range as in this study. The low R_{eco} fluxes reported from this study lead to relatively high NEE fluxes at the polygonal center, benefited by moderate GPP fluxes, compared to other tundra sites. Furthermore, the comparison revealed that comparatively high estimates of NEE were reported solely from wet and sedge-dominated sites (Table 7), but these sites can also act as net source for atmospheric CO_2 (Oechel *et al.*, 1995). The GPP fluxes in some arctic regions are distinctly higher than in the Lena River Delta (Olivas *et al.*, 2011, Ström *et al.*, 2012, Vourlitis *et al.*, 2000, Zamolodchikov *et al.*, 2000). The low GPP fluxes at the polygonal rim are causing, despite low R_{eco} fluxes, a comparatively low NEE at the rim.

Table 7: Comparison of daily averaged CO_2 fluxes from arctic tundra sites. The sites are similar in vegetation and soil composition. All listed fluxes were measured with the closed chamber technique. *: standard error estimated

Location	Tundra type	Period	NEE (g C m^{-2} d^{-1})	GPP (g C m^{-2} d^{-1})	R_{eco} (g C m^{-2} d^{-1})	Ref
Lena River Delta, RU (72°N,127°E)	pol. rim pol. center	Jul-Sep 2015	-0.6 ± 0.4 -1.6 ± 0.3	-1.4 ± 0.4 -2.3 ± 0.2	0.8 ± 0.2 0.7 ± 0.1	a
Lek Vorkuta, RU (67°N, 63°E)	shrub sedge bog	Jul-Aug 1996	-0.6 ± 0.3 -1.0 ± 0.2	-4.5 ± 0.4 -3.2 ± 0.4	3.9 ± 0.3 2.2 ± 0.3	b
Prudhoe Bay, US (70°N, 149°W)	pol. tundra	Jun-Aug 1994	-0.6 ± 0.4	-5.2 ± 0.6	4.6 ± 0.3	c
Lek Vorkuta, RU (67°N, 63°E)	wet peaty tundra	Jun-Sep 2001	-1.1 ± 0.2	-1.9 ± 0.2*	0.9 ± 0.2*	d
Daring Lake, CA (65°N, 111°W)	dry heath mesic birch wet sedge	Jun-Sep 2004	-0.01 ± 0.1 -0.4 ± 0.3 -0.9 ± 0.1	-1.7 ± 0.3 -3.2 ± 0.5 -1.7 ± 0.1	1.8 ± 0.2 2.8 ± 0.3 0.8 ± 0.1	e
Barrow, US (71°N, 157°W)	pol. rim pol. center pol. rim pol. center	Jun-Aug 2005 Jun-Aug 2006	-0.1 ± 0.5 -0.2 ± 0.2 -0.7 ± 0.2 -0.8 ± 0.2	-3.7 ± 0.2 -3.1 ± 0.1 -3.1 ± 0.3 -2.3 ± 0.2	3.6 ± 0.3 2.9 ± 0.1 2.4 ± 0.2 1.5 ± 0.2	f
Barrow, US (71°N, 157°W)	pol. center	Jun-Aug 1992	0.04 ± 0.05	-0.8 ± 0.1	0.8 ± 0.1	g
Zackenberg, GL (74°N, 20°W)	sedge-dom. fen	Jun-Aug	-2.6 ± 0.3	-5.6 ± 0.4	3.0 ± 0.1	h

a: This study; b: Zamolodchikov *et al.* (2000); c: Vourlitis *et al.* (2000); d: Heikkinen *et al.* (2004); e: Nobrega and Grogan (2008); f: Olivas *et al.* (2011); g: Oechel *et al.* (1995); h: Ström *et al.* (2012)

6.1.2. Environmental controls on CO_2 fluxes

The polygonal tundra on Samoylov Island in the Lena River Delta has to be considered as an ecosystem with low GPP due to low vascular plant coverage with a maximum leaf coverage of 0.3 (Kutzbach *et al.*, 2007b). Mosses, which have a high leaf coverage (> 0.9), are dominant at both microsites and have, similar to lichens, a much lower photosynthetic capacity than vascular plants (Brown *et al.*, 1980). Furthermore, photosynthesis of vascular plants in arctic tundra ecosystems is restricted by a low nutrient availability. This is true for most tundra soils due to often water-logged and cold soil conditions (Oechel *et al.*, 1998), as these conditions ensure low microbial decomposition rates (Hobbie *et al.*, 2002), which in turn lead to a low supply of bioavailable nutrients (Beermann *et al.*, 2015). However, following the explanation of Kutzbach *et al.* (2007b), the soils at the study site can be considered as extremely nutrient-poor as the study site is one of the coldest permafrost regions on the earth (Romanovsky *et al.*, 2010), the parent material consists of nutrient-poor sands and the Holocene river terrace is due to its elevation not regularly

flooded, so that fresh nutrient input via water transport is lacking. Additionally, the net radiation at the study site from June to August is with a mean of 85 W m^{-2} (1999-2011) lower than those reported from most other arctic tundra sites (Boike *et al.*, 2013). These factors might explain the comparatively low GPP fluxes at the polygonal rim and center at the study site compared to other arctic tundra sites.

Differences in GPP fluxes between the rim and center are also related to the vascular plant coverage. The polygonal center has a much higher abundance of sedges while the rim is moss-dominated (Table 4) and the sparsely spread vascular plants have shorter and fewer leaves. Therefore, the photosynthetic capacity of the center is higher, which results in higher GPP. Additionally, limited water availability due to the elevation of the polygonal rim allows moisture to run off and desiccate the moss layer at the rim, which then would lead to decreasing GPP fluxes (Olivas *et al.*, 2011). On the other hand, Olivas *et al.* (2011) found GPP fluxes to be higher at the polygonal rim than at the polygonal center (Table 7). They related low GPP fluxes at the center to submersion of the moss layer and vascular plants at the center, which requires a constant WT above the soil surface. At the polygonal center from this study, the WT was frequently below the soil surface so that submersion is impeded partwise. This difference in GPP fluxes between both study sites reveals the importance of the water level and fluctuations throughout the season as they obviously can have an impact on GPP fluxes. However, the addition of WT and VWC values as parameter did not improve the GPP model (Table 2). An impact of hydrological conditions on GPP fluxes in this study might be low due to missing continuous plant submersion or might be masked due to contrasting PAR values and WT/VWC fluctuations.

Differences in NEE fluxes between the microsites can also be related to their different soil conditions. Cold and water-logged soil conditions, such as in polygonal depressions like the centers, inhibits decomposition and mineralization of SOM due to oxygen limitation which causes low microbial activity (Hobbie *et al.*, 2002). On the other hand, the moisture run-off at the rim creates dry conditions at the rim, which increases soil oxygen availability and therefore enhances R_{eco} and R_H (Oechel *et al.*, 1998). The higher diurnal amplitude of the soil temperature (Figure 15), a product of the thermic buffer function of the standing water at the center, leads to higher daily soil temperatures at the polygonal rim compared to the center. These higher temperatures are causing higher decomposition rates and

therefore higher R_H fluxes in relation to sites with high water levels. Hence, low NEE estimates at the rim are occurring not only because of lower GPP but also due to higher R_{eco} fluxes compared to the center. In general, respiration fluxes from the polygonal tundra of the Lena River Delta are expected to be low since the factors controlling R_{eco} and R_H are not favorable for a high respiration rates at this site (Gorham, 1991). This finding is in good agreement with Nobrega and Grogan (2008) who compared a wet sedge with a dry heath and a mesic birch site and found that the NEE at the wet sedge site is highest (Table 7). They concluded that SOC accumulation in wet-sedge tundra is highest because respiration is restricted due to the water-logged conditions.

Interestingly, measurements of CO_2 fluxes at the polygonal rim show an increase of NEE throughout September. This increase cannot be explained with higher PAR or temperature during this time of the season and at the polygonal center the net CO_2 uptake was continuously decreasing during September. Instead, the increase of net CO_2 uptake at the rim towards the end of measurement period can be related to the photosynthetic activity of mosses. Mosses can remain photosynthetic active for years (Collins & Oechel, 1974) and Kutzbach *et al.* (2007b) considered the September at the EC footprint area as period where C uptake occurs mostly due to moss photosynthesis. During this time of the growing season, mosses can still assimilate substantial amounts of CO_2 because they tend to reach light saturation at lower irradiance (Harley *et al.*, 1989). The photosynthetic activity of mosses declines rapidly when they face desiccation, because they cannot control their tissue water content (Turetsky *et al.*, 2012). It was also shown that mosses face light stress during times of high PAR (Murray *et al.*, 1993). This light stress causes delayed senescence and more late-season photosynthesis (Zona *et al.*, 2011). Therefore, the photosynthetic activity at the polygonal rim is expected to be low during warm and dry weather periods like at the beginning of September (Figure 15) and during times of high PAR. With continuous rainfall, dew formation and lower PAR in mid-September, the mosses resume metabolic active, which leads to increasing net CO_2 uptake at the rim.

6.1.3. Heterotrophic respiration fluxes in arctic tundra ecosystems

The comparison of R_H fluxes in 2015 from sampling plots that were trenched in 2014 to those that were trenched in 2015 showed no significant differences (Figure 26). In

contrast to that, the contribution of R_H to R_{eco} fluxes at the rim in 2014 was remarkably higher as in 2015 and the measured R_H fluxes partwise exceeded the measured R_{eco} fluxes. It is assumed that these high R_H fluxes are an artefact of the root-trenching, most likely due to the additional decomposition of residual roots which is one of the main drawbacks of this method (Figure 4) (Subke *et al.*, 2006). However, Shurpali *et al.* (2008) suggested that this artefact contribute little to R_H fluxes several months after the treatment. It is therefore assumed, that the root-trenching method produced reliable R_H fluxes at the study site in 2015 as no evidence of a significant over- or underestimation was observed one year after the treatment.

To date, there are just a few estimates of growing season R_H fluxes from arctic tundra ecosystems (Table 8). Differences in R_H fluxes between the tundra sites may be caused by different time of waiting after the treatment. Nobrega and Grogan (2008) started the R_H measurements one day after clipping, while measurements for this as well as for the study of Biasi *et al.* (2014) started about one year after the treatment. Therefore, even though the partitioning approach for seasonal estimates of R_H fluxes is similar for all studies, a comparison has to be handled with caution. The few R_H flux estimates from other arctic tundra sites are comparatively higher than the R_H values from the Lena River Delta (Table 8). Considerable higher R_H fluxes throughout the growing season were measured at a mesic birch and a dry heath site at Daring Lake in Canada (Nobrega & Grogan, 2008) and at a bare peat site in the subarctic tundra at Seida, Russia (Biasi *et al.*, 2014). Both sites contained substantial higher amounts of SOC in the organic-rich layer, which most likely explain higher R_H fluxes due to higher decomposition rates. R_H fluxes within the same range as in this study were solely measured at a wet sedge site in Daring Lake where soil and environmental conditions like ALD, soil temperature, vegetation and SOC were similar and at a dry peat site in Seida. Despite these differences, the averaged contributions of R_H to R_{eco} of 42% at the center and 60% at the rim are in good agreement with those observed at Seida (37 – 64%) and Daring Lake (44 – 64%). Similar contributions were determined from an arctic tussock tundra site where R_H makes up approximately 40% of growing season R_{eco} (Segal & Sullivan, 2014) and from a moist acidic tussock tundra site (Hicks Pries *et al.*, 2013). In contrast to these results, Dorrepaal *et al.* (2009) determined a substantial higher contribution of R_H to R_{eco} with about 70% in a subarctic peatland.

Table 8: Comparison of daily averaged R_H fluxes. The differences between the sites are most probably caused by substrate availability, with higher R_H fluxes simultaneously to higher SOC contents. All listed fluxes were measured with the closed chamber technique.

Location	Tundra type	Period	R_H (g C m^{-2} d^{-1})	Ref
Lena River Delta, RU (72°N,127°E)	polygonal rim polygonal center	Jul-Sep 2015	0.5 ± 0.1 0.3 ± 0.02	a
Daring Lake, CA (65°N, 111°W)	dry heath mesic birch wet sedge	Jun-Sep 2004	0.8 ± 0.1 1.8 ± 0.2 0.4 ± 0.1	b
Seida, RU (67°N, 63°E)	dry peat moist peat bare peat shrub tundra heath	Jun-Sep 2008	0.4 ± 0.03 0.6 ± 0.2 1.0 ± 0.04 0.6 ± 0.07	c

a: This study; b: Nobrega and Grogan (2008); c: Biasi *et al.* (2014)

6.1.4. Spatial variability of heterotrophic respiration fluxes

The partitioning of R_{eco} fluxes revealed a higher contribution of R_H to R_{eco} at the polygonal rim compared to the polygonal center. This difference of the R_H/R_{eco} ratio can be related to differences in vascular plant coverage and moisture conditions between both microsites. Higher GPP as at the center compared to the rim causes also higher rates of R_A and in turn lowers the contribution of R_H to R_{eco}. Additionally, anoxic soil conditions due to standing water at the center are not favorable for decomposition of SOM. Furthermore, Nobrega and Grogan (2008) concluded that consistently moderate moisture conditions, as at the rim microsite, promotes fast decomposition of SOM and therefore ensures high R_H rates. In general, R_H fluxes are expected to correlate with SOC contents, where higher SOC contents promote higher R_H fluxes (Biasi *et al.*, 2014, Lavoie *et al.*, 2011). However, SOC contents at the polygonal center were about two-times higher in the upper soil layer compared to the rim (Figure 18 and Figure 19), but R_H fluxes were lower. This relationship is most likely masked by other environmental factors, most dominantly by anoxic conditions at the center and higher abundance of vascular plants. Furthermore, other factors such as soil physical conditions (Schimel *et al.*, 1994) as well as the soil microbial community composition and quantity (Elberling *et al.*, 2008a) can influence the R_H/R_{eco} ratio.

Höfle (2015) reported differences of the SOM composition in the polygonal tundra on Samoylov Island: The SOM of polygonal centers consist of mostly undecomposed

plant-derived SOM with relatively young ^{14}C ages, whereas the rims consist of much older, little-decomposed plant material. Based on these findings, a slow microbial SOM degradation at the rim is suggested (Höfle, 2015). However, the differences of the R_{eco} and R_H fluxes between rim and center from this study lead to an opposing assumption. The fact that at the center, despite higher GPP fluxes, the R_{eco} and R_H fluxes are lower compared to those from the rim, indicates a higher microbial decomposition rate at the rim. It could be suggested that higher ^{14}C ages with increasing soil depth, found by Höfle (2015) at the polygonal rim, are because of high decomposition rates of fresh plant material at this microsite. In general, easily decomposable C compounds with young ^{14}C ages (available from fresh plant material) are mineralized faster as more stable C compounds (von Lützow *et al.*, 2008, Walz *et al.*, 2017), and the amount of more stable C compounds increases with soil depth (Schädel *et al.*, 2014), which could lead to a pronounced age stratification in the soil. In turn, younger ^{14}C ages at the center might be caused by accumulation of recent plant material due to low decomposition rates in this water-logged environment, observed by low R_{eco} and R_H fluxes in this study. Furthermore, cryoturbation in the soils of polygonal rims could heave SOM with relatively old ^{14}C ages upward into soil layers with younger SOM, which would lead to a pronounced age stratification in these soils.

The averaged contribution of R_H to R_{eco} fluxes during the measurement period in 2015 were 42% at the center and 60% at the rim. Thus, Hypothesis 3, that the contribution of R_H on R_{eco} is below 50% during the growing season, can be supported for R_H fluxes at the polygonal center, but has to be rejected for R_H fluxes at the rim. Neither at the rim nor at the center was a seasonal trend of the R_H/R_{eco} ratio observed. This is in contrast to a study from Segal and Sullivan (2014) where the R_H/R_{eco} ratio increased towards the end of the growing season, most likely due to deepening of the active layer which increases substrate availability for R_H processes. This effect might be missed in this study because of smaller changes in ALD (Figure 15) as well as lower soil temperatures throughout the growing season at the study site compared to other arctic tundra sites. Also other factors like increased substrate availability due to plant senescence and root mortality are suggested to lead to an increased R_H/R_{eco} ratio towards the end of the growing season in prairie grasslands (Gomez-Casanovas *et al.*, 2012). Whether these factors are of major

importance in arctic tundra ecosystems remains uncertain as it was recently shown that increased substrate availability via priming has minor effects on R_H fluxes in the active layer (Walz *et al.*, 2017). Even at the end of the measurement period, considerable GPP fluxes were measured, which in turn means that substantial amounts of plants are still photosynthetically active. Therefore, these active plants are not yet providing dead plant material as substrate to prime microbial decomposition, which would lead to higher R_H fluxes. Based on this finding, it is concluded that the investigation period was too short to observe significant changes in the R_H/R_{eco} ratio and an increase of this ratio may be observed later in the year. Therefore, Hypothesis 4, that the R_H/R_{eco} ratio has a distinct seasonality with higher values towards the end of the season cannot be answered.

Interestingly, significant correlations of the WT fluctuations with the R_H/R_{eco} ratio and R_A fluxes (Figure 27), but no correlation between R_H fluxes and WT were observed. Most likely, the R_A fluxes are negatively affected by high WT due to submersion of the moss layer and vascular leaf area as submersion can lead to plant stress which reduces productivity and nutrient turnover (Gebauer *et al.*, 1995). R_H fluxes might be unaffected by variations of high standing water as the decomposition of SOM takes place in deeper parts of the soil, which are permanently water-saturated. Only in times of remarkable low WT the R_H/R_{eco} ratio increases, which shows low R_A contribution during these periods. Too low soil moisture contents can limit the growth and productivity of an ecosystem (Chen *et al.*, 2015) as desiccation lowers the photosynthetic activity (Turetsky *et al.*, 2012) and in turn lowers R_A fluxes. This could lead to the observed increase of the R_H/R_{eco} ratio simultaneously to a lower water table. These findings show the importance of the WT and VWC for R_{eco} fluxes. The relationship between R_A fluxes and WT fluctuations explain the need of WT and VWC for the reproduction of the R_{eco} fluxes (and not for the R_H fluxes) over the complete measurement period using the empirical Q_{10} model.

6.2. CH_4 fluxes

6.2.1. Factors regulating CH_4 fluxes

The CH_4 emissions from the polygonal rim and center in 2015 can partwise be explained with environmental variables (Table 6). In contrast to that, no significant correlation was found between CH_4 emissions from polygonal rim and center in 2014. However, the CH_4

emissions in 2014 showed a much lower range as in 2015 (Figure 31 and Figure 32) and the measurements are limited to just 17 days in August. This may cause poor correlations with environmental variables as within this rather short period the environmental variables also showed low variations (Figure 12 and Figure 13). The environmental parameter with the highest explanatory power of the CH_4 fluxes in 2015 for both microsites was the ALD. Therefore, Hypothesis 5, that the soil temperature has the highest explanatory power of CH_4 fluxes, is rejected. However, this finding is in good agreement with other studies who found the ALD to be an important predictor of CH_4 emissions (Friborg *et al.*, 2000, van Huissteden *et al.*, 2005). A relationship between ALD and CH_4 emissions could indicate a substantial contribution to CH_4 emissions from deeper soil layers (Wille *et al.*, 2008). A higher active layer increases the microbial active soil column and are accompanied with higher soil temperatures, which causes higher methanogenic activity (Wagner *et al.*, 2007). In contrast to that, Olefeldt *et al.* (2013) found no correlation between CH_4 emissions and ALD by assembling several studies on CH_4 fluxes from arctic ecosystems. However, the relationship of ALD and CH_4 emissions is likely to be masked in many ecosystems by decreasing soil temperatures with increasing soil depth, which causes lower microbial activity (Conrad, 1996), even if the microorganisms are adapted to cold conditions (Wagner *et al.*, 2007). In turn, the soil temperature has been identified by many studies to be one of the main environmental parameter controlling CH_4 emissions in wetlands (e.g. McEwing *et al.*, 2015, Olefeldt *et al.*, 2013, Wille *et al.*, 2008). In this study, the soil temperature poorly explained CH_4 emissions from the polygonal rim, whereas at the center the correlation was slightly better (Table 6). This is in accordance to Olefeldt *et al.* (2013), who suggested that ecosystems with a WT at or above the soil surface are more sensitive to soil temperature variability than drier ecosystems. It was previously shown that a good correlation between soil temperature and CH_4 fluxes only occurs at inundated sites, with a WT distinctly above the soil surface (Nykänen *et al.*, 1998). If the WT is close to the soil surface or even below, as at the polygonal rim and center, the upcoming methane oxidation is suggested to mask the relationship between soil temperature and CH_4 emissions (Kutzbach *et al.*, 2004, Zhu *et al.*, 2014). As a result of that, CH_4 fluxes can often be related to the WT fluctuations (Marushchak *et al.*, 2016, Olefeldt *et al.*, 2013). However, at polygonal rim and center, WT and VWC had a weak explanatory power of the CH_4 emissions in 2015 (Table 6). The effect

of WT fluctuations on CH_4 emissions are described as an on-off switch (Christensen *et al.*, 2003). Some authors suggested that a water table just slightly below the soil surface can cause high CH_4 oxidation rates (Kutzbach *et al.*, 2004, Whalen *et al.*, 1996). Even under water-saturated soil conditions substantial amounts of CH_4 can be oxidized by brown mosses at the study site (Liebner *et al.*, 2011). Furthermore, it was shown that CH_4 emissions are not always well correlated with water table fluctuations and that dry periods can lower CH_4 emissions considerably even after rewetting (Brown *et al.*, 2014). All these findings can lead to a weak correlation between the water table and CH_4 emissions.

Another factor regulating CH_4 production and consumption processes might be given by the pH value. Both methanotrophs and methanogens are known to be neutrophilic (Hanson & Hanson, 1996, Whalen, 2005) and the optimum pH of methane production and oxidation in subarctic peatlands is suggested to be 5.5-7.5 and 5.0-6.5, respectively (Dunfield *et al.*, 1993). On the other hand, Valentine *et al.* (1994) observed a significant reduction of CH_4 production potential by lowering the pH from 7.0 to 5.5 in a northern fen and Kamal and Varma (2008) suggested more acidic pH values as favorable for the growth of methanotrophs. The comparison between the pH values of the porewater analysis from the center (Figure 20) and CH_4 fluxes (Figure 32) reveals a linear relationship between emissions and pH. Here, highest emissions were measured during times when the pH was most acidic ($R^2 = 0.73$ – data not shown). This might give evidence for an impact of soil porewater pH on CH_4 emissions. However, as data on porewater pH are very scarce during the measurement period, the assumed relationship cannot be fully investigated.

6.2.2. CH_4 fluxes in comparison with other arctic tundra sites

The averaged CH_4 fluxes were compared with reported CH_4 fluxes from arctic tundra sites that are similar in vegetation and soil composition (Table 9). In general, the comparison revealed large differences of the CH_4 emissions between study sites and sampling years. These differences might be caused due to different environmental conditions, different sampling strategies and measurement periods. For instance, methodological differences are the chamber size and equipment as well as closure times, sampling periods and

frequencies. Nevertheless, as all listed studies were conducted in the polygonal tundra, or at least in ecosystems that are similar to the polygonal tundra, this comparison provides a profound overview about CH_4 fluxes from these ecosystems.

The determined CH_4 fluxes from this study are at the lower end in comparison with CH_4 fluxes from other studies (Table 9). A set of studies from wet tundra sites reported more than four-fold higher CH_4 fluxes compared to the polygonal center CH_4 emissions from this study in 2015 (Bartlett *et al.*, 1992, McEwing *et al.*, 2015, Ström *et al.*, 2012, van Huissteden *et al.*, 2005, Vaughn *et al.*, 2016). Studies of CH_4 emissions from relatively dry tundra sites also determined partially distinctly higher CH_4 fluxes compared to the polygonal rim of this study (van Huissteden *et al.*, 2005, Vaughn *et al.*, 2016). Only a few studies determined CH_4 emissions from wet tundra (Heikkinen *et al.*, 2002, Marushchak *et al.*, 2016) and dry tundra ecosystems (Davidson *et al.*, 2016) that were lower as CH_4 emissions from this study.

The rather low CH_4 emissions from the polygonal tundra on Samoylov Island can be related to low SOM contents and permafrost temperatures. Furthermore, the soils of the polygonal tundra on Samoylov Island are characterized by a sandy texture, which is not a favorable habitat for methane producing microbes (Wagner *et al.*, 1999). The low permafrost temperature at the study site (Boike *et al.*, 2013, Romanovsky *et al.*, 2010) is suggested to lead to low CH_4 production rates as methanogenesis is controlled by temperature (Whalen, 2005). The soil organic matter contents are of major importance for CH_4 emissions. The comparison between CH_4 fluxes from this and other studies (Table 9) shows that highest CH_4 emissions were measured in organic soils (Bartlett *et al.*, 1992, McEwing *et al.*, 2015, Ström *et al.*, 2012, Vaughn *et al.*, 2016), while CH_4 emissions from mineral soils are generally lower. This is in good agreement with Knoblauch *et al.* (2015) who suggested that low SOM contents in the polygonal tundra of the Lena River Delta are a reason for comparatively low CH_4 emissions. Furthermore, SOM contents are found to be positively correlated with CH_4 emissions across several tundra ecosystems (Christensen *et al.*, 1995).

Table 9: Comparison of daily averaged CH_4 fluxes measured at various arctic tundra sites. The sites are similar in vegetation and land cover class. All listed fluxes were measured with the closed chamber technique. The soils are categorized as organic if SOC contents are > 20%. *: standard error not available

Location	Tundra type	Period	Soil	CH_4 flux (mg m^{-2} d^{-1})	Ref
Lena River Delta, RU (72°N, 127°E)	polygonal center polygonal rim polygonal center polygonal rim	August 2014 Jul-Sep 2015	mineral mineral mineral mineral	38.4 ± 2.2 1.7 ± 0.2 24.1 ± 2.9 1.7 ± 0.6	a
Yukon Delta, US (60°N, 162°W)	wet tundra dry upland tundra	Jul-Aug 1988	organic organic	143.6 ± 31.1 2.3 ± 1.1	b
Lek Vorkuta, RU (67°N, 63°E)	wet flark	Jun-Sep 1999	organic	6.0 ± *	c
Lena River Delta, RU (72°N, 127°E)	polygonal center polygonal rim	Aug 1999	mineral mineral	28.0 ± 5.4 4.3 ± 0.8	d
Tiksi, RU (72°N, 130°E)	wet sedge tundra	Jul-Aug 1993	organic	46.3 ± *	e
Lena River Delta, RU (72°N, 127°E)	polygonal centers polygonal rim	Jul-Sep 2006	mineral mineral	86.2 ± 25 4.9 ± 10	f
Zackenberg, GL (74°N, 20°W)	sedge-dom. wet tundra	Jun-Aug	organic	130.6 ± 13	g
Chokurdakh, RU (71°N, 147°E)	wet (pol.) tundra dry (pol.) tundra	Jul 2004	organic mineral	171.4 ± * 4.3 ± *	h
Lena River Delta, RU (72°N, 127°E)	polygonal center polygonal rim	Jun-Sep 1999	mineral mineral	53.2 ± 8.7 4.7 ± 2.5	i
Seida, RU (67°N, 63°E)	sedge-dom. tundra	Jul-Oct 2007 May-Oct 2008	organic	10.1 ± 1.0 6.8 ± 1.3	j
Barrow, US (71°N, 157°W)	wet sedge tundra	Jul-Sep 2013	organic	108.5 ± 10.8	k
Barrow, US (71°N, 157°W)	wet sedge tundra dry tundra	Jun-Aug 2014	organic organic	40.3 ± 48.5 1.4 ± 3.6	l
Barrow, US (71°N, 157°W)	polygonal center polygonal rim	Jul-Oct 2013	organic organic	122.2 ± 63.6 24.2 ± 18.0	m

a: This study; b: Bartlett *et al.* (1992); c: Heikkinen *et al.* (2002); d: Kutzbach *et al.* (2004); e: Nakano *et al.* (2000); f: Sachs *et al.* (2010); g: Ström *et al.* (2012); h: van Huissteden *et al.* (2005); i: Wagner *et al.* (2003); j: Marushchak *et al.* (2016); k: McEwing *et al.* (2015); l: Davidson *et al.* (2016); m: Vaughn *et al.* (2016)

6.2.3. CH_4 fluxes in comparison with earlier studies from Samoylov Island

Beside this study, three other studies focused on CH_4 emissions from the polygonal tundra on Samoylov Island on the microscale (Kutzbach *et al.*, 2004, Sachs *et al.*, 2010, Wagner *et al.*, 2003). Between these studies very large differences of CH_4 emissions from polygonal center and rim were determined: Kutzbach *et al.* (2004) found CH_4 fluxes from a polygonal center that were within the same range as determined in this study in 2015, even though the CH_4 emissions were measured just in August. On the other hand, Wagner *et al.* (2003) and Sachs *et al.* (2010) found the CH_4 fluxes from a polygonal center to be

substantial higher compared to CH_4 emissions from this study (Table 9). Additionally, the CH_4 emissions from polygonal rims were within the same range between the three studies, but differ significantly to determined fluxes from this study. These differences most likely display the large temporal and spatial variability of CH_4 fluxes on microsite even within the same study site. Variable biotic and abiotic conditions between the study years most likely cause these differences. For instance, different pH values are suggested to could have an impact on CH_4 production and oxidation rates (see section 6.3.1.). While the soil porewater at the center from this study was slightly acidic (Figure 20), Wagner *et al.* (2003) measured pH values between 7.4 and 7.9. These slightly alkaline pH values could increase the rates of methanogenesis and decrease the methane oxidation (Kamal & Varma, 2008, Valentine *et al.*, 1994), which would partly explain higher measured CH_4 emissions from Wagner *et al.* (2003) compared to those from this study. Furthermore, disparities in the sampling procedure as well as the calculation of the CH_4 fluxes might explain the fluxes differences between years. The use of different regression models for the flux calculation can lead to substantial differences of the fluxes (Kutzbach *et al.*, 2007a). While in this study as well as in the study from Kutzbach *et al.* (2004), the CH_4 emissions were calculated using a linear regression model, Sachs *et al.* (2010) used a non-linear regression model for the flux calculation (Figure 33). It is well known that there is a non-linear nature of gas concentration evolution over time in closed chambers due to disturbance of the gas concentration gradient during the chamber measurement (Hutchinson *et al.*, 2000, Livingston *et al.*, 2006). Nevertheless, as mentioned in the section 4.5.1., a linear regression model can produce a better flux estimate for a non-linear concentration-over-time curve than a non-linear regression model (Görres *et al.*, 2014).

Furthermore, initial pressure shocks could lead to an overestimation of CH_4 emissions, but it remains uncertain, if they can explain the discrepancies of CH_4 emissions from this study to those from Wagner *et al.* (2003) and Sachs *et al.* (2010). At least initial pressure shocks could possibly explain the distinct non-linear flux evaluation of CH_4 fluxes measured by Sachs *et al.* (2010) (Figure 33). In general, if no attention is paid to initial pressure shocks, the CH_4 fluxes can be substantially overestimated even if the flux calculation was done with a linear regression model (Christiansen *et al.*, 2011). This especially holds true for flux

estimates based on measurements, where samples are taken in intervals of up to several minutes or based on one-point measurements (like Wagner *et al.* (2003)), as it is possible that initial pressure shocks are missed.

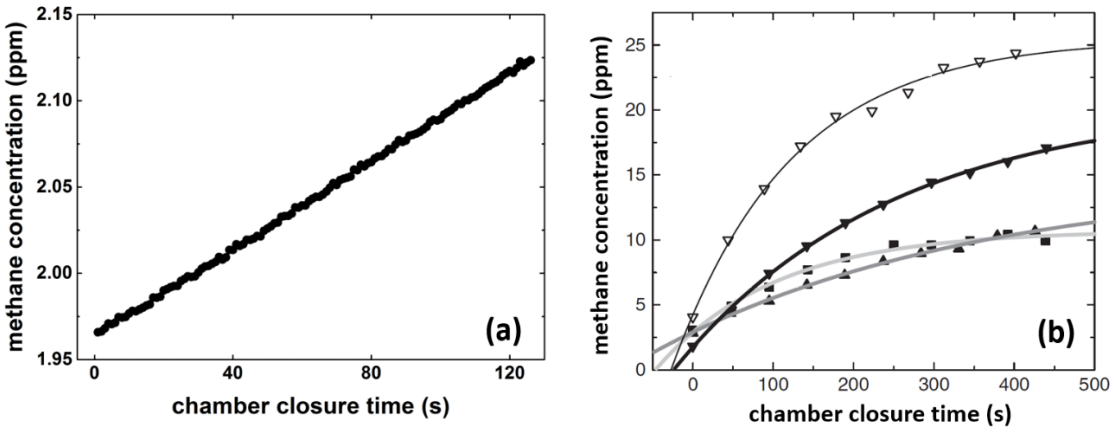

Figure 33: Examples of different concentration-over-time curves of CH_4 fluxes. Panel (a) shows the concentration-over-time curve from CH_4 fluxes measured in this study. Panel (b) is modified after figure 4 in Sachs *et al.* (2010). The distinct non-linearity of the CH_4 fluxes measured by Sachs *et al.* (2010) might be an artefact of the chamber placement, called initial pressure shocks. Note the different scale of both axis between panel (a) and (b).

The measured CH_4 fluxes in 2014 and 2015 from this study showed no difference between years in CH_4 emissions at the polygonal rim (Table 9). In contrast to that, the CH_4 emissions at the center were distinctly higher in 2014 compared to 2015. This difference might demonstrate the inter-annual variability of CH_4 emissions at the polygonal tundra. A possible reason for higher CH_4 emissions in 2014 is the higher air temperature in August 2014 (about 2 °C higher as in August 2015). As mentioned in section 6.3.1., the temperature is assumed to be a major driver of CH_4 fluxes and could therefore be a possible explanation for CH_4 flux differences between the studies in 2014 and 2015. If the measured CH_4 emissions in 2014 are compared to a period of same length in 2015, where highest CH_4 emissions occurred, the gap between the emissions decreases: Between 24 August and 13 September 2015 a daily averaged CH_4 emission of 0.37 ± 0.08 µg m^{-2} s^{-1} was measured, which is close to the mean emissions of 0.45 ± 0.03 µg m^{-2} s^{-1} in 2014. It might be possible that the measurement period in 2014 only contains the peak of CH_4 emissions, which occurred later in 2015. This would result in higher mean CH_4 emissions in comparison to the same period in 2015, where the peak emissions were measured about three weeks later (Figure 32). However, the measurement period in 2014 was too

short to gain a sufficient insight into the seasonality of the CH emissions for reliable estimates of the CH_4 flux dynamics in 2014.

6.2.4. CH_4 flux differences on the microscale

A considerable difference between CH_4 emissions of the polygonal center and rim was observed in this study (Figure 31 and Figure 32). These differences can be attributed to a set of differing environmental and physical controls influencing CH_4 production, oxidation as well as release mechanisms. One of the main factors leading to a substantial difference between microsites is the water table (e.g. Harazono *et al.*, 2006, Marushchak *et al.*, 2016, Olefeldt *et al.*, 2013). With a water table close to the soil surface, the methane production zone at the center has a higher thickness as at the rim, where the water table is just a few centimeters above the permafrost table (Figure 16). This difference causes most likely higher CH_4 production rates at the polygonal center compared to the rim. Due to non-water-saturated conditions at the rim, most parts of the active layer are well aerated, which means a higher thickness of the methane oxidation zone in relation to the center. Additionally, due to non-water-saturated conditions, ebullition as transport mechanism of CH_4 molecules from the soil to the atmosphere is lacking at the rim.

The vegetation composition is another factor that possibly explains the CH_4 flux differences between the microsites. At the polygonal center, higher growth forms and abundance of *Carex Aquatilis* were observed compared to the rim (Table 4). It is well established that the abundance of sedges is an important factor controlling CH_4 emissions (King *et al.*, 1998, Verville *et al.*, 1998) as they provide a transport mechanism for CH_4 where oxic zones of the soil are bypassed, namely plant-mediated transport (Kutzbach *et al.*, 2004). Also the height of vascular plants is suggested to cause higher CH_4 emission rates due greater CH_4 transport capacities as well as enhancement of substrate supply for methanogenesis with taller plants (von Fischer *et al.*, 2010). Substrate availability is identified as one of the main drivers of CH_4 fluxes (Christensen *et al.*, 2003, McEwing *et al.*, 2015). In deeper soil layers at the polygonal center, the substrate availability, higher SOC and N values serve here as proxy for higher substrate availability, was distinctly higher as at the rim (Figure 18 and Figure 19). On the other hand, vascular plants are transporting oxygen to their roots which supports methanotrophic activity in the surrounding soil

(Conrad, 1996, Harazono *et al.*, 2006), but this effect is suggested to play a minor role at the center due to presumably high CH_4 production rates in the soil. There is evidence that in mosses of water-logged soils higher methanotrophic activity takes place compared to unsaturated soils (Vecherskaya *et al.*, 1993), probably due to symbiotic-like relations of mosses and methanotrophs as in brown mosses (Liebner *et al.*, 2011). These findings lead to the suggestion that methanotrophic activity is higher at the polygonal center as on the rim, lowering the difference of CH_4 emissions between the microsites. However, this effect might has just a low impact on total CH_4 fluxes as in water-saturated soils the CH_4 production rate exceed the rate of methane oxidation by far. Furthermore, it is suggested that the higher ALD at the center causes higher CH_4 emissions. An enlargement of the ALD is accompanied by an increase of the methane production zone, which is supported by the correlation of ALD with measured CH_4 emissions from rim and center (Table 6). In contrast to that, Olefeldt *et al.* (2013) found no correlation between CH_4 emissions and active layer depth by compiling various studies on CH_4 fluxes across permafrost landscapes. The different dependencies of CH_4 fluxes on environmental parameters across different arctic tundra sites highlight the complicated the determination of their individual impact on CH_4 production, oxidation and transport mechanisms.

The averaged CH_4 emissions at the polygonal rim show that this microsite acts as net source for atmospheric CH_4 (Table 9). Furthermore, not a single measured CH_4 flux showed a net uptake of CH_4 neither at the rim, nor at the center (Figure 31 and Figure 32). Therefore, Hypothesis 6, that the polygonal rim act as sink for atmospheric CH_4 is rejected. This is in contrast to other studies who found substantial net CH_4 uptake rates in non-water-saturated high arctic tundra soils in Zackenberg, Greenland (Jørgensen *et al.*, 2015) and antarctic tundra soils (Zhu *et al.*, 2014). These CH_4 uptake rates are positively correlated to soil temperatures. In this study, however, no significant correlation between CH_4 emissions and soil temperature was observed, but a correlation might be masked due to simultaneously increasing methanogenesis with higher soil temperatures. It is suggested that substrate availability and soil temperatures are of major importance for the differences of CH_4 sink strengths between these ecosystems. The SOC contents of dry tundra soils in Greenland are lower than those at the polygonal rim (Figure 19 and Elberling *et al.* (2008b)). This most likely lowers the methanogenesis in these soils as a low

substrate availability is not favorable for CH_4 production (Ström *et al.*, 2012). The soil temperatures at the polygonal rim were higher than soil temperatures at antarctic tundra soils (Figure 15 and Zhu *et al.* (2014)). As the CH_4 production has a lower temperature dependence than the CH_4 oxidation (Dunfield *et al.*, 1993), higher soil temperatures in the oxic soil layers lead to a higher increase of CH_4 oxidation rates compared to the increase of CH_4 production. As a result, the lower substrate availability in Greenland soils and higher soil temperatures in antarctic soils lead to a higher impact of CH_4 oxidation on the CH_4 fluxes, which can cause in particular cases a net CH_4 sink. In contrast to this, the rather high substrate supply and low soil temperature at the polygonal rim are not promoting the CH_4 sink function of this microsite.

6.3. CO_2 and CH_4 budgets in the polygonal tundra

The modeled CO_2 and mean CH_4 fluxes from polygonal rim and center were used to calculate the CO_2 and CH_4 budget of the measurement period in 2015 of the EC footprint area of the EC system and the polygonal tundra of Samoylov Island (Table 10). Based on the surface classification from Muster *et al.* (2012), the polygonal rim makes up 65% of the polygonal tundra of Samoylov Island, whereas the center represent 19%. Open water bodies make up 16% of the polygonal tundra. As CO_2 and CH_4 fluxes from this microsite are missing in this study, the estimates of CO_2 were taken from Abnizova *et al.* (2012) and estimates of CH_4 from Knoblauch *et al.* (2015).

Table 10: Calculation of the CO_2 and CH_4 budget for the measurement period in 2015. The budgets were calculated for the polygonal tundra on Samoylov Island.

Land cover class	Coverage[a] (%)	CO_2 flux (g CO_2 m^{-2} d^{-1})	Total CO_2 flux (Kg CO_2 ha^{-1} d^{-1})	CH_4 flux (mg CH_4 m^{-2} d^{-1})	Total CH_4 flux (Kg CO_2-equ ha^{-1} d^{-1})
Dry tundra	65	-2.3	-14.8	1.7	0.4
Wet tundra	19	-5.9	-11.2	25.5	1.7
Water	16	6.8[b]	10.9	26.0[c]	1.4
Total	100	-	-15.3	-	3.4
EC fluxes	-	-	-24.6[h], -21.0[d], -15.1[e]	-	6.2[h], 6.0[f], 6.5[g]

a: Muster *et al.* (2012); b: Abnizova *et al.* (2012); c: Knoblauch *et al.* (2015); d: Kutzbach *et al.* (2007b); e: Runkle *et al.* (2013); f: Wille *et al.* (2008); g: Sachs *et al.* (2008); h: Kutzbach *et al.* unpublished.

The calculated total CO_2 budget from the individual microsites polygonal rim, center and ponds is in agreement with estimates of CO_2 fluxes calculated with EC measurements

during the same period (Kutzbach *et al.,* unpublished). With -15.3 Kg CO_2 ha^{-1} d^{-1}, the calculated CO_2 budget is also in agreement to EC footprint estimates from other years (Kutzbach *et al.*, 2007b, Runkle *et al.*, 2013). The differences of EC footprint estimates between years demonstrate the inter-annual variability of the CO_2 fluxes at the study site, which are caused, among others, by differing meteorological conditions. For instance, variety of PAR can lead to different GPP fluxes between years, as PAR is the most important driver of photosynthesis. During the growing season in 2003, the average air temperature in July was about 2 °C higher than in 2015 (Figure 16) and total rainfall was twice as high as during the measurement period in 2015 (Figure 15) (Kutzbach *et al.*, 2007b). These differences can cause different CO_2 NEE fluxes as temperature and precipitation rates affect all of the NEE underlying processes (e.g. Hobbie *et al.*, 2002, Luo & Zhou, 2006, Schlesinger, 2013). Furthermore, the estimates of the outgassing CO_2 from polygonal ponds are related to high variabilities (Abnizova *et al.*, 2012), which could cause a strong bias of the estimate.

On polygonal tundra-scale, the polygonal rim displays a stronger CO_2 sink as the center, which supports Hypothesis 7. This is remarkable as almost three-fold lower net CO_2 uptake fluxes were measured at the rim compared to the center (Table 5). Therefore, small changes of the CO_2 NEE at the rims can have large impacts on the CO_2 budget of the polygonal tundra. This highlights the importance of polygonal rims for the CO_2 sink strength.

Considerably lower CH_4 emissions of the polygonal tundra area were calculated with chamber flux estimates from this study compared to EC measurements from other investigation periods (Sachs *et al.*, 2008, Wille *et al.*, 2008). Also a first estimate of CH_4 emissions from EC measurements (Kutzbach *et al.,* unpublished) revealed higher CH_4 emissions than the summed CH_4 fluxes for the polygonal tundra from the single microsites rim, center and ponds. This difference most likely reflects the distinct spatial variability of CH_4 fluxes in the polygonal tundra and highlights the difficulties of reliable estimates of CH_4 emissions from these landscapes. The WT, one of the main drivers of CH_4 production, is highly variable on the spatial scale; For instance, at the polygonal center from the study site the water table is partly below the soil surface, which causes high rates of CH_4 oxidation in the upper soil layer. Most likely these conditions are highly heterogeneous

across polygonal centers on Samoylov Island. This could lead to a substantial bias in the budget calculation. Furthermore, the CH_4 emission value from the ponds used for the calculation is representing a mean of measurements from an open water body and a pond margin (Knoblauch *et al.*, 2015). This value is related to uncertainties as it remains unclear how pond margins and open water bodies are distributed in the polygonal tundra. Therefore, it might be possible that a substantial source is missed or underestimated in the CH_4 budget calculation based on the fluxes from the single microsites.

Considering the 34-fold higher GWP of CH_4 on a 100-year timescale compared to CO_2 (Myhre *et al.*, 2013), the CH_4 emissions might display an important contributor to the overall greenhouse gas balance of the polygonal tundra. The conversion of CH_4 emissions into CO_2-equivalents revealed that the net uptake of atmospheric CO_2 of -15.3 kg CO_2 ha^{-1} d^{-1} was about five-fold higher as the CH_4 emissions of 3.4 Kg CO_2-eq ha^{-1} d^{-1}. Therefore, the polygonal tundra of Samoylov Island displayed a robust sink for atmospheric carbon in 2015. If the same calculation is conducted with CO_2 and CH_4 fluxes from 2014, the polygonal tundra represents a net source for atmospheric carbon as CO_2 fluxes are with 3.7 Kg CO_2 ha^{-1} d^{-1} a small and the CH_4 fluxes with 8.1 Kg CO_2-eq ha^{-1} d^{-1} a large source. However, CH_4 and CO_2 flux measurements in 2014 are restricted to just one month and it might be possible that those fluxes show a different trend over the complete growing season. Nevertheless, this finding emphasizes the inter-annual variability of C dynamics between soils and atmosphere in the polygonal tundra.

7. Conclusion and Outlook

This study examined the contributions of GPP, R_{eco}, R_H and R_A to CO_2 NEE fluxes on the microscale in the polygonal tundra. Both investigated microsites represent a sink for atmospheric CO_2 during the measurement periods July to September 2015 and July to August 2014. The sink function is more pronounced at the polygonal center compared to the polygonal rim site (Hypothesis 1 is confirmed) and was stronger in 2015 than in 2014. It is concluded, that the difference in CO_2 fluxes between the two microsites occurs mainly due to R_{eco} being suppressed under the water-saturated conditions and not primarily because of higher GPP at the center (supports Hypothesis 2). This assumption holds also true for R_H fluxes, which represent the first *in situ* measurements of R_H fluxes over almost a complete growing season from a Russian arctic tundra site. The substantial differences identified in NEE between the two investigated microsites show the importance of microscale measurements for reliable estimates of CO_2 surface-atmosphere fluxes from arctic tundra sites and highlight the important role of soil moisture conditions on CO_2 fluxes.

The contribution of R_H to R_{eco} fluxes differs between the microsites. At the polygonal center the average contribution of R_H to R_{eco} is 42% (Hypothesis 3 is supported), while at the polygonal rim the average contribution of R_H is comparatively higher at 60% (Hypothesis 3 is rejected). This difference is most likely related to differences in vascular plant coverage and soil moisture conditions. The R_H/R_{eco} ratio was not found to increase towards the end of the growing season, and it is concluded that the measurement period was too short to observe any seasonality in the R_H/R_{eco} ratio (Hypothesis 4 cannot be examined). Instead, the R_H/R_{eco} ratio and the R_A fluxes were found to correlate with the WT at the polygonal center. This might be an effect of low R_A fluxes during times of high WT due to the submersion of vascular plants, while during times of low WT, the R_H gains more importance on the R_H/R_{eco} ratio due to well-aerated soils and mosses could desiccate, resulting in low R_A fluxes.

In the future Arctic, rainfall is predicted to increase (Christensen *et al.*, 2013) and this work shows for the polygonal tundra on Samolyov Island that high levels of soil moisture conditions cause this environment to function as a stronger CO_2 sink. Hereby, R_A and R_H

fluxes respond differently to changing moisture conditions. On the other hand, the modeling of CO_2 fluxes revealed that both R_H and R_A fluxes correlate positively with rising temperatures, although Hicks Pries *et al.* (2015) have shown a different response of these fluxes to warming in other arctic tundra ecosystems. Therefore, it remains uncertain whether future climate change will cause the polygonal tundra to act as stronger CO_2 sink or if it will turn into a CO_2 source. This work shows that the hydrological conditions are of major importance for R_A and R_H fluxes. Therefore, it is recommended that future studies determining partitioned CO_2 fluxes from arctic tundra ecosystems should focus on the role of hydrological conditions as driver of these fluxes to obtain an in-depth insight into this relationship.

In order to determine the individual impacts of hydrological conditions and temperature on the R_H and R_A fluxes, it would be useful to perform both warming and wetting experiments under field conditions. So far, a number of studies have determined the temperature response of NEE, GPP, and R_{eco} fluxes in arctic ecosystems with warming experiments (e.g. Frey *et al.*, 2008, Natali *et al.*, 2011, Voigt *et al.*, 2016), however, much less research has focused on the response of R_A and R_H fluxes to increased temperatures (Hicks Pries *et al.*, 2015). Wetting experiments in arctic tundra ecosystems to determine the individual response of R_A and R_H fluxes to changing hydrological conditions are lacking so far, despite their importance as highlighted in this study.

This study also determined CH_4 fluxes from different microsites in the polygonal tundra. The measured CH_4 emissions are rather low in comparison to arctic tundra sites with organic-rich soils, which highlights the importance of substrate availability for CH_4 production. The rather low CH_4 emissions found in this study in comparison to other studies from the same site (Samoylov Island) highlight not only the high temporal and spatial variability of CH_4 emissions, but also the importance of an accurate measurement procedure. ALD was the environmental parameter with the highest explanatory power of CH_4 fluxes from the polygonal center and rim (Hypothesis 5 is rejected). In contrast to other studies, the dry polygonal rim was not found to function as a CH_4 sink (Hypothesis 6 rejected). It is concluded that low soil temperatures (causing low CH_4 oxidation rates) and high substrate availability (causing high CH_4 production rates) were the main factors causing the polygonal rim to function as a source of CH_4. These findings show the varying

impact of different environmental conditions in arctic tundra ecosystems on CH_4 fluxes, which complicates estimates of total CH_4 emissions from arctic tundra landscapes. Future studies conducting CH_4 flux measurements on the microsite scale across a range of arctic tundra landscapes are required to better estimate the recent contribution of CH_4 fluxes to the global C cycle and the future response of these fluxes to global warming.

The calculation of CO_2 and CH_4 budgets for the polygonal tundra on Samoylov Island revealed that the polygonal rims act as a stronger net CO_2 sink than the polygonal centers (Hypothesis 7 is supported). Considering the GWP of CH_4 on a 100-year timescale, the CH_4 emissions from the polygonal tundra are five-fold lower than its net CO_2 uptake. However, on the shorter term, calculating the budget with the fluxes measured in 2014 revealed that this ecosystem acted as net source for atmospheric C over a period of one month, which highlights the pronounced inter-annual variability of these fluxes. Furthermore, the observed differences in CH_4 emissions and partitioned CO_2 fluxes between the microsites clearly show that modelling approaches of C budgets on larger scales should always be supported by microscale measurements to take the pronounced spatial heterogeneity of arctic tundra ecosystems and its impact on C fluxes into account.

In order to gain a quantitative understanding of the contribution of greenhouse gas emissions from arctic ecosystems to global warming, future studies should also focus on other greenhouse gases in addition to CO_2 and CH_4. For instance, soil warming increases N_2O emissions from arctic tundra sites (Voigt *et al.*, 2016). Furthermore, little effort has been made so far in determining methyl halide fluxes in arctic tundra ecosystems. This is critical as it was shown that several arctic and subarctic ecosystems emit considerable amounts of chloroform ($CHCl_3$) (Johnsen *et al.*, 2016) as well as methyl chloride (CH_3Cl) (Hardacre *et al.*, 2009). Both N_2O and methyl halides emissions can be of major importance due to their much higher GWP compared to CO_2.

References

Abnizova A, Siemens J, Langer M, Boike J (2012) Small ponds with major impact: The relevance of ponds and lakes in permafrost landscapes to carbon dioxide emissions. Global Biogeochemical Cycles, **26**, GB2041.

Bartlett KB, Crill PM, Sass RL, Harriss RC, Dise NB (1992) Methane emissions from tundra environments in the Yukon-Kuskokwim Delta, Alaska. Journal of Geophysical Research-Atmospheres, **97**, 16645-16660.

Beer C (2008) Soil science: The Arctic carbon count. Nature Geoscience, **1**, 569-570.

Beermann F, Teltewskoi A, Fiencke C, Pfeiffer EM, Kutzbach L (2015) Stoichiometric analysis of nutrient availability (N, P, K) within soils of polygonal tundra. Biogeochemistry, **122**, 211-227.

Belshe EF, Schuur EA, Bolker BM (2013) Tundra ecosystems observed to be CO2 sources due to differential amplification of the carbon cycle. Ecology Letters, **16**, 1307-1315.

Biasi C, Jokinen S, Marushchak ME, Hamalainen K, Trubnikova T, Oinonen M, Martikainen PJ (2014) Microbial Respiration in Arctic Upland and Peat Soils as a Source of Atmospheric Carbon Dioxide. Ecosystems, **17**, 112-126.

Blok D, Heijmans M, Schaepman-Strub G, Kononov AV, Maximov TC, Berendse F (2010) Shrub expansion may reduce summer permafrost thaw in Siberian tundra. Global Change Biology, **16**, 1296-1305.

Boike J, Grüber M, Langer M, Piel K, Scheritz M (2012) Orthomosaic of Samoylov Island, Lena Delta, Siberia. pp Page, PANGAEA.

Boike J, Kattenstroth B, Abramova K *et al.* (2013) Baseline characteristics of climate, permafrost and land cover from a new permafrost observatory in the Lena River Delta, Siberia (1998-2011). Biogeosciences, **10**, 2105-2128.

Boike J, Veh G, Viitanen L-K, Bornemann N, Stoof G, Muster S (2015) Visible and near-infrared orthomosaic of Samoylov Island, Siberia, summer 2015 (5.3 GB). pp Page, PANGAEA.

Boike J, Wille C, Abnizova A (2008) Climatology and summer energy and water balance of polygonal tundra in the Lena River Delta, Siberia. Journal of Geophysical Research-Biogeosciences, **113**, G03025.

Bolshiyanov D, Makarov A, Savelieva L (2015) Lena River delta formation during the Holocene. Biogeosciences, **12**, 579-593.

Bond-Lamberty B, Bronson D, Bladyka E, Gower ST (2011) A comparison of trenched plot techniques for partitioning soil respiration. Soil Biology and Biochemistry, **43**, 2108-2114.

Brown J, Miller PC, Tieszen LL, Bunnell F (1980) *An arctic ecosystem: the coastal tundra at Barrow, Alaska*, Dowden, Hutchinson & Ross, Inc., Stroudsberg, PA, USA.

Brown MG, Humphreys ER, Moore TR, Roulet NT, Lafleur PM (2014) Evidence for a nonmonotonic relationship between ecosystem-scale peatland methane emissions and water table depth. Journal of Geophysical Research: Biogeosciences, **119**, 826-835.

Bubier J, Crill P, Mosedale A, Frolking S, Linder E (2003) Peatland responses to varying interannual moisture conditions as measured by automatic CO2 chambers. Global Biogeochemical Cycles, **17**, 1066.

Burnham KP, Anderson DR (2004) Multimodel inference - understanding AIC and BIC in model selection. Sociological Methods & Research, **33**, 261-304.

CAVM-Team (2003) Circumpolar Arctic Vegetation Map, Scale 1: 7.500. 000. Conservation of Arctic Flora and Fauna (CAFF) Map No. 1. US Fish and Wildlife Service, Anchorage, Alaska. pp Page.

Chanton JP (2005) The effect of gas transport on the isotope signature of methane in wetlands. Organic Geochemistry, **36**, 753-768.

Chapin FS, Sturm M, Serreze MC *et al.* (2005) Role of land-surface changes in Arctic summer warming. Science, **310**, 657-660.

Chapin FS, Woodwell GM, Randerson JT *et al.* (2006) Reconciling Carbon-cycle Concepts, Terminology, and Methods. Ecosystems, **9**, 1041-1050.

Chen J, Luo YQ, Xia JY *et al.* (2016) Differential responses of ecosystem respiration components to experimental warming in a meadow grassland on the Tibetan Plateau. Agricultural and Forest Meteorology, **220**, 21-29.

Chen J, Shi WY, Cao JJ (2015) Effects of Grazing on Ecosystem CO2 Exchange in a Meadow Grassland on the Tibetan Plateau During the Growing Season. Environmental Management, **55**, 347-359.

Christensen JH, Krishna Kumar K, Aldrian E *et al.* (2013) Climate Phenomena and their Relevance for Future Regional Climate Change. In: *Climate Change 2013: The Physical Science Basis. Contribution of Working Group I to the Fifth Assessment Report of the Intergovernmental Panel on Climate Change.* (eds Stocker TF, Qin D, Plattner G-K, Tignor M, Allen SK, Boschung J, Nauels A, Xia Y, Bex V, Midgley PM) pp Page. Cambridge, United Kingdom and New York, NY, USA, Cambridge University Press.

Christensen T, Jonasson S, Callaghan T, Havstrom M (1995) Spatial variation in high-latitude methane flux along a transect across Siberian and European tundra environments. Journal of Geophysical Research, **100**, 21035-21045.

Christensen TR, Ekberg A, Ström L *et al.* (2003) Factors controlling large scale variations in methane emissions from wetlands. Geophysical Research Letters, **30**, 1414.

Christiansen JR, Korhonen JFJ, Juszczak R, Giebels M, Pihlatie M (2011) Assessing the effects of chamber placement, manual sampling and headspace mixing on CH4 fluxes in a laboratory experiment. Plant and Soil, **343**, 171-185.

Ciais P, Sabine C, Bala G *et al.* (2013) Carbon and Other Biogeochemical Cycles. In: *Climate Change 2013: The Physical Science Basis. Contribution of Working Group I to the Fifth Assessment Report of the Intergovernmental Panel on Climate Change.* (eds Stocker TF, Qin D, Plattner

G-K, Tignor M, Allen SK, Boschung J, Nauels A, Xia Y, Bex V, Midgley PM) pp Page. Cambridge, United Kingdom and New York, NY, USA, Cambridge University Press.

Collins NJ, Oechel WC (1974) Pattern of growth and translocation of photosynthate in a tundra moss, Polytrichum-Alpinum. Canadian Journal of Botany-Revue Canadienne De Botanique, **52**, 355-363.

Conrad R (1996) Soil microorganisms as controllers of atmospheric trace gases (H2, CO, CH4, OCS, N2O, and NO). Microbiological Reviews, **60**, 609-640.

Davidson EA, Savage K, Verchot LV, Navarro R (2002) Minimizing artifacts and biases in chamber-based measurements of soil respiration. Agricultural and Forest Meteorology, **113**, 21-37.

Davidson SJ, Sloan VL, Phoenix GK, Wagner R, Fisher JP, Oechel WC, Zona D (2016) Vegetation Type Dominates the Spatial Variability in CH4 Emissions Across Multiple Arctic Tundra Landscapes. Ecosystems, **19**, 1116-1132.

Dedysh SN (2002) Methanotrophic bacteria of acidic Sphagnum peat bogs. Microbiology, **71**, 638-650.

Denmead OT (2008) Approaches to measuring fluxes of methane and nitrous oxide between landscapes and the atmosphere. Plant and Soil, **309**, 5-24.

Diaz-Pines E, Schindlbacher A, Pfeffer M, Jandl R, Zechmeister-Boltenstern S, Rubio A (2010) Root trenching: a useful tool to estimate autotrophic soil respiration? A case study in an Austrian mountain forest. European Journal of Forest Research, **129**, 101-109.

Dlugokencky EJ, Nisbet EG, Fisher R, Lowry D (2011) Global atmospheric methane: budget, changes and dangers. Philosophical Transactions of the Royal Society A - Mathematical Physical and Engineering Sciences, **369**, 2058-2072.

Dorrepaal E, Toet S, van Logtestijn RSP, Swart E, van de Weg MJ, Callaghan TV, Aerts R (2009) Carbon respiration from subsurface peat accelerated by climate warming in the subarctic. Nature, **460**, 616-619.

Dunfield P, Dumont R, Moore TR (1993) Methane production and consumption in temperate and subarctic peat soils: response to temperature and pH. Soil Biology and Biochemistry, **25**, 321-326.

Durbin J, Watson GS (1950) Testing for serial correlation in least squares regression. Biometrika, **37**, 409-428.

Eckhardt T, Kutzbach L (2016) MATLAB code to calculate gas fluxes from chamber-based methods. pp Page, PANGAEA.

Edwards NT, Ross-Todd BM (1983) Soil carbon dynamics in a mixed deciduous forest following clear-cutting with and without residue removal. Soil Science Society of America Journal, **47**, 1014-1021.

Elberling B, Nordstrom C, Grondahl L *et al.* (2008a) High-arctic soil CO2 and CH4 production controlled by temperature, water, freezing and snow. Advances in Ecological Research, Vol 40: High-Arctic Ecosystem Dynamics in a Changing Climate, **40**, 441-472.

Elberling B, Tamstorf MP, Michelsen A *et al.* (2008b) Soil and plant community-characteristics and dynamics at Zackenberg. Advances in Ecological Research, **40**, 223-248.

Elovskaya VV (1987) Classification and diagnostics of frozen soils of Yakutia. Yakutian filial SO AN USSR, 172 pp *(in Russian)*.

Elsgaard L, Görres C-M, Hoffmann CC, Blicher-Mathiesen G, Schelde K, Petersen SO (2012) Net ecosystem exchange of CO2 and carbon balance for eight temperate organic soils under agricultural management. Agriculture, Ecosystems & Environment, **162**, 52-67.

Epron D, Nouvellon Y, Deleporte P *et al.* (2006) Soil carbon balance in a clonal Eucalyptus plantation in Congo: effects of logging on carbon inputs and soil CO2 efflux. Global Change Biology, **12**, 1021-1031.

French HM (1996) *The periglacial environment,* London, UK, Longman.

Frey SD, Drijber R, Smith H, Melillo J (2008) Microbial biomass, functional capacity, and community structure after 12 years of soil warming. Soil Biology & Biochemistry, **40**, 2904-2907.

Friborg T, Christensen TR, Hansen BU, Nordstroem C, Soegaard H (2000) Trace gas exchange in a high-Arctic valley: 2. Landscape CH4 fluxes measured and modeled using eddy correlation data. Global Biogeochemical Cycles, **14**, 715-723.

Gebauer RLE, Reynolds JF, Tenhunen JD (1995) Growth and allocation of the arctic sedges Eriophorum-Angustifolium and Eriophorum-Vaginatum - effects of variable soil oxygen and nutrient availability. Oecologia, **104**, 330-339.

Godin E, Fortier D, Coulombe S (2014) Effects of thermo-erosion gullying on hydrologic flow networks, discharge and soil loss. Environmental Research Letters, **9**, 105010.

Gomez-Casanovas N, Matamala R, Cook DR, Gonzalez-Meler MA (2012) Net ecosystem exchange modifies the relationship between the autotrophic and heterotrophic components of soil respiration with abiotic factors in prairie grasslands. Global Change Biology, **18**, 2532-2545.

Gorham E (1991) Northern peatlands: role in the carbon cycle and probable responses to climatic warming. Ecological Applications, **1**, 182-195.

Görres CM, Kutzbach L, Elsgaard L (2014) Comparative modeling of annual CO2 flux of temperate peat soils under permanent grassland management. Agriculture, Ecosystems & Environment, **186**, 64-76.

Grigoriev N (1960) The temperature of permafrost in the Lena delta basin–deposit conditions and properties of the permafrost in Yakutia. Yakutsk, **2**, 97-101.

Grogan P, Chapin FS (2000) Initial effects of experimental warming on above- and belowground components of net ecosystem CO2 exchange in arctic tundra. Oecologia, **125**, 512-520.

Grosse G, Harden J, Turetsky M *et al.* (2011) Vulnerability of high-latitude soil organic carbon in North America to disturbance. Journal of Geophysical Research-Biogeosciences, **116**, G00K06.

Hanson PJ, Edwards NT, Garten CT, Andrews JA (2000) Separating root and soil microbial contributions to soil respiration: A review of methods and observations. Biogeochemistry, **48**, 115-146.

Hanson RS, Hanson TE (1996) Methanotrophic bacteria. Microbiological Reviews, **60**, 439-471.

Harazono Y, Mano M, Miyata A *et al.* (2006) Temporal and spatial differences of methane flux at arctic tundra in Alaska. Memoirs of National Institute of Polar Research. Special issue, **59**, 79-95.

Hardacre CJ, Blei E, Heal MR (2009) Growing season methyl bromide and methyl chloride fluxes at a sub-arctic wetland in Sweden. Geophysical Research Letters, **36**, L12401.

Harley PC, Tenhunen JD, Murray KJ, Beyers J (1989) Irradiance and temperature effects on photosynthesis of tussock tundra Sphagnum mosses from the foothills of the Philip Smith Mountains, Alaska. Oecologia, **79**, 251-259.

Heikkinen JEP, Elsakov V, Martikainen PJ (2002) Carbon dioxide and methane dynamics and annual carbon balance in tundra wetland in NE Europe, Russia. Global Biogeochemical Cycles, **16**, 1115.

Heikkinen JEP, Virtanen T, Huttunen JT, Elsakov V, Martikainen PJ (2004) Carbon balance in East European tundra. Global Biogeochemical Cycles, **18**, GB1023.

Hicks Pries CE, Logtestijn RS, Schuur EA, Natali SM, Cornelissen JH, Aerts R, Dorrepaal E (2015) Decadal warming causes a consistent and persistent shift from heterotrophic to autotrophic respiration in contrasting permafrost ecosystems. Global Change Biology, **21**, 4508-4519.

Hicks Pries CE, Schuur EA, Crummer KG (2013) Thawing permafrost increases old soil and autotrophic respiration in tundra: partitioning ecosystem respiration using delta (13)C and (14)C. Glob Chang Biol, **19**, 649-661.

Hobbie SE, Nadelhoffer KJ, Hogberg P (2002) A synthesis: The role of nutrients as constraints on carbon balances in boreal and arctic regions. Plant and Soil, **242**, 163-170.

Höfle ST (2015) Organic matter composition and dynamic in polygonal tundra soils. Dissertation, University of Cologne, 2015, pp 110.

Högberg P, Nordgren A, Buchmann N *et al.* (2001) Large-scale forest girdling shows that current photosynthesis drives soil respiration. Nature, **411**, 789-792.

Hudson JMG, Henry GHR, Cornwell WK (2011) Taller and larger: shifts in Arctic tundra leaf traits after 16 years of experimental warming. Global Change Biology, **17**, 1013-1021.

Hugelius G, Strauss J, Zubrzycki S *et al.* (2014) Estimated stocks of circumpolar permafrost carbon with quantified uncertainty ranges and identified data gaps. Biogeosciences, **11**, 6573-6593.

Hutchinson GL, Livingston GP (2001) Vents and seals in non-steady-state chambers used for measuring gas exchange between soil and the atmosphere. European Journal of Soil Science, **52**, 675-682.

Hutchinson GL, Livingston GP, Healy RW, Striegl RG (2000) Chamber measurement of surface-atmosphere trace gas exchange: Numerical evaluation of dependence on soil, interfacial layer, and source/sink properties. Journal of Geophysical Research-Atmospheres, **105**, 8865-8875.

IPCC (2013) *Climate Change 2013: The Physical Science Basis. Contribution of Working Group I to the Fifth Assessment Report of the Intergovernmental Panel on Climate Change,* Cambridge, United Kingdom and New York, NY, USA, Cambridge University Press.

Jia GJ, Epstein HE, Walker DA (2009) Vegetation greening in the Canadian Arctic related to decadal warming. J Environ Monit, **11**, 2231-2238.

Joabsson A, Christensen TR, Wallen B (1999) Vascular plant controls on methane emissions from northern peatforming wetlands. Trends in Ecology & Evolution, **14**, 385-388.

Johnsen AR, Jacobsen OS, Gudmundsson L, Albers CN (2016) Chloroform emissions from arctic and subarctic ecosystems in Greenland and Northern Scandinavia. Biogeochemistry, **130**, 53-65.

Johnson LC, Shaver GR, Cades DH *et al.* (2000) Plant carbon-nutrient interactions control CO2 exchange in Alaskan wet sedge tundra ecosystems. Ecology, **81**, 453-469.

Johnston CE, Ewing SA, Harden JW *et al.* (2014) Erratum: Effect of permafrost thaw on CO2 and CH4 exchange in a western Alaska peatland chronosequence (2013Environ. Res. Lett.9085004). Environmental Research Letters, **9**, 109601.

Jones BM, Stoker JM, Gibbs AE *et al.* (2013) Quantifying landscape change in an arctic coastal lowland using repeat airborne LiDAR. Environmental Research Letters, **8**, 045025.

Jørgensen CJ, Johansen KML, Westergaard-Nielsen A, Elberling B (2015) Net regional methane sink in High Arctic soils of northeast Greenland. Nature Geoscience, **8**, 20-23.

Jorgenson MT, Grosse G (2016) Remote Sensing of Landscape Change in Permafrost Regions. Permafrost and Periglacial Processes, **27**, 324-338.

Kamal S, Varma A (2008) Peatland microbiology. In: *Microbiology of Extreme Soils.* pp Page., Springer.

King JY, Reeburgh WS, Regli SK (1998) Methane emission and transport by arctic sedges in Alaska: Results of a vegetation removal experiment. Journal of Geophysical Research-Atmospheres, **103**, 29083-29092.

Knoblauch C, Beer C, Sosnin A, Wagner D, Pfeiffer EM (2013) Predicting long-term carbon mineralization and trace gas production from thawing permafrost of Northeast Siberia. Glob Chang Biol, **19**, 1160-1172.

Knoblauch C, Spott O, Evgrafova S, Kutzbach L, Pfeiffer EM (2015) Regulation of methane production, oxidation, and emission by vascular plants and bryophytes in ponds of the northeast Siberian polygonal tundra. Journal of Geophysical Research-Biogeosciences, **120**, 2525-2541.

Knoblauch C, Zimmermann U, Blumenberg M, Michaelis W, Pfeiffer E (2008) Methane turnover and temperature response of methane-oxidizing bacteria in permafrost-affected soils of northeast Siberia. Soil Biology and Biochemistry, **40**, 3004-3013.

Koskinen M, Minkkinen K, Ojanen P, Kamarainen M, Laurila T, Lohila A (2014) Measurements of CO2 exchange with an automated chamber system throughout the year: challenges in measuring night-time respiration on porous peat soil. Biogeosciences, **11**, 347-363.

Koven CD, Ringeval B, Friedlingstein P *et al.* (2011) Permafrost carbon-climate feedbacks accelerate global warming. Proceedings of the National Academy of Sciences of the United States of America, **108**, 14769-14774.

Kuhry P, Dorrepaal E, Hugelius G, Schuur EAG, Tarnocai C (2010) Potential Remobilization of Belowground Permafrost Carbon under Future Global Warming. Permafrost and Periglacial Processes, **21**, 208-214.

Kutzbach L (2006) The exchange of energy, water and carbon dioxide between wet arctic tundra and the atmosphere at the Lena River Delta, Northern Siberia. Berichte zur Polar-und Meeresforschung (Reports on Polar and Marine Research), **541**, pp 160.

Kutzbach L, Schneider J, Sachs T *et al.* (2007a) CO2 flux determination by closed-chamber methods can be seriously biased by inappropriate application of linear regression. Biogeosciences, **4**, 1005-1025.

Kutzbach L, Wagner D, Pfeiffer EM (2004) Effect of microrelief and vegetation on methane emission from wet polygonal tundra, Lena Delta, Northern Siberia. Biogeochemistry, **69**, 341-362.

Kutzbach L, Wille C, Pfeiffer EM (2007b) The exchange of carbon dioxide between wet arctic tundra and the atmosphere at the Lena River Delta, Northern Siberia. Biogeosciences, **4**, 869-890.

Kuzyakov Y (2006) Sources of CO2 efflux from soil and review of partitioning methods. Soil Biology and Biochemistry, **38**, 425-448.

Kwon MJ, Heimann M, Kolle O *et al.* (2016) Long-term drainage reduces CO2 uptake and increases CO2 emission on a Siberian floodplain due to shifts in vegetation community and soil thermal characteristics. Biogeosciences, **13**, 4219-4235.

Lai DYF (2009) Methane Dynamics in Northern Peatlands: A Review. Pedosphere, **19**, 409-421.

Lai DYF, Roulet NT, Humphreys ER, Moore TR, Dalva M (2012) The effect of atmospheric turbulence and chamber deployment period on autochamber CO2 and CH4 flux measurements in an ombrotrophic peatland. Biogeosciences, **9**, 3305-3322.

Laisk A, Kiirats O, Oja V (1984) Assimilatory power (postillumination CO2 uptake) in leaves - measurement, environmental dependencies, and kinetic-properties. Plant Physiology, **76**, 723-729.

Lavoie M, Mack M, Schuur E (2011) Effects of elevated nitrogen and temperature on carbon and nitrogen dynamics in Alaskan arctic and boreal soils. Journal of Geophysical Research: Biogeosciences, **116**, G03013.

Lee H, Schuur EAG, Inglett KS, Lavoie M, Chanton JP (2012) The rate of permafrost carbon release under aerobic and anaerobic conditions and its potential effects on climate. Global Change Biology, **18**, 515-527.

Liebner S, Zeyer J, Wagner D, Schubert C, Pfeiffer E-M, Knoblauch C (2011) Methane oxidation associated with submerged brown mosses reduces methane emissions from Siberian polygonal tundra. Journal of Ecology, **99**, 914-922.

Livingston GP, Hutchinson GL, Spartalian K (2005) Diffusion theory improves chamber-based measurements of trace gas emissions. Geophysical Research Letters, **32**, L24817.

Livingston GP, Hutchinson GL, Spartalian K (2006) Trace Gas Emission in Chambers. Soil Science Society of America Journal, **70**, 1459.

Loranty MM, Goetz SJ, Beck PSA (2011) Tundra vegetation effects on pan-Arctic albedo. Environmental Research Letters, **6**, 029601.

Luo Y, Zhou X (2006) *Soil respiration and the environment,* Amsterdam Boston, Elsevier Academic Press.

Mahecha MD, Reichstein M, Carvalhais N *et al.* (2010) Global Convergence in the Temperature Sensitivity of Respiration at Ecosystem Level. Science, **329**, 838-840.

Marushchak ME, Friborg T, Biasi C *et al.* (2016) Methane dynamics in the subarctic tundra: combining stable isotope analyses, plot- and ecosystem-scale flux measurements. Biogeosciences, **13**, 597-608.

Marushchak ME, Kiepe I, Biasi C *et al.* (2013) Carbon dioxide balance of subarctic tundra from plot to regional scales. Biogeosciences, **10**, 437-452.

Mastepanov M, Sigsgaard C, Dlugokencky EJ, Houweling S, Ström L, Tamstorf MP, Christensen TR (2008) Large tundra methane burst during onset of freezing. Nature, **456**, 628-630.

Mastepanov M, Sigsgaard C, Tagesson T, Ström L, Tamstorf MP, Lund M, Christensen TR (2013) Revisiting factors controlling methane emissions from high-Arctic tundra. Biogeosciences, **10**, 5139-5158.

Mauritz M, Bracho R, Celis G *et al.* (2017) Non-linear CO2 flux response to seven years of experimentally induced permafrost thaw. Global Change Biology, 1-20.

McEwing KR, Fisher JP, Zona D (2015) Environmental and vegetation controls on the spatial variability of CH4 emission from wet-sedge and tussock tundra ecosystems in the Arctic. Plant and Soil, **388**, 37-52.

McGuire AD, Anderson LG, Christensen TR *et al.* (2009) Sensitivity of the carbon cycle in the Arctic to climate change. Ecological Monographs, **79**, 523-555.

McGuire AD, Christensen TR, Hayes D *et al.* (2012) An assessment of the carbon balance of Arctic tundra: comparisons among observations, process models, and atmospheric inversions. Biogeosciences, **9**, 3185-3204.

Murray K, Tenhunen J, Nowak R (1993) Photoinhibition as a control on photosynthesis and production of Sphagnum mosses. Oecologia, **96**, 200-207.

Muster S, Langer M, Heim B, Westermann S, Boike J (2012) Subpixel heterogeneity of ice-wedge polygonal tundra: a multi-scale analysis of land cover and evapotranspiration in the Lena River Delta, Siberia. Tellus B*,* **64**, 17301.

Myhre G, Shindell D, Bréon F-M *et al.* (2013) Anthropogenic and Natural Radiative Forcing. In: *Climate Change 2013: The Physical Science Basis. Contribution of Working Group I to the Fifth Assessment Report of the Intergovernmental Panel on Climate Change.* (eds Stocker TF, Qin D, Plattner G-K, Tignor M, Allen SK, Boschung J, Nauels A, Xia Y, Bex V, Midgley PM) pp Page. Cambridge, United Kingdom and New York, NY, USA, Cambridge University Press.

Nakano T, Kuniyoshi S, Fukuda M (2000) Temporal variation in methane emission from tundra wetlands in a permafrost area, northeastern Siberia. Atmospheric Environment*,* **34**, 1205-1213.

Natali SM, Schuur EAG, Rubin RL (2012) Increased plant productivity in Alaskan tundra as a result of experimental warming of soil and permafrost. Journal of Ecology*,* **100**, 488-498.

Natali SM, Schuur EAG, Trucco C, Hicks Pries CE, Crummer KG, Baron Lopez AF (2011) Effects of experimental warming of air, soil and permafrost on carbon balance in Alaskan tundra. Global Change Biology*,* **17**, 1394-1407.

Nobrega S, Grogan P (2008) Landscape and Ecosystem-Level Controls on Net Carbon Dioxide Exchange along a Natural Moisture Gradient in Canadian Low Arctic Tundra. Ecosystems*,* **11**, 377-396.

Nykänen H, Alm J, Silvola J, Tolonen K, Martikainen PJ (1998) Methane fluxes on boreal peatlands of different fertility and the effect of long-term experimental lowering of the water table on flux rates. Global Biogeochemical Cycles*,* **12**, 53-69.

Oechel WC, Vourlitis GL, Hastings SJ, Ault RP, Bryant P (1998) The effects of water table manipulation and elevated temperature on the net CO2 flux of wet sedge tundra ecosystems. Global Change Biology*,* **4**, 77-90.

Oechel WC, Vourlitis GL, Hastings SJ, Bochkarev SA (1995) Change in arctic CO2 flux over 2 decades - effects of climate-change at Barrow, Alaska. Ecological Applications*,* **5**, 846-855.

Oechel WC, Vourlitis GL, Hastings SJ, Zulueta RC, Hinzman L, Kane D (2000) Acclimation of ecosystem CO2 exchange in the Alaskan Arctic in response to decadal climate warming. Nature*,* **406**, 978-981.

Olefeldt D, Turetsky MR, Crill PM, McGuire AD (2013) Environmental and physical controls on northern terrestrial methane emissions across permafrost zones. Glob Chang Biol*,* **19**, 589-603.

Olivas PC, Oberbauer SF, Tweedie C, Oechel WC, Lin D, Kuchy A (2011) Effects of Fine-Scale Topography on CO2 Flux Components of Alaskan Coastal Plain Tundra: Response to Contrasting Growing Seasons. Arctic, Antarctic, and Alpine Research*,* **43**, 256-266.

ORNL DAAC (2014) MODIS Collection 5 Land Products Global Subsetting and Visualization Tool. ORNL DAAC, Oak Ridge, Tennessee, USA. August 25, 2015. Subset obtained for MOD13Q1 product at 72.373N,126.4978W, time period: 2000-02-18 to 2016-07-28, and subset size: 0.25 x 0.25 km. pp Page, ORNL Distributed Active Archive Center.

Parmentier FJW, van der Molen MK, van Huissteden J *et al.* (2011) Longer growing seasons do not increase net carbon uptake in the northeastern Siberian tundra. Journal of Geophysical Research, **116**, G04013.

Pearson RG, Phillips SJ, Loranty MM, Beck PSA, Damoulas T, Knight SJ, Goetz SJ (2013) Shifts in Arctic vegetation and associated feedbacks under climate change. Nature Clim. Change, **3**, 673-677.

Pedersen AR, Petersen SO, Schelde K (2010) A comprehensive approach to soil-atmosphere trace-gas flux estimation with static chambers. European Journal of Soil Science, **61**, 888-902.

Pihlatie MK, Christiansen JR, Aaltonen H *et al.* (2013) Comparison of static chambers to measure CH4 emissions from soils. Agricultural and Forest Meteorology, **171**, 124-136.

Ping CL, Bockheim JG, Kimble JM, Michaelson GJ, Walker DA (1998) Characteristics of cryogenic soils along a latitudinal transect in Arctic Alaska. Journal of Geophysical Research-Atmospheres, **103**, 28917-28928.

Ping CL, Jastrow JD, Jorgenson MT, Michaelson GJ, Shur YL (2015) Permafrost soils and carbon cycling. SOIL, **1**, 147-171.

Prater JL, Chanton JP, Whiting GJ (2007) Variation in methane production pathways associated with permafrost decomposition in collapse scar bogs of Alberta, Canada. Global Biogeochemical Cycles, **21**, GB4004.

Preuss I, Knoblauch C, Gebert J, Pfeiffer E-M (2013) Improved quantification of microbial CH4 oxidation efficiency in arctic wetland soils using carbon isotope fractionation. Biogeosciences, **10**, 2539–2552.

Redeker KR, Baird AJ, Teh YA (2015) Quantifying wind and pressure effects on trace gas fluxes across the soil–atmosphere interface. Biogeosciences, **12**, 7423-7434.

Rekacewicz P, UNEP/GRID-Arendal (1998) Data from International Peramfrost Association, 1998. Circumpolar Active-layer Permafrost-System (CAPS), version 1.0. http://nsidc.org/cryosphere/frozenground/whereis_fg.html (22.03.2013).

Rodeghiero M, Cescatti A (2005) Main determinants of forest soil respiration along an elevation/temperature gradient in the Italian Alps. Global Change Biology, **11**, 1024-1041.

Romanovsky VE, Drozdov DS, Oberman NG *et al.* (2010) Thermal State of Permafrost in Russia. Permafrost and Periglacial Processes, **21**, 136-155.

Runkle BRK, Sachs T, Wille C, Pfeiffer EM, Kutzbach L (2013) Bulk partitioning the growing season net ecosystem exchange of CO2 in Siberian tundra reveals the seasonality of its carbon sequestration strength. Biogeosciences, **10**, 1337-1349.

Saarnio S, Alm J, Silvola J, Lohila A, Nykanen H, Martikainen PJ (1997) Seasonal variation in CH4 emissions and production and oxidation potentials at microsites on an oligotrophic pine fen. Oecologia, **110**, 414-422.

Sachs T, Giebels M, Boike J, Kutzbach L (2010) Environmental controls on CH4 emission from polygonal tundra on the microsite scale in the Lena river delta, Siberia. Global Change Biology, **16**, 3096–3110.

Sachs T, Wille C, Boike J, Kutzbach L (2008) Environmental controls on ecosystem-scale CH4emission from polygonal tundra in the Lena River Delta, Siberia. Journal of Geophysical Research, **113**, G00A03.

Salmon VG, Soucy P, Mauritz M, Celis G, Natali SM, Mack MC, Schuur EAG (2016) Nitrogen availability increases in a tundra ecosystem during five years of experimental permafrost thaw. Global Change Biology, **22**, 1927-1941.

Schädel C, Schuur EA, Bracho R *et al.* (2014) Circumpolar assessment of permafrost C quality and its vulnerability over time using long-term incubation data. Global Change Biology, **20**, 641-652.

Schaeffer SM, Sharp E, Schimel JP, Welker JM (2013) Soil-plant N processes in a High Arctic ecosystem, NW Greenland are altered by long-term experimental warming and higher rainfall. Global Change Biology, **19**, 3529-3539.

Schimel DS, Braswell BH, Holland EA *et al.* (1994) Climatic, edaphic, and biotic controls over storage and turnover of carbon in soils. Global Biogeochemical Cycles, **8**, 279-293.

Schlesinger WH (2013) *Biogeochemistry : an analysis of global change,* Amsterdam, Elsevier, AP.

Schneider J, Grosse G, Wagner D (2009) Land cover classification of tundra environments in the Arctic Lena Delta based on Landsat 7 ETM+ data and its application for upscaling of methane emissions. Remote Sensing of Environment, **113**, 380-391.

Schneider J, Jungkunst HF, Wolf U *et al.* (2016) Russian boreal peatlands dominate the natural European methane budget. Environmental Research Letters, **11**, 014004.

Schneider J, Kutzbach L, Wilmking M (2011) Carbon dioxide exchange fluxes of a boreal peatland over a complete growing season, Komi Republic, NW Russia. Biogeochemistry, **111**, 485-513.

Schneider von Deimling T, Meinshausen M, Levermann A, Huber V, Frieler K, Lawrence DM, Brovkin V (2012) Estimating the near-surface permafrost-carbon feedback on global warming. Biogeosciences, **9**, 649-665.

Schoeneberger P, Wysocki D, Benham E (2012) Soil Survey Staff. 2012. Field book for describing and sampling soils, Version 3.0. Natural Resources Conservation Service, National Soil Survey Center, Lincoln, NE, 36.

Schuur E, Abbott B, Bowden W *et al.* (2013) Expert assessment of vulnerability of permafrost carbon to climate change. Climatic Change, **119**, 359-374.

Schuur EA, Vogel JG, Crummer KG, Lee H, Sickman JO, Osterkamp TE (2009) The effect of permafrost thaw on old carbon release and net carbon exchange from tundra. Nature, **459**, 556-559.

Schuur EAG, Abbott B, Permafrost Carbon N (2011) High risk of permafrost thaw. Nature, **480**, 32-33.

Schuur EAG, Bockheim J, Canadell JG *et al.* (2008) Vulnerability of permafrost carbon to climate change: Implications for the global carbon cycle. Bioscience, **58**, 701-714.

Schuur EAG, Crummer KG, Vogel JG, Mack MC (2007) Plant species composition and productivity following permafrost thaw and thermokarst in alaskan tundra. Ecosystems, **10**, 280-292.

Schwamborn G, Rachold V, Grigoriev MN (2002) Late Quaternary sedimentation history of the Lena Delta. Quaternary International, **89**, 119-134.

Segal AD, Sullivan PF (2014) Identifying the sources and uncertainties of ecosystem respiration in Arctic tussock tundra. Biogeochemistry, **121**, 489-503.

Shurpali NJ, Hyvönen NP, Huttunen JT, Biasi C, Nykänen H, Pekkarinen N, Martikainen PJ (2008) Bare soil and reed canary grass ecosystem respiration in peat extraction sites in Eastern Finland. Tellus B, **60**, 200-209.

Ström L, Tagesson T, Mastepanov M, Christensen TR (2012) Presence of Eriophorum scheuchzeri enhances substrate availability and methane emission in an Arctic wetland. Soil Biology & Biochemistry, **45**, 61-70.

Subke J-A, Inglima I, Francesca Cotrufo M (2006) Trends and methodological impacts in soil CO2 efflux partitioning: A metaanalytical review. Global Change Biology, **12**, 921-943.

Suseela V, Conant RT, Wallenstein MD, Dukes JS (2012) Effects of soil moisture on the temperature sensitivity of heterotrophic respiration vary seasonally in an old-field climate change experiment. Global Change Biology, **18**, 336-348.

Swann AL, Fung IY, Levis S, Bonan GB, Doney SC (2010) Changes in Arctic vegetation amplify high-latitude warming through the greenhouse effect. Proceedings of the National Academy of Sciences of the United States of America, **107**, 1295-1300.

Tape K, Sturm M, Racine C (2006) The evidence for shrub expansion in Northern Alaska and the Pan-Arctic. Global Change Biology, **12**, 686-702.

Tarnocai C, Canadell JG, Schuur EAG, Kuhry P, Mazhitova G, Zimov S (2009) Soil organic carbon pools in the northern circumpolar permafrost region. Global Biogeochemical Cycles, **23**, GB2023.

Tokida T, Miyazaki T, Mizoguchi M, Nagata O, Takakai F, Kagemoto A, Hatano R (2007) Falling atmospheric pressure as a trigger for methane ebullition from peatland. Global Biogeochemical Cycles, **21**, GB2003.

Trucco C, Schuur EAG, Natali SM, Belshe EF, Bracho R, Vogel J (2012) Seven-year trends of CO2 exchange in a tundra ecosystem affected by long-term permafrost thaw. Journal of Geophysical Research: Biogeosciences, **117**, G02031.

Turetsky MR, Bond-Lamberty B, Euskirchen E, Talbot J, Frolking S, McGuire AD, Tuittila ES (2012) The resilience and functional role of moss in boreal and arctic ecosystems. New Phytologist, **196**, 49-67.

Valentine DW, Holland EA, Schimel DS (1994) Ecosystem and physiological controls over methane production in northern wetlands. Journal of Geophysical Research: Atmospheres, **99**, 1563-1571.

van't Hoff JH (1898) Lectures on theoretical and physical chemistry, Part 1: Chemical dynamics. Edward Arnold, London.

van Everdingen R (2005) Multi-language glossary of permafrost and related ground-ice terms: National Snow and Ice Data Center. Data Center for Glaciology.

van Huissteden J, Maximov TC, Dolman AJ (2005) High methane flux from an arctic floodplain (Indigirka lowlands, eastern Siberia). Journal of Geophysical Research-Biogeosciences, **110**, G02002.

Vaughn LJS, Conrad ME, Bill M, Torn MS (2016) Isotopic insights into methane production, oxidation, and emissions in Arctic polygon tundra. Global Change Biology, **22**, 3487-3502.

Vecherskaya MS, Galchenko VF, Sokolova EN, Samarkin VA (1993) Activity and species composition of aerobic methanotrophic communities in tundra soils. Current Microbiology, **27**, 181-184.

Verville J, Hobbie S, Chapin FS, Hooper D (1998) Response of tundra CH4 and CO2 flux tomanipulation of temperature and vegetation. Biogeochemistry, **41**, 215-235.

Voigt C, Lamprecht RE, Marushchak ME *et al.* (2016) Warming of subarctic tundra increases emissions of all three important greenhouse gases–carbon dioxide, methane, and nitrous oxide. Global Change Biology.

von Fischer JC, Rhew RC, Ames GM, Fosdick BK, von Fischer PE (2010) Vegetation height and other controls of spatial variability in methane emissions from the Arctic coastal tundra at Barrow, Alaska. Journal of Geophysical Research: Biogeosciences, **115**, G00I03.

von Lützow M, Kögel-Knabner I, Ludwig B *et al.* (2008) Stabilization mechanisms of organic matter in four temperate soils: development and application of a conceptual model. Journal of Plant Nutrition and Soil Science, **171**, 111-124.

Vourlitis GL, Oechel WC, Hope A *et al.* (2000) Physiological models for scaling plot measurements of CO2 flux across an arctic tundra landscape. Ecological Applications, **10**, 60-72.

Wagner D, Gattinger A, Embacher A, Pfeiffer E, Schloter M, Lipski A (2007) Methanogenic activity and biomass in Holocene permafrost deposits of the Lena Delta, Siberian Arctic and its implication for the global methane budget. Global Change Biology, **13**, 1089-1099.

Wagner D, Kobabe S, Pfeiffer EM, Hubberten HW (2003) Microbial controls on methane fluxes from a polygonal tundra of the Lena Delta, Siberia. Permafrost and Periglacial Processes, **14**, 173-185.

Wagner D, Pfeiffer EM, Bock E (1999) Methane production in aerated marshland and model soils: effects of microflora and soil texture. Soil Biology & Biochemistry, **31**, 999-1006.

Walker MD, Wahren CH, Hollister RD *et al.* (2006) Plant community responses to experimental warming across the tundra biome. Proceedings of the National Academy of Sciences, **103**, 1342-1346.

Walz J, Knoblauch C, Böhme L, Pfeiffer E-M (2017) Regulation of soil organic matter decomposition in permafrost-affected Siberian tundra soils - Impact of oxygen availability, freezing and thawing, temperature, and labile organic matter. Soil Biology and Biochemistry, **110**, 34-43.

Whalen S, Reeburgh W, Reimers C (1996) Control of tundra methane emission by microbial oxidation. In: *Landscape function and disturbance in arctic tundra.* pp Page., Springer.

Whalen SC (2005) Biogeochemistry of methane exchange between natural wetlands and the atmosphere. Environmental Engineering Science, **22**, 73-94.

Whalen SC, Reeburgh WS (1992) Interannual variations in tundra methane emission: A 4-year time series at fixed sites. Global Biogeochemical Cycles, **6**, 139-159.

Wille C, Kutzbach L, Sachs T, Wagner D, Pfeiffer E-M (2008) Methane emission from Siberian arctic polygonal tundra: eddy covariance measurements and modeling. Global Change Biology, **14**, 1395-1408.

Wilson RM, Fitzhugh L, Whiting GJ *et al.* (2017) Greenhouse gas balance over thaw-freeze cycles in discontinuous zone permafrost. Journal of Geophysical Research: Biogeosciences, doi:10.1002/2016JG003600.

Wilson TB, Meyers TP (2007) Determining vegetation indices from solar and photosynthetically active radiation fluxes. Agricultural and Forest Meteorology, **144**, 160-179.

Wohlfahrt G, Pilloni S, Hortnagl L, Hammerle A (2010) Estimating carbon dioxide fluxes from temperate mountain grasslands using broad-band vegetation indices. Biogeosciences, **7**, 683-694.

WRB IWG (2014) *World reference base for soil resources 2014 international soil classification system for naming soils and creating legends for soil maps,* FAO, Rome.

Xu LK, Baldocchi DD, Tang JW (2004) How soil moisture, rain pulses, and growth alter the response of ecosystem respiration to temperature. Global Biogeochemical Cycles, **18**, GB4002.

Yavitt JB, Lang GE (1990) Methane production in contrasting wetland sites - response to organic-chemical components of peat and to sulfate reduction. Geomicrobiology Journal, **8**, 27-46.

Zamolodchikov D, Karelin D, Ivaschenko A (2000) Sensitivity of tundra carbon balance to ambient temperature. Water, Air and Soil Pollution, **119**, 157-169.

Zhang T, Barry RG, Knowles K, Heginbottom JA, Brown J (2008) Statistics and characteristics of permafrost and ground-ice distribution in the Northern Hemisphere. Polar Geography, **31**, 47-68.

Zhu R, Ma D, Xu H (2014) Summertime N2O, CH4 and CO2 exchanges from a tundra marsh and an upland tundra in maritime Antarctica. Atmospheric Environment, **83**, 269-281.

Zimov SA, Davydov SP, Zimova GM, Davydova AI, Schuur EAG, Dutta K, Chapin FS (2006) Permafrost carbon: Stock and decomposability of a globally significant carbon pool. Geophysical Research Letters, **33**, L20502.

Zona D, Gioli B, Commane R *et al.* (2016) Cold season emissions dominate the Arctic tundra methane budget. Proceedings of the National Academy of Sciences of the United States of America, **113**, 40-45.

Zona D, Oechel WC, Richards JH, Hastings S, Kopetz I, Ikawa H, Oberbauer S (2011) Light-stress avoidance mechanisms in a Sphagnum-dominated wet coastal Arctic tundra ecosystem in Alaska. Ecology, **92**, 633-644.

Zubrzycki S, Kutzbach L, Grosse G, Desyatkin A, Pfeiffer EM (2013) Organic carbon and total nitrogen stocks in soils of the Lena River Delta. Biogeosciences, **10**, 3507-3524.

Acknowledgements

First of all, I would like to thank my doctoral advisors *Eva-Maria Pfeiffer* and *Christian Knoblauch* for giving me a lot of freedom to develop and to work on this project. Thank you for entrusting me with this PhD project! I am especially grateful to *Eva-Maria Pfeiffer* for her effort in making the Institute of Soil Science one of the big players in the area of permafrost research, giving me constructive criticism on my manuscript and supporting me in many ways. Special thanks go to *Christian Knoblauch* for supporting me through all stages of my project. He assisted me patiently with ideas, discussions and constructive criticism and revised my manuscript thoroughly.

Furthermore, I would like to thank *Lars Kutzbach* for open-minded, fruitful discussions and new ideas on my project. I was lucky to receive *Richard Seifert* as my advisory panel chair, where he was pushing me to finish this thesis. I needed this pressure, thank you!

I would also like to thank all members at the Institute of Soil Science. From my point of view, it seems not easy to share an office with me. Therefore, I am very grateful to my #506 and #428 mates *Norman Rüggen, Kerstin Hansen, Nana Molina Gámez, Olga Vybornova, Lutz Beckebanze, Norman Rößger* and *Josefine Walz* for their patience. Many unnecessary questions and my chaotic way of working challenged their patience. The fact that we are organizing a regular barbecue on the rooftop tells a lot about our team spirit. Thank you guys! It was a pleasure to write my thesis simultaneously to *Josefine Walz*' thesis. There were lot of worries, questions and findings to share. Most probably, I would still write my thesis without this "push-effect" due to passing every phase of thesis-writing together. After all this time, I am proud to call you, *Josi,* a friend of mine.

Furthermore, I would like to thank *Christian Wille* and *David Holl* for supporting me intensely by developing the CO_2 models and working with MATLAB. It was very helpful to have *Volker Kleinschmidt* at my side when I made my first steps in developing a chamber. I was lucky to work together with *Gillian Simpson*, who was doing her M.Sc. thesis. Sometimes I wasn't sure who the doctoral and who the master student was. Your thoroughness helped me a lot, *Gillian*!

Working on this project contained two incredible field trips to the research station Samoylov Island. I am grateful to *Waldemar Schneider, Michail Grigoriev, Irina Fedorova,*

Sasha Makarov and especially *Günter 'Molo' Stoof* as well as all members from the Samoylov research station for technical and logistical support during these trips. Beside the participants from Hamburg, I would like to thank *Niko Bornemann*, *Dima Bolshiyanov, Peter Schreiber, Julia Boike* and *Katrin Kohnert* for making these field trips memorable.

This work would not be possible without my family and friends who were giving me never ending emotional support. Most of all, I would like to thank my beloved companion *Swantje* and my daughter *Liv.* You were cheering me up, when I needed it, you were giving me the freedom I needed for completing this work, you were supporting me in every way. It must be love! Thank you!

It was a pleasure to be part of the School of Integrated Climate System Sciences (SICSS), who were giving me the opportunity to extend my scientific skills and brought me together with PhD students from highly diverse disciplines.

This study was supported by the interdisciplinary Russian-German project CarboPerm, funded by the German Federal Ministry of Education and Research (BMBF Grant No. 03G0836A).

Eidesstattliche Versicherung

Hiermit versichere ich an Eides statt, dass ich die vorliegende Arbeit im Promotionsstudiengang Erdsystemwissenschaften selbstständig verfasst und keine anderen Hilfsmittel – insbesondere keine im Quellenverzeichnis nicht benannten Internet-Quellen – benutzt habe. Alle Stellen, die wörtlich oder sinngemäß aus Veröffentlichungen entnommen wurden, sind als solche kenntlich gemacht.

Ich versichere weiterhin, dass ich die Arbeit vorher nicht in einem anderen Prüfungsverfahren eingereicht habe und die eingereichte schriftliche Fassung der auf dem elektronischen Speichermedium entspricht.

Hamburg, den 03.05.2017

(Tim Eckhardt)